Department of the Navy
Naval Ordnance Test Station
Contract N123(60530)31686A

AN EXPERIMENTAL INVESTIGATION OF A FULLY CAVITATING TWO-DIMENSIONAL FLAT PLATE HYDROFOIL NEAR A FREE SURFACE

Thomas Emmett Dawson
and
E. R. Bate, Jr.

Hydrodynamics Laboratory
Karman Laboratory of Fluid Mechanics and Jet Propulsion
California Institute of Technology
Pasadena, California

Approved by
A. J. Acosta

Report No. E-118.12

October 1962

INTRODUCTORY REMARKS

The work to be described in this report was performed mainly by one of us (Dawson) as part of the requirements for an Aeronautical Engineer's degree at the California Institute of Technology (June, 1959). It is thought, however, that the information gained in this research would be of interest to other people engaged in hydrofoil research even at this late date.

ABSTRACT

An experimental program was conducted to investigate the characteristics of a fully cavitating two-dimensional flat plate hydrofoil in the presence of a free surface. The submergence of the hydrofoil was varied from the planing condition at the free surface to a depth corresponding to 2.16 model chords. Near the surface the cavities formed by venting to the atmosphere, but at the deeper submergences, they had to be artificially formed by supplying them with air.

The normal force, the moment about the leading edge, the center of pressure location, the cavity length, and the volumetric air flow rate into the cavity are presented as functions of angle of attack, cavitation number, Froude number, and proximity to the free surface.

TABLE OF CONTENTS

NOMENCLATURE

Symbols	Definition	Units
b	Span	Feet
c	Chord length	Feet
$C_f = \frac{F_n}{\rho U^2 c/2}$	Normal force coefficient	Dimensionless
$C_{m_{le}} = \frac{M}{\rho U^2 bc/2}$	Moment coefficient about leading edge (positive nose up)	Dimensionless
$C_P = \frac{p - p_c}{\rho U^2/2}$	Pressure coefficient	Dimensionless
$C_Q = \frac{Q}{Ubc \sin a}$	Air volume flow rate coefficient	Dimensionless
$F = \frac{U}{\sqrt{gc}}$	Froude number	Dimensionless
F_n	Normal force	Pounds
$K = \frac{p_\infty - p_c}{\rho U^2/2}$	Cavitation number	Dimensionless
l	Cavity length from leading edge	Feet
M	Moment about leading edge (positive nose up)	Foot pounds
p	Pressure on wetted surface of hydrofoil	Pounds/square foot
p_c	Cavity pressure	Pounds/square foot
p_∞	Upstream pressure at depth of leading edge	Pounds/square foot
Q	Air volume flow rate	Cubic feet/second
s	Foil submergence (see page 7)	Feet
U	Free stream velocity	Feet/second
a	Angle of attack	Degrees
ρ	Water density	Slugs/cubic foot

Purpose of Study

The interest in the effects of cavitation in various fields of hydrodynamics is evidenced by the long list of theoretical and experimental research programs which have been conducted for many years. Most of this research has been directed toward reducing or eliminating the undesirable aspects associated with this flow condition, of which mechanical damage to propellers or pump and turbine impellers is a noteworthy example. In addition to this it is known that the occurrence of extensive cavitation in turbomachines usually causes deterioration in performance.

Supercavitating sections have been proposed as a possible means for reducing or eliminating damage to hydrofoils which must operate in a cavitating flow regime (supercavitation is said to occur when the cavity length exceeds the chord length of the hydrofoil). In this case, a steady cavity completely envelops the foil section thereby reducing the damage and noise caused by the repeated formation and collapse of an unsteady cavity. A great deal of work, however, must yet be done to understand fully this flow condition and to improve the efficiency of these supercavitating sections. The promise of being able to extend the operating speed of hydrofoils without many of the problems usually associated with cavitation has thus awakened interest in this type of hydrofoil for application to propellers, ship stabilization, underwater ordnance, hydrofoil craft, and various other aspects of naval architecture.

Important contributions have already been made in determining the performance of two-dimensional, cavitating hydrofoils and verifying two-dimensional theories in an infinite fluid. In this category can be cited the closed tunnel experiments of Parkin (1)* and those by Silberman (2) in a free jet tunnel.

Two-dimensional theories were developed by Wu (3) and (5), and Tulin (4). These theories do not account for the presence of

---

* Numbers in parenthesis refer to references at the end of this text.

stream boundaries nor do they take into account the effects of gravity. Parkin (8) worked out (approximately) the effect of gravity in an infinite fluid.

The complete theoretical treatment of a cavitating hydrofoil in the presence of gravity having arbitrary submergence in a stream with a free surface does not seem to exist. Special cases, however, have been treated. Green (10) and (11) solves the problem in a stream of infinite and finite depth, but he does not consider gravity, and he only treats the case of $K = 0$. Cumberbatch (12) considers gravity, but he restricts the problem to the case where the hydrofoil is at the free surface, ie., planing only, and his solution is for a stream of infinite depth.

Due to different assumptions made in the formulation of the various theories and the differences between the theoretical models used, it is difficult to compare the theoretical results that have been obtained. Likewise, comparisons between theory and experiment are not always justified. Finally, not much is known about comparisons between experiments performed in different facilities due to tunnel boundary effects. In particular, a comparison between the present experiment and the two previously mentioned is hard to justify due to the extreme disparity of tunnel boundary conditions. References (6), (7), and (17) consider the effects of tunnel boundaries on cavitating bodies, and Appendix I gives the approximate effect of the tunnel bottom on the lift of a hydrofoil planing on the free surface. There were no tunnel boundary corrections applied to the experiments previously mentioned. However, Silberman finds that the differences between the results of free jet experiments, closed tunnel experiments, and infinite fluid theory are negligibly small "for all but the smallest cavitation numbers," and he gives $K = 0.12$ as the limit, above which wall effects apparently are unimportant. The experiments of Parkin and Silberman were carried out with the model relatively far from the boundaries, and their effects should be expected to become more important for the case when the model is allowed to come close to one of them as in the present experiment.

The experiment of Silberman was carried out in a vertical tunnel and Parkin's results were obtained in a horizontal tunnel. Between the two experiments, the effect of gravity was rotated through 90°. Since the experimental results agreed so well with each other and with the zero gravity theory at the higher cavitation numbers, this might mean that the effects of gravity are very small for large cavitation numbers ($K > 0.12$) when the model is relatively far from any boundaries.

Few hydrofoils can be regarded as operating in an infinite fluid. In fact, most are operated near a free surface, as for example, the case of a hydrofoil-supported boat. In view of the added experimental difficulties and the increased number of independent parameters introduced by the presence of the free surface, it is not surprising that few experimenters have explored its influence. In fact, for cavitating flows of the sort described herein, only the work of Johnson (9) on curved hydrofoils of low aspect ratio appears in the readily available literature. Because of the high speed and low aspect ratios of these tests, it was not possible to determine separately the effects of the free surface and cavitation number; nor was it possible to make direct comparison with the two-dimensional theories developed in (3), (4), and (5) or the other experiments previously mentioned.

From the foregoing remarks it is obvious that much work, experimental as well as theoretical, remains to be done before all situations of interest to users of hydrofoils are thoroughly explained. It is also evident that no one theory or combinations of theories now available will adequately cover the range of variables that could be expected to occur. The present program is an experimental one which is intended to give some preliminary information on the effect of the proximity of a free surface on the cavitating flow past a flat plate two-dimensional hydrofoil.

Equipment

The Free-Surface Water Tunnel of the Hydrodynamics Laboratory at the California Institute of Technology was the facility used for this work. Knapp, et al (13) gives a complete description of this tunnel, and Figure 1a shows the working section. This tunnel is a vertical-return, closed loop capable of a velocity of up to 27 fps. Since the low velocity of the working section does not permit vapor cavitation, air was forced into the wake of the hydrofoil to form and sustain a cavity. Such forced cavitation simulates in all important respects vapor cavitation on bodies which have fixed separation points and permits cavitation research in low speed facilities that do not have pressurization control. O'Neill and Swanson (14) have experimented with artificial cavities behind discs.

The installation of a full span hydrofoil in the working section of the tunnel was not considered feasible due to mounting and instrumentation difficulties. Therefore, a narrower two-dimensional test section (Fig. 1b) was constructed and installed in the center of the tunnel working section at the upstream end. The two parallel walls of the test section were constructed of plexiglass for flow visualization, and their upstream ends terminated in wedge shaped aluminum splitter plates. The model was mounted directly to an aluminum disk which in turn fitted into a rectangular aluminum plate. This aluminum plate formed an integral part of one of the walls of the test section and could be moved vertically with respect to the wall, thereby varying the submergence of the model. The disc could be rotated with respect to the plate and in this way the angle of attack of the model could be changed.

The apertures for supplying air to the cavity and for measuring the cavity pressure were located on the circular disk downstream from the model mounting location. To insure against water in the line that measured the cavity pressure, a three-way valve was installed with one side connected to the laboratory air main. This enabled the lines to be cleared with high pressure air prior to each reading (see Fig. 4 for a schematic drawing).

Description of Model

The model was in the form of a wedge constructed from 416 stainless steel. The wedge angle was 6 degrees, the chord 4.50 inches, and the span 3.25 inches (Figs. 2b and 3). In operation, the cavity would spring from the sharp leading edge, leaving the top surface unwetted and the bottom surface fully wetted.

A new method of providing pressure taps was used for this model. Grooves were milled in the bottom surface and 1/16-inch diameter brass tubes were laid in these grooves. Transparent epoxy resin was molded into the grooves, completely covering the brass tubes, and then ground smooth in the plane of the bottom surface of the model. Piezometer orifices of 0.020 inch diameter were drilled perpendicular to the wetted surface of the hydrofoil through the epoxy into each tube along the centerline of the model. The transparent epoxy covering the brass tubes enabled them to be seen easily and hence facilitated the drilling operation.

Experimental Procedure

The pressure from the ten orifices on the model, the tunnel total head, and the cavity pressure were measured by water manometers. The air volume flow rate was measured by means of a Fisher Porter Flowmeter. Figures 1a and 4 show a photograph and a schematic drawing of the experimental setup. The cavity lengths were measured by means of a yardstick fixed to the tunnel wall. By sighting perpendicular to the flow at the point of closure of the cavity, it was possible to measure the cavity lengths on the yardstick. A more accurate method for measuring cavity lengths was not deemed necessary due to difficulty in determining the end of the cavity. In all of the runs, the cavity closure was a re-entrant jet. Under the influence of gravity, the jet fell and struck the lower surface of the cavity. The resulting turbulent mixing of water combined with the frothy nature of the flow at this point due to escaping cavity air, made it difficult to determine the cavity closure point.

The pressure measurements are considered accurate to within 0.01 feet of water. The air flow rate is considered accurate to within 5 percent. Cavity lengths are considered accurate to within 0.5 inches.

Zero angle of attack was determined with the aid of two additional piezometer orifices which had been drilled in the model. One was located on the upper surface and the other on the lower surface at equal distances from the leading edge. By pitching the model to reduce the pressure difference between these two orifices to zero, it was possible to align the chordplane of the wedge parallel to the flow. This angle was repeatable to within 0.25 degrees. The angle of attack of the flat plate is defined with respect to the wetted or lower surface of the model. Since the included wedge angle of the model is 6 degrees, zero angle of attack for the flat plate differed by 3 degrees from zero angle of attack for the wedge.

The Free-Surface Water Tunnel, as originally designed and constructed, had a free surface boundary layer remover, or skimmer. This served to remove the boundary layer on the free surface which had built up through the tunnel so that the velocity profile in the working section would be uniform up to and including the free surface. However, a flatter water surface was obtained in the two-dimensional test section when the skimmer was made inoperative by plugging the water scoop with a streamlined fairing. The majority of runs were conducted with the skimmer plugged.

Figure 5 shows the results of a velocity survey near the free surface on the centerline of the test section with the skimmer plugged. The velocity at the free surface is about 75 percent of the free stream value, and at a depth of one inch the velocity has returned to 98 percent of the free stream value. To determine what effects this velocity defect had on the experimental data that was taken near the free surface, additional runs were made near the surface with the skimmer unplugged. This effect was small and the results are shown in Figures 24 and 35.

A calibration of the two-dimensional test section was made with the model removed. The velocity at the center of the test section

was related to the tunnel total head. Boundary layer surveys were made with an impact probe at the position of the leading edge of the hydrofoil. The results of these boundary layer surveys are shown in Figure 6. The boundary layers were slightly larger than predicted by turbulent boundary layer theory on a plane wall. The displacement thickness was found to be 0.045 inches as compared to 0.032 inches from the theory. Mendelsohn and Polhamus (15) show that a boundary layer thickness equal to four percent of the span does not affect the forces acting at the centerline of a two-dimensional fully wetted airfoil by more than one percent. For the purpose of this study, the boundary layer effect on the pressure distribution at midspan is assumed to be small.

The independent parameters were angle of attack, model depth, velocity, and air flow rate to the cavity. The quantities measured were model pressure distribution, cavity pressure, and cavity length. The force and moment acting on the model and the location of the center of pressure were obtained from a numerical integration of the pressure distribution. The submergence, s is defined from the undisturbed free surface to the pivot point on the model, 0.833c from the leading edge and 0.044c above the bottom or wetted surface. s is positive below the free surface and negative if above.

Discussion of Results

The results are presented in Figures 18 through 43. The quantities obtained were: the normal force coefficient, C_f, the moment coefficient about the leading edge, $C_{m_{le}}$, the center of pressure location aft of the leading edge, the cavity length ratio, ℓ/c, and the air volume flow rate coefficient, C_Q. The results are presented with respect to the angle of attack, α, the cavitation number, K, the submergence ratio, s/c, and the Froude number, F.

1. Normal Force and Moment Coefficients

The normal force and moment coefficients are presented in Figures 18 through 35, and compared to Wu's infinite fluid, no-gravity theory. The agreement between the present experiment and the theory is good at the deeper submergences and the smaller angles of attack. As the hydrofoil approaches the free surface, the experimental normal force coefficients become larger than those predicted by Wu's theory. Figure 25 shows this effect at an attack angle of 8 degrees. The results of the experiments of Silberman and Parkin at 8 degrees are also shown on this figure. Agreement is good between the three experiments for cavitation numbers larger than K = 0.12 and at the deepest submergence for the present experiment. At cavitation numbers smaller than K = 0.12 the present experiment follows more closely the theory of Wu (again, at the deepest submergence) than the results of Silberman (Parkin had no data at these lower cavitation numbers).

Figure 26 shows the behavior of C_f as a function of submergence for a cavitation number of zero. The values of C_f for this figure were obtained by extrapolating C_f to K = 0 at each submergence and each angle of attack by drawing a line through the data points parallel to Wu's theory. It is thought that this extrapolation is justified at the deeper submergences on the basis of the good agreement between the theory and the experimental points. Near the surface, the data points are very near K = 0 and the value of C_f corresponding to zero cavitation number is not too sensitive to the method used for extrapolation. The negative cavitation numbers that occur near the surface are a consequence of the definition of p_o. p_o is defined as the pressure at a depth below the free surface corresponding to the submergence of the leading edge of the hydrofoil, and when the foil is above the surface, this quantity is a negative number. Actually, all cavitation numbers that are less than zero should probably be set equal to zero, since at the submergences near the surface the cavity was open to atmospheric air.

At the deeper submergences, the agreement between the experiment at α = 6 degrees and the result of the classical Rayleigh theory (which is the limit of Green's planing theory when the submergence-to-chord ratio is made large) is good. As the submergence is decreased the force coefficient is increased as the zero gravity theory of Green predicts.* Cumberbatch worked out the gravity case for planing, and the values from his theory at F = 3 and 4.5 (the Froude number range in this experiment) for α = 6 degrees are shown on the figure. Though the force coefficients increase for submergences close to the free surface, the value at the free surface (the planing case) is lower than the value predicted by the theory of Cumberbatch even at the lowest value of the Froude number. This discrepancy might be accounted for by the relatively large angles of attack and the effects of the bottom. The Froude number or gravity effect is present in the experimental results, and it seems to have a greater effect on the force coefficients than the theory of Cumberbatch predicts. Figure 27 shows the variation of C_f as a function of Froude number at two submergences, one deep, and the other planing. There does not seem to be any recognizable dependence of the force coefficient on the Froude number at either of the submergences. Any dependence, however, might not be apparent because of the relatively small range of Froude numbers presented.

2. Center of Pressure

Figure 36 shows the effect of angle of attack on the center of pressure. At all submergences the center of pressure moves aft on the hydrofoil as the angle of attack is increased. The cavitation number was not taken out of the experimental data. There was no apparent dependence between center of pressure location and cavitation number.

---

* Reference (18) shows the theory of Green plotted as a function of depth.

Figure 37 shows the effect of the free surface on the center of pressure location. This location remains essentially constant for each angle of attack up to the free surface. Upon passing through the surface, however, the center of pressure moves aft for all angles of attack.

3. Cavity Length

The original data of cavity length to chord length ratio, ℓ/c, are plotted in Figures 38 through 40 at the submergence ratios of 2.16, 1.50, and 0.83. The cavity lengths decrease with decreasing submergence, with decreasing angle of attack, and with increasing cavitation number.

Few experimental data are available for comparison of length ratios. However, we can cite Silberman (2) again. The comparison of length data with that of Silberman at 8 degrees can be seen on Figure 41. No fairing of curves through the experimental data of Reference 2 was attempted. At a given cavitation number, say K = 0.10, the length ratio in the present experiment is less than that of Silberman by a factor of about two for the submergence ratio, 1.60. This difference could be due to the gravity effect, since the Minnesota experiment was performed in a vertical, free jet tunnel in which gravity was parallel to the flow. Figure 41 shows experimental results at α = 8 degrees as well as the theory of Parkin both for F = 2.83 and 3.68. As can be seen from this figure the Froude number dependence is practically negligible in this range and the experimental length ratios for a given cavitation number and Froude number are smaller than Parkin's theoretical lengths by a factor of about two. A comparison of experimental cavity lengths to the exact and linear theories of Wu (3) and (5) is shown in Figure 37 also.

The experimental data do not agree with the only other experiment available, nor do they agree with the linearized theory of Wu (5) or the infinite fluid, gravity theory of Parkin (8). The agreement is good with the exact infinite fluid theory of Wu (3). The ef-

fects of gravity on cavity lengths in the velocity range of this experiment were not able to be resolved.

The discrepancy between the present experiment and the other results shown in Figure 41 can possibly be explained by the influence of the tunnel boundaries and the free surface. However, tunnel boundary corrections have not been applied to these results.

4. Air Volume Flow Rate

The air volume flow rate coefficient data are plotted in Figures 42 and 43 at $s/c = 2.16$ and 0.83. The difficulty of measurement of the air flow rate results in scattered and not too reproducible data. However, these results do show the order of magnitude of the air flow at two submergences. For purposes of comparison, one three-dimensional experiment and theory of Cox and Clayden (16) and another three-dimensional experiment of Swanson and O'Neill (14) are available. The results of these two experiments are shown on Figures 42 and 43. The Froude number dependence found by the other investigators does not seem to be present in this experiment since the Froude numbers for the experimental points shown ranged from $F = 3.5$ to $F = 4.5$.

As the submergence is decreased at constant angle of attack and cavitation number, the air flow is also decreased. The curves of Cox and Clayden (16) and Swanson and O'Neill (14) show a radical decrease in air flow for a small increase in K. The results of the present experiment do not show this behavior. The air flow measurments in the other experiments were obtained when the cavity end consisted of thin vortices, and the noted sharp reduction in air flow occured when these vortices disappeared and a re-entrant jet formed. The cavities in the present experiment were entirely the re-entrant jet type (see Figures 7 through 11).

5. Pressure Distribution

Representative plots of the experimentally obtained pressure

distributions are shown in Figures 12 through 17. The experimental points in these figures represent the pressure tap locations. Since the model was extremely thin near its leading edge it was not feasible to install a pressure tap at a position near the stagnation point; thus the first pressure tap is at x/c = .092. The stagnation point location was determined by tests with tufts at several angles of attack and velocities. In all cases it was sufficiently close to the leading edge so that the determination of the normal force by numerical integration of the pressure distribution curve was considered accurate if the stagnation point was assumed at x/c = 0.* The value used for C_P at the stagnation point in the data reduction was C_P = 1.00. This was an error, since the pressure coefficient was based on the cavity pressure and not free stream pressure. The value of the pressure coefficient at the stagnation point should have been $C_P = (1.00 + K)$. Upon examination of the pressure distribution curves it can be seen that this error will be negligibly small even for rather large values of the cavitation number in the determination of the total area under the curves. For this reason, none of the values of the force coefficients were recalculated nor the curves redrawn.

Figure 17b shows a comparison between one of the experimentally determined pressure distributions near the free surface and the planing theory of Cumberbatch for similar Froude number. The agreement is good over the range of experimental points except near the leading edge. Extrapolation of the theory indicates that the location of the stagnation point might possibly be farther aft on the foil than was indicated by this experiment when the foil is near the free surface. The tests using tufts were not performed near the surface since spray and deformation of the surface made it difficult to see the tufts. For this reason, the stagnation point location was

---

* For small α, the location of the stagnation point can approximately be given by $x/c = \frac{17}{48}\,\alpha^4$ from Wu, Ref. (3)

assumed to remain the same as that determined at the deeper submergences.

6. Summary

An experiment was performed to determine the force and cavitation characteristics of a fully cavitating flat plate hydrofoil in the presence of a free surface. The submergence of the hydrofoil was an important variable in the experiment.

I. At the deeper submergences the normal force coefficient agreed well with experiments performed by Parkin and Silberman and with the infinite fluid, no-gravity theory of Wu.

II. Upon approaching the free surface, the normal force increased in magnitude, but not to the extent predicted by the planing theory of Green. Cumberbatch takes into account the effects of gravity, but the present experiment indicates that the theory underestimates this gravity effect.

III. Cavity lengths agreed well with Wu's exact theory, and did not agree with Parkin or Wu's linear theories. There was no recognizable dependence of cavity length on the Froude number, but this could be due to the small range of Froude numbers chosen.

IV. Tunnel boundary effects become important at small cavitation numbers. More work needs to be done to understand exactly what influence they have on experimental results.

ADDENDUM

Dawson's original thesis contained a linearized theory for the flow past a cavitating flat plate in the presence of a free surface and a comparison of this theory, the experimental data, and Green's nonlinear theory. Prior to publishing the present report, Schot in Reference (18) solved the same linearized problem and compared his results with Green's theory. Dawson's analysis is not included in the present report, since a similar treatment has subsequently appeared in published form.

A comparison between the results of experiments and theories of cavitating bodies near a free surface introduces the problem of determining the submergence of the body. For a semi-infinite flow (no bottom), or when the bottom is very far away from the hydrofoil, the only significant physical depth parameter is the spray sheet thickness. In the case of the flow in which a bottom is present and the upstream depth can be specified, the submergence of the hydrofoil is still not easy to define due to local deformation of the free surface. Again, the spray sheet thickness is probably the best measure of the submergence. Due to the difficulty of measuring the spray sheet thickness, the submergence in the present experiment was defined with respect to the undisturbed free surface, and it was not thought justified to present the comparison of the experimental results and the theory of Green.

APPENDIX I

A simple estimate of the tunnel bottom effect on a planing surface at small angles of attack:

In this scheme, the hydrofoil is represented by a vortex of strength Γ. To calculate the vortex strength, the Weissinger two-point method will be used. The vortex is placed at the one-quarter chord point on the foil (the center of pressure) and the condition of flow tangency is satisfied at the three-quarter chord point.

If v is the perturbation velocity perpendicular to the plate then at the three-quarter chord point the boundary condition is $v/U = dy/dx = -\alpha$ or $v = -\alpha U$. The flow is sketched in Fig. I-1.

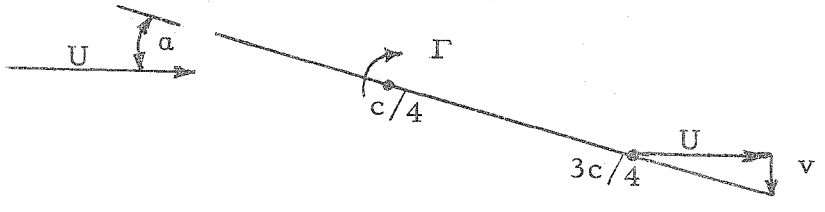

Fig. I-1

The velocity at a distance c/2 from a vortex of strength Γ is $v = -\Gamma/2\pi c/2$ so that $\Gamma = -v\pi c = \alpha U\pi c$. In an infinite fluid, with velocity U, the lift on a vortex of strength is $L = \rho U\Gamma$ where ρ is the density of the fluid. Planing theory for no gravity predicts a lift that is just half of the value for the infinite fluid. For this analysis, the lift on the planing hydrofoil will be: $L = \rho U \Gamma/2$. The lift is then:

$$L = 1/2\rho U^2 \pi\alpha c$$

and the lift coefficient is

$$C_L = \frac{L}{\rho U^2 c/2} = \pi\alpha$$

A planing surface in the presence of a tunnel bottom is now considered, Fig. I-2

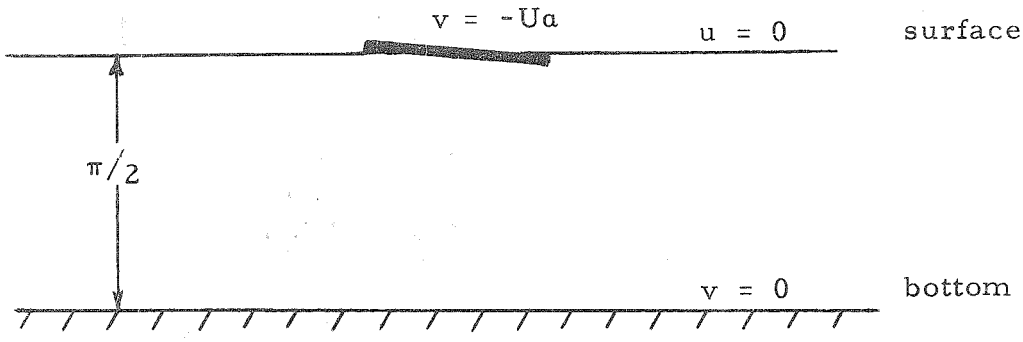

Fig. I-2

The flat plate can be replaced by a vortex at the one-quarter chord point but in order to satisfy the boundary conditions shown in Fig. I-2, the infinite sequence of alternating vortices of equal strength, as shown in Fig. I-3, will be necessary.

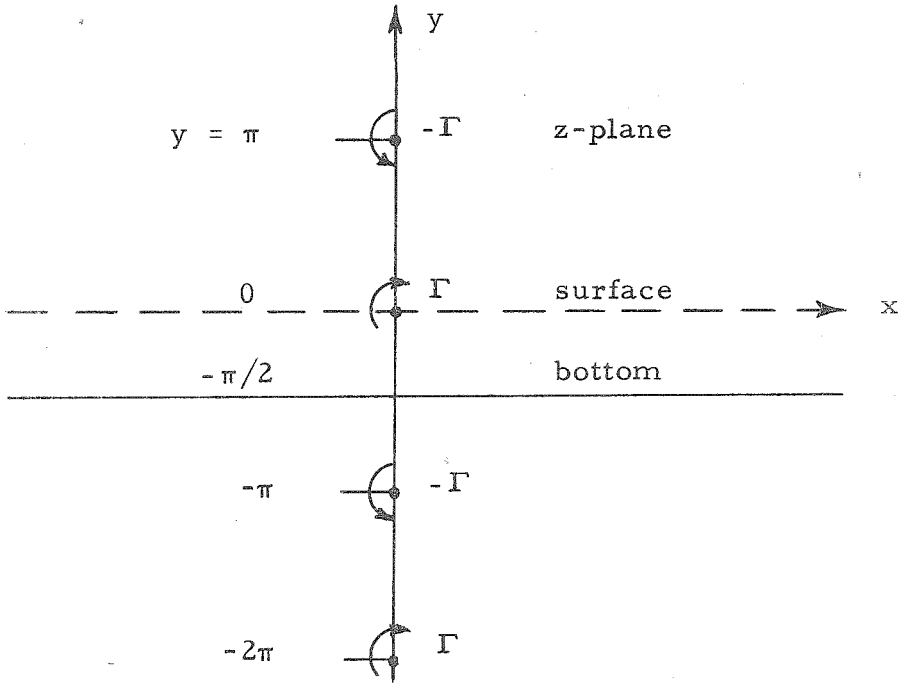

Fig. I-3

On the lines of symmetry $z = 0 \pm n\pi i$ there are no horizontal velocities, u, due to the vortices. Similarly on the lines of symmetry, $z = -\frac{\pi}{2} \pm n\pi i$ there are no vertical velocities, v, due to the vortices.

The potential due to a single vortex is

$$G(z) = \phi + i\psi = \frac{i\Gamma}{2\pi} \ln z$$

and for the sequence in Fig. I-3 the total potential due to all vortices is

$$F(z) = \frac{i\Gamma}{2\pi} \sum_{-\infty}^{+\infty} (-1)^n \ln(z - n\pi)$$

This series has a sum*

$$F(z) = \frac{i\Gamma}{2\pi} \ln \tanh \frac{z}{2}$$

so that

$$u - iv = \frac{dF}{dz} = \frac{i\Gamma}{2\pi} \operatorname{cosech} z.$$

At $z = c/2$,

$$v = -\frac{\Gamma}{2\pi} \operatorname{cosech} \frac{c}{2} = -U\alpha,$$

hence,

$$\Gamma = 2\pi U\alpha \sinh \frac{c}{2}$$

and

$$L = \pi\rho U^2 \alpha \sinh \frac{c}{2}$$

---

* Copson, E. T., Theory of Functions of a Complex Variable

Finally the lift coefficient is obtained

$$C_L = \frac{L}{\rho U^2 \, c/2} = \frac{2\pi\alpha}{c} \sinh \frac{c}{2}$$

However, the dimension of interest is the distance to the solid boundary, h. Let the ratio of the chord to this distance, h, be $\sigma = c/h = c/\pi/2$ or $c = 2\sigma/\pi$. Therefore,

$$C_L = \frac{4\alpha}{\sigma} \sinh \frac{\pi\sigma}{4}$$

is the lift coefficient of a planing flat plate hydrofoil with a solid lower boundary and no gravity.

The hyperbolic sine can be expanded

$$\sinh x = x + \frac{1}{6} x^3 + \ldots\ldots$$

so that

$$C_L = \frac{4\alpha}{\sigma} \left[\frac{\pi\sigma}{4} + \frac{1}{6} \left(\frac{\pi\sigma}{4}\right)^3 + \ldots\ldots \right]$$

or

$$C_L = \pi\alpha \left[1 + 0.103\sigma^2 + \ldots\ldots\right]$$

Therefore, it can be seen that the presence of a lower boundary always increases the lift. The effect is fairly small even for $\sigma = 1$ in which case there is a ten percent increase in lift. In the case of this experiment near the surface, $\sigma = 0.2$ so that

$$\frac{C_L}{C_{L\infty}} = 1.004$$

which is not significant.

REFERENCES

1. Parkin, Blaine R., "Experiments on Circular Arc and Flat Plate Hydrofoils in Noncavitating and Full Cavity Flows", California Institute of Technology, Hydrodynamics Laboratory, Report No. 47-6, February 1956.

2. Silberman, Edward, "Experimental Studies of Supercavitating Flow about Simple Two-Dimensional Bodies in a Jet", University of Minnesota, St. Anthony Falls Hydraulic Laboratory, Project Report No. 59, April 1958.

3. Wu, T.Y., "A Free Streamline Theory for Two-Dimensional, Fully Cavitated Hydrofoils", California Institute of Technology, Hydrodynamics Laboratory, Report No. 21-17, July 1955.

4. Tulin, M.P., "Supercavitating Flow Past Foils and Struts", Symposium on Cavitation in Hydrodynamics, National Physical Laboratory, Teddington, England, Paper No. 16, September 1955.

5. Wu, T.Y., "A Note on the Linear and Nonlinear Theories for Fully Cavitated Hydrofoils", California Institute of Technology, Hydrodynamics Laboratory, Report No. 21-22, August 1956.

6. Birkhoff, C., Plesset, M., and Simmons, N., "Wall Effects in Cavity Flow", Parts I and II, Quarterly of Applied Mathematics, Vol. VIII, No. 2, July 1950.

7. Cohen, Hirsch, and Tu, Yih-o, "Wall Effects on Supercavitating Flow Past Foils", Rensselaer Polytechnic Institute, RPI Math. Report No. 6, October 1956.

8. Parkin, Blaine R., "A Note on the Cavity Flow Past a Hydrofoil in a Liquid with Gravity", California Institute of Technology, Engineering Division Report No. 47-9, December 1957.

9. Johnson, Virgil E., Jr., "The Influence of Depth of Submersion, Aspect Ratio and Thickness on Supercavitating Hydrofoils Operating at Zero Cavitation Number", Second Symposium on Naval Hydrodynamics, Washington, D.C., August 1958.

10. Green, A.E., "Note on the Gliding of a Plate on the Surface of a Stream", Proceedings of Cambridge Philosophical Society, Vol. 32, 1936, pages 248-252.

11. Green, A.E., "The Gliding of a Plate on a Stream of Finite Depth", Proceedings of Cambridge Philosophical Society, Part I, Vol. 31, 1955, pp. 584-603, Part II, Vol. 32, 1936, pp. 67-85.

12. Cumberbatch, E., "Two-Dimensional Planing at High Froude Number", Journal of Fluid Mechanics, Vol. 4, Part 5, September 1958, pp. 466-478.

13. Knapp, R.T., Levy, J., O'Neill, J.P., and Brown, F.B., "The Hydrodynamics Laboratory at the California Institute of Technology", Transactions, A.S.M.E., Vol. 70, No. 5, July 1948, pp. 437-457.

14. Swanson, W.M., and O'Neill, J.P., "The Stability of an Air-Maintained Cavity Behind a Stationary Object in Flowing Water", California Institute of Technology, Hydrodynamics Laboratory, Memorandum Report No. M-24.3, September 1951.

15. Mendelsohn, R.A., and Polhamus, J.F., "Effect of the Tunnel-Wall Boundary Layer on Test Results of a Wing Protruding from a Tunnel Wall", NACA TN No. 1244, April 1947.

16. Cox, R.N., and Clayden, W.A., "Air Entrainment at the Rear of a Steady Cavity", Symposium on Cavitation in Hydrodynamics, National Physical Laboratory, Teddington, England, Paper No. 12, September 1955.

17. Cohen, H., and DiPrima, R.C., "Wall Effects in Cavitating Flows", Second Symposium on Naval Hydrodynamics, ONR, Aug. 25-29, 1958.

18. Schot, S.H., "Surface Tension and Free Surface Effects in Steady Two-Dimensional Cavity Flow about Slender Bodies", DTMB Report No. 1566, January, 1962.

LIST OF FIGURES

continued

continued

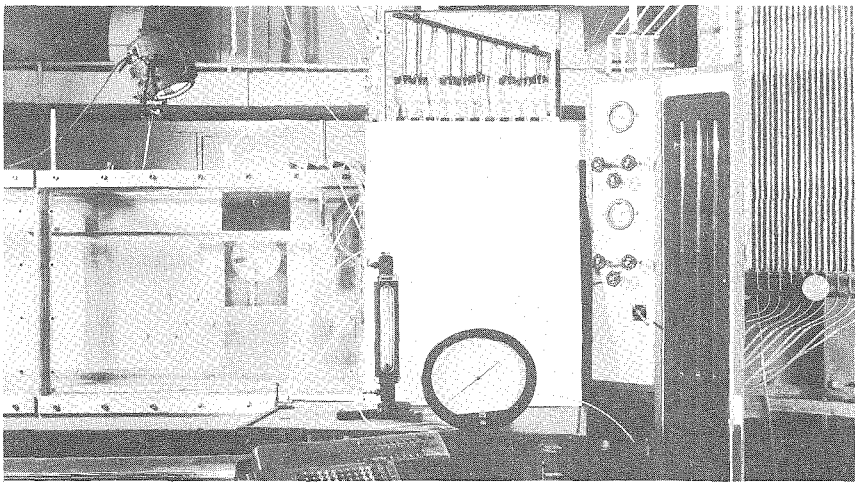

Fig. 1a - The General Arrangement of the Experimental Apparatus Showing the Two-Dimensional Test Section Installed in the Working Section of the Free-Surface Water Tunnel. The Hydrofoil also Can be Seen in a Position Corresponding to s/c = -0.06.

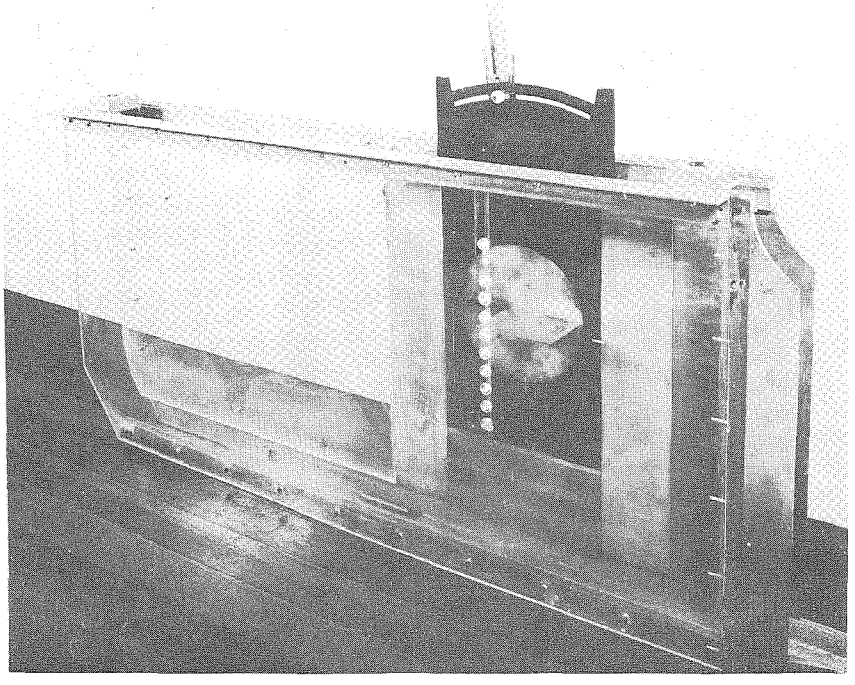

Fig. 1b - A View of the Two-Dimensional Test Section Showing the Leading Edges and General Construction. The Mounting Plate and Hydrofoil Can also be Seen Installed.

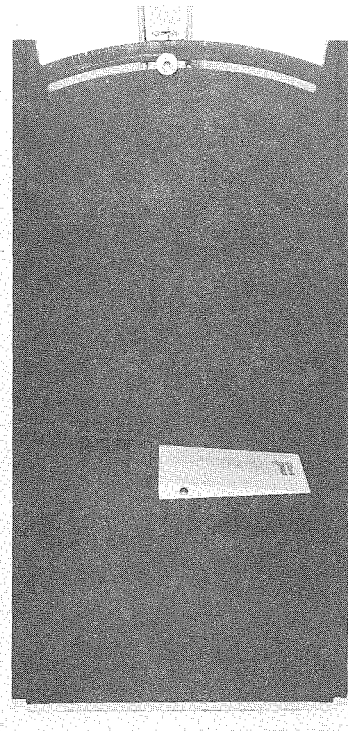

Fig. 2a - The Mounting Plate and the Hydrofoil Showing the Cavity Pressure Probe and the Opening for Forcing Air into the Cavity. The Circular Plate and Arc for Varying the Angle of Attack also Can be Seen.

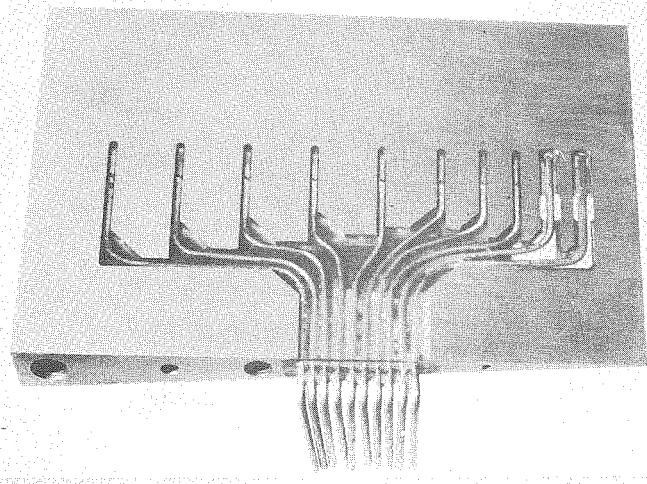

Fig. 2b - A View of the Wedge Hydrofoil Showing the Wetted Surface, Piezometer Orifices, and General Construction.

A	B	C	D	E	F
.500"	.500"	.497"	.506"	.433"	.314"
G	H	I	J		
.253"	.245"	.239"	.413"		

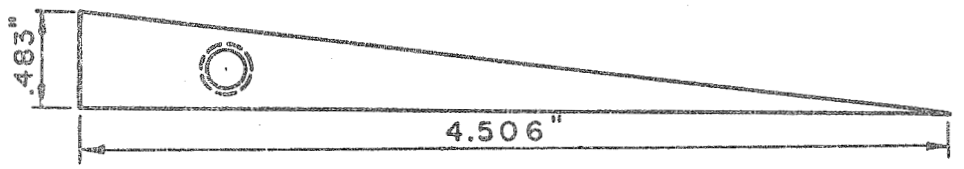

NOTE: PRESSURE TAP POSITIONS NOT TO SCALE

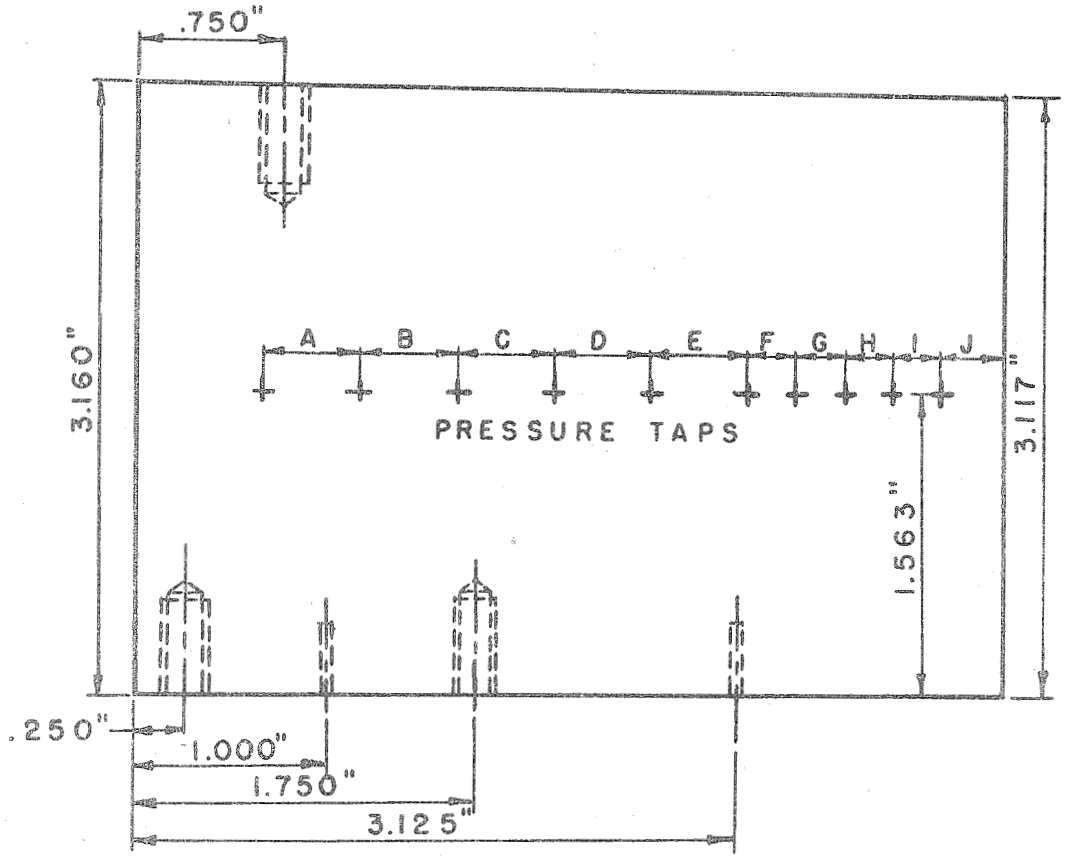

Fig. 3 - A Side and Bottom View of the Wedge Hydrofoil Tested Showing Additional Details of the Construction and the Location of the Piezometer Orifices.

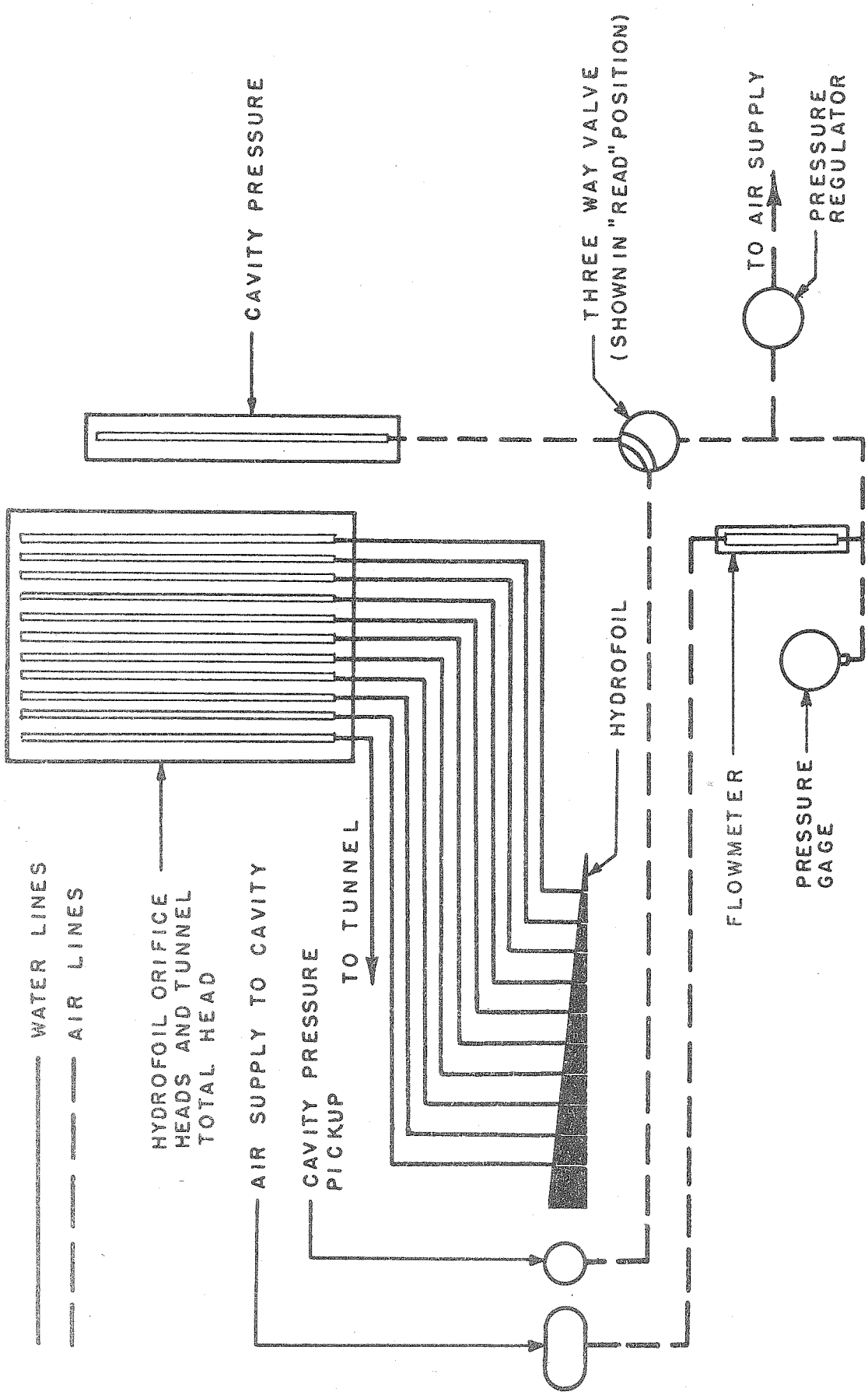

Fig. 4 - A Schematic Diagram of the Setup of the Experimental Apparatus.

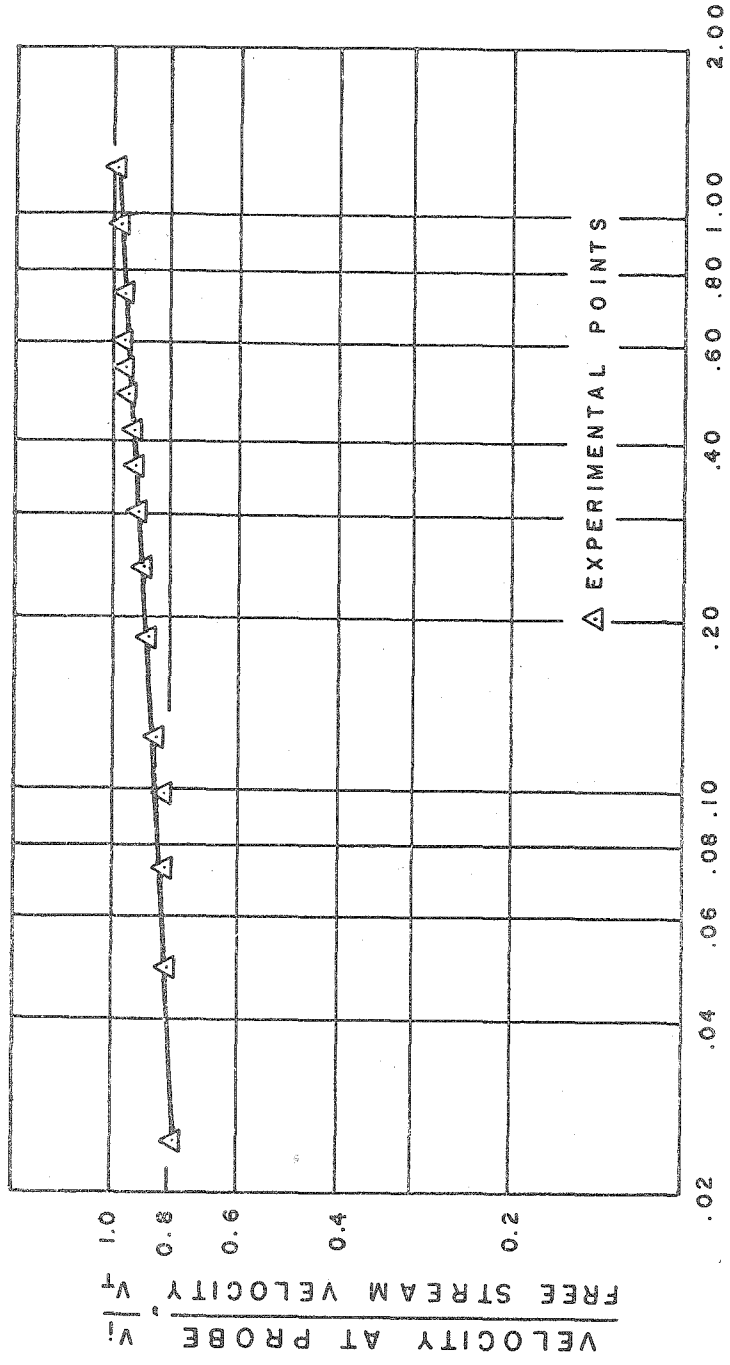

Fig. 5 - A Plot of the Velocity Profile Near the Free Surface and on the Centerline of the Two-Dimensional Test Section. (Skimmer Not Operating)

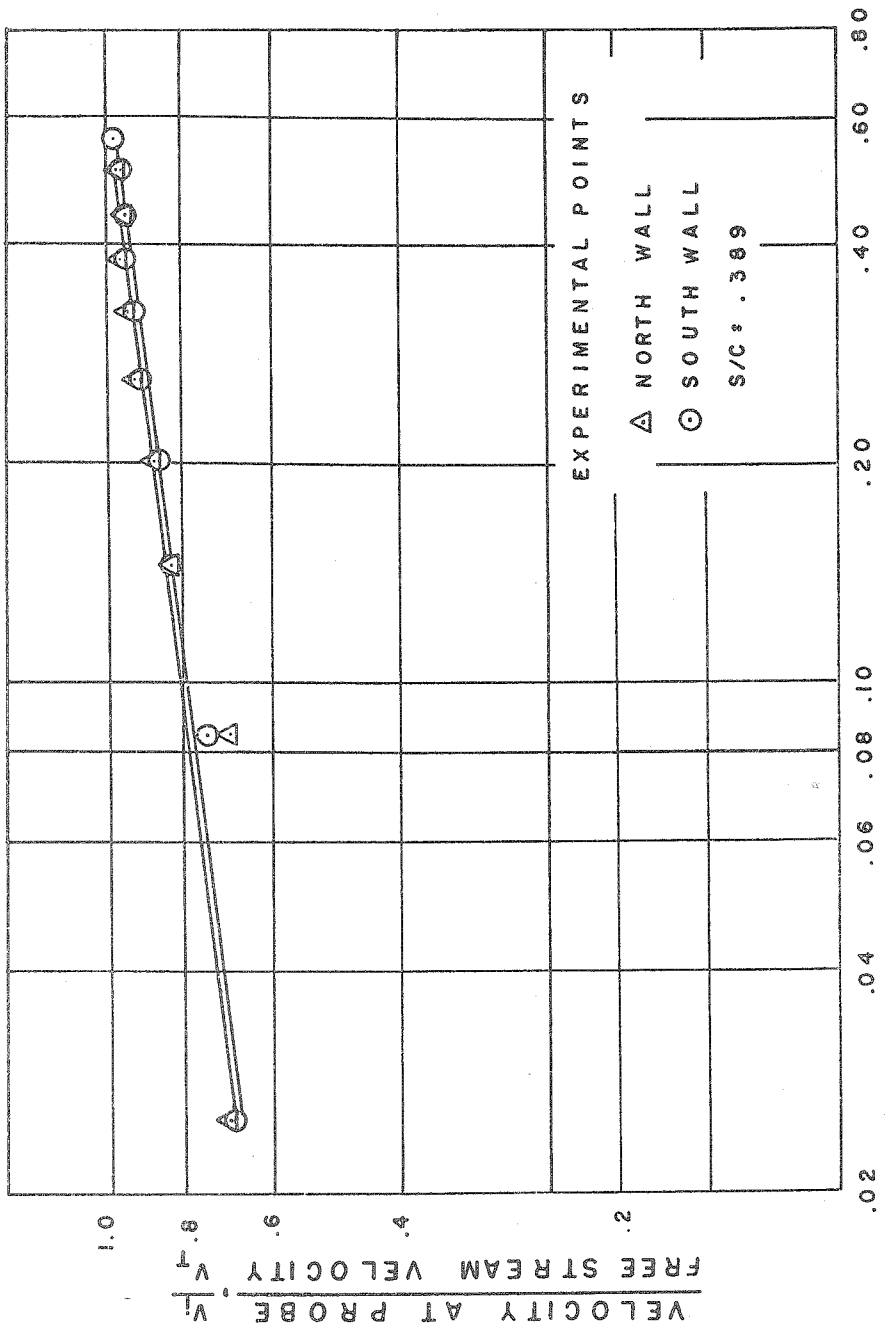

Fig. 6 - A Plot of the Velocity Profiles on the Walls of the Two-Dimensional Test Section at the Position of the Leading Edge of the Hydrofoil.

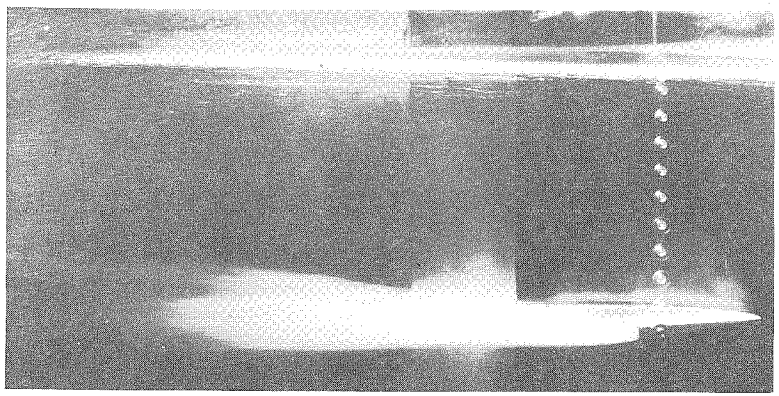

(a) $s/c = 2.16$, $\alpha = 10^{\circ}$, $K = 0.182$, $\ell/c = 2.53$

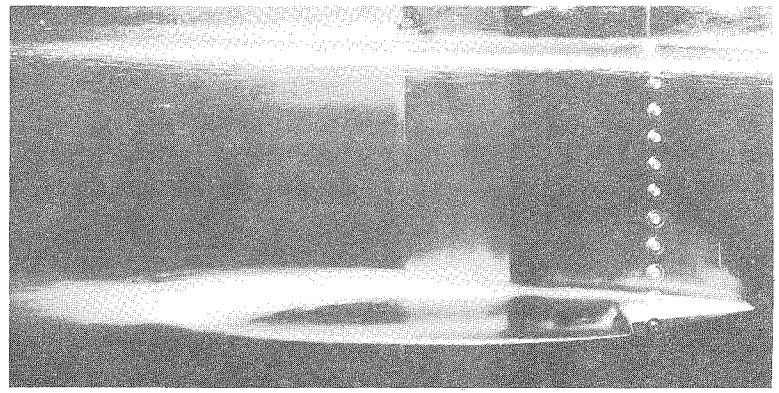

(b) $s/c = 2.16$, $\alpha = 12^{\circ}$, $K = 0.132$, $\ell/c = 4.18$

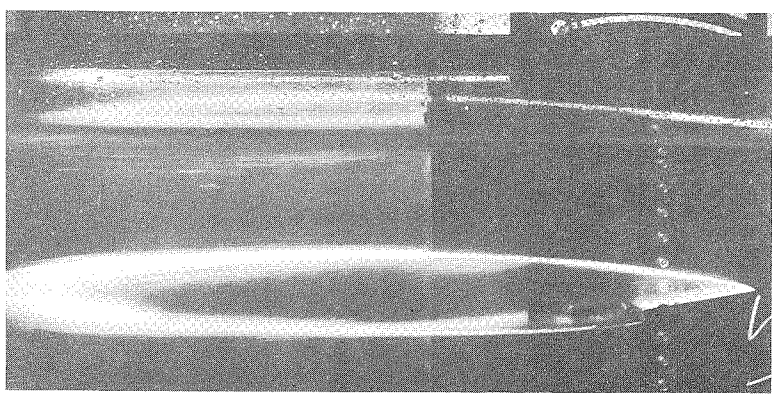

(c) $s/c = 1.50$, $\alpha = 16^{\circ}$, $K = 0.109$, $\ell/c = 6.92$

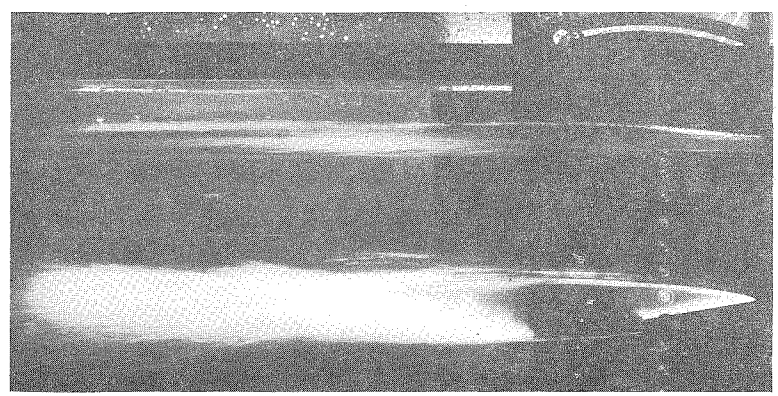

(d) $s/c = 1.50$, $\alpha = 16^{\circ}$, $K = 0.144$, $\ell/c = 3.60$

Fig. 7 - Photos of Typical Cavities Under Varying Conditions which Show the Bowing of the Free Surface.

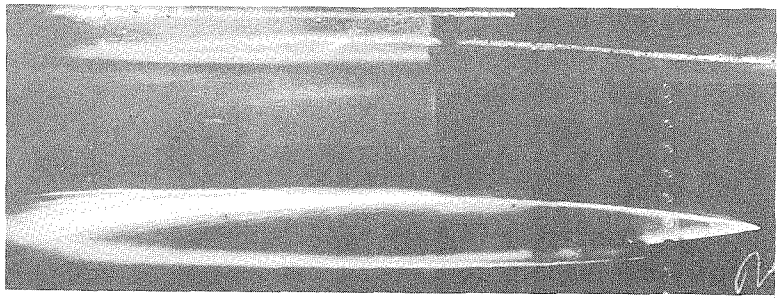

(a) $s/c = 1.50$, $\alpha = 14^{\circ}$, $K = 0.099$, $\ell/c = 6.58$

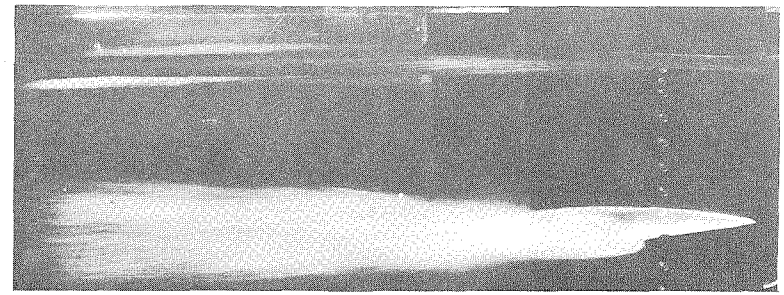

(b) $s/c = 1.50$, $\alpha = 14^{\circ}$, $K = 0.190$, $\ell/c = 2.80$

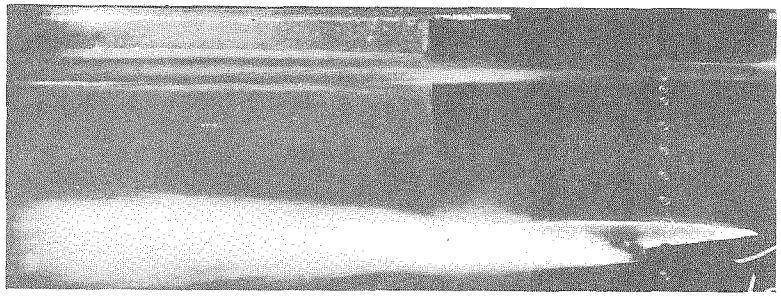

(c) $s/c = 1.50$, $\alpha = 12^{\circ}$, $K = 0.169$, $\ell/c = 2.80$

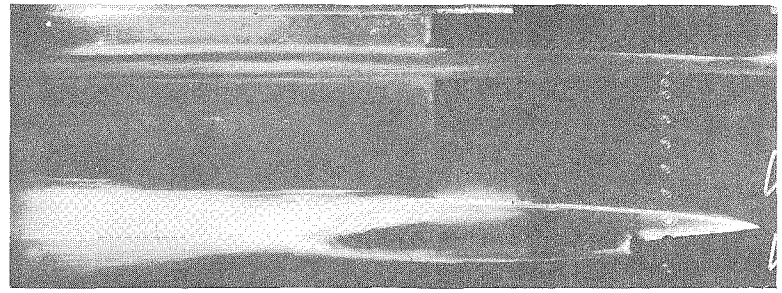

(d) $s/c = 1.50$, $\alpha = 12^{\circ}$, $K = 0.109$, $\ell/c = 4.26$

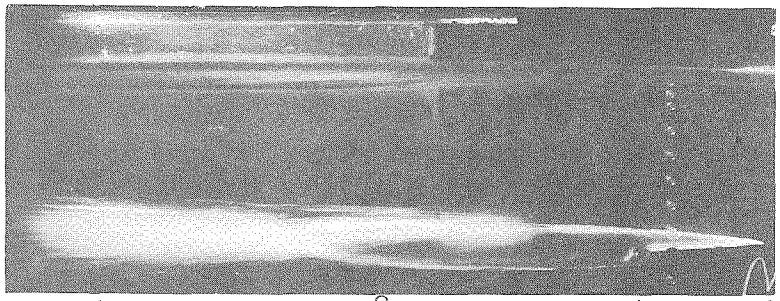

(e) $s/c = 1.50$, $\alpha = 10^{\circ}$, $K = 0.101$, $\ell/c = 3.86$

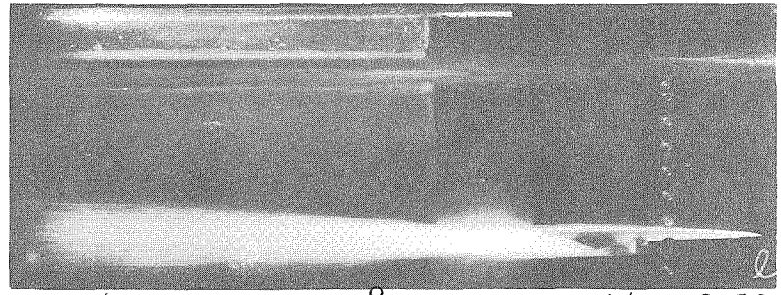

(f) $s/c = 1.50$, $\alpha = 8^{\circ}$, $K = 0.115$, $\ell/c = 2.53$

Fig. 8 - Photos of Typical Cavities Under Varying Conditions which Show the Bowing of the Free Surface.

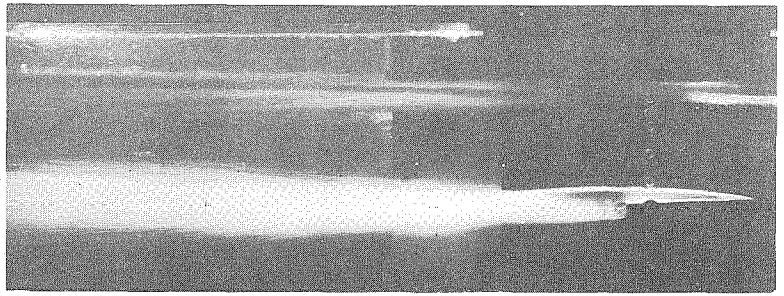

(a) $s/c = 0.83$, $\alpha = 8^{\circ}$, $K = 0.128$, $\ell/c = 1.86$

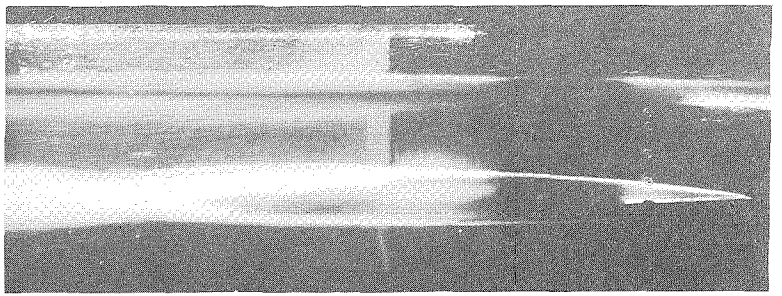

(b) $s/c = 0.83$, $\alpha = 8^{\circ}$, $K = 0.058$, $\ell/c = 4.93$

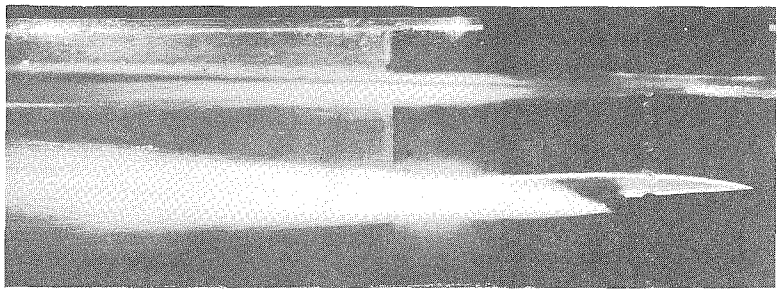

(c) $s/c = 0.83$, $\alpha = 10^{\circ}$, $K = 0.146$, $\ell/c = 2.13$

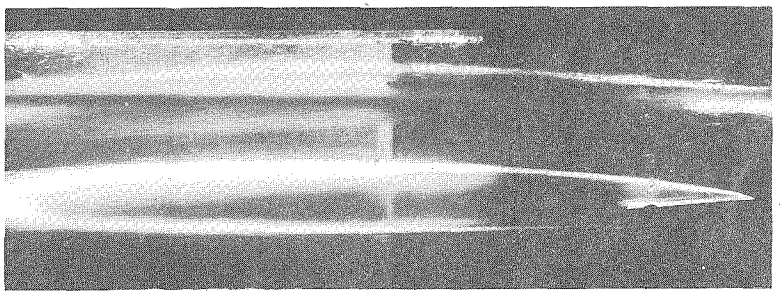

(d) $s/c = 0.83$, $\alpha = 10^{\circ}$, $K = 0.061$, $\ell/c = 6.26$

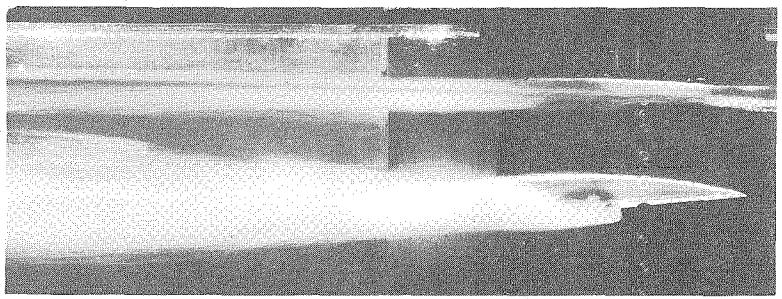

(e) $s/c = 0.83$, $\alpha = 12^{\circ}$, $K = 0.145$, $\ell/c = 2.53$

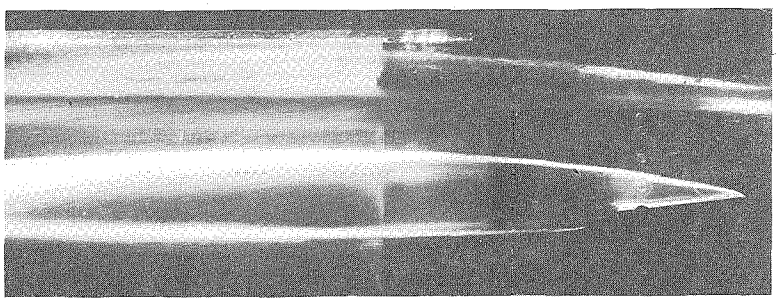

(f) $s/c = 0.83$, $\alpha = 12^{\circ}$, $K = 0.063$, $\ell/c = 6.92$

Fig. 9 - Photos of Typical Cavities Under Varying Conditions which Show the Bowing of the Free Surface.

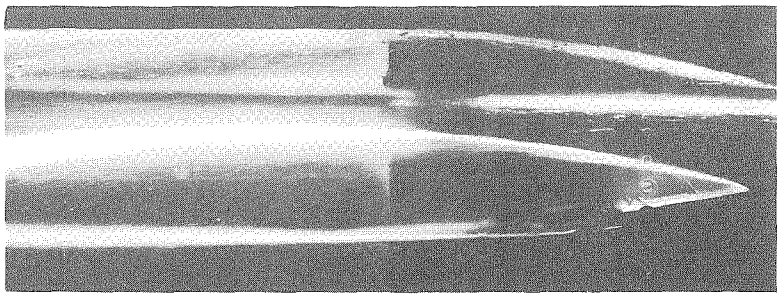

(a) s/c = 0.83, $\alpha = 16^{\circ}$, K = 0.073, $\ell/c = 7.99$

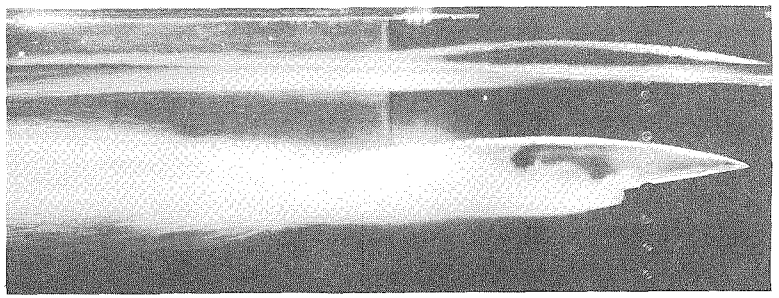

(b) s/c = 0.83, $\alpha = 16^{\circ}$, K = 0.141, $\ell/c = 2.80$

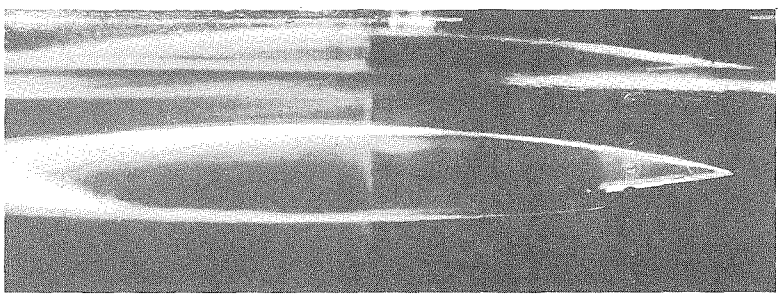

(c) s/c = 0.83, $\alpha = 14^{\circ}$, K = 0.071, $\ell/c = 6.13$

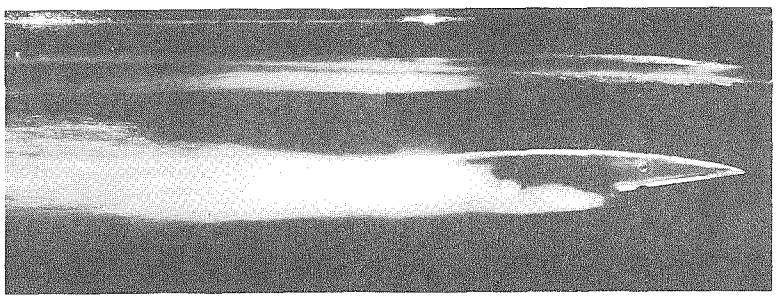

(d) s/c = 0.83, $\alpha = 14^{\circ}$, K = 0.143, $\ell/c = 2.93$

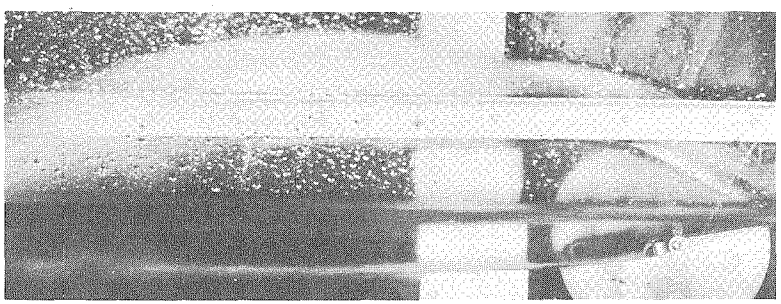

(e) s/c = 0.16, $\alpha = 16^{\circ}$, K = -0.005

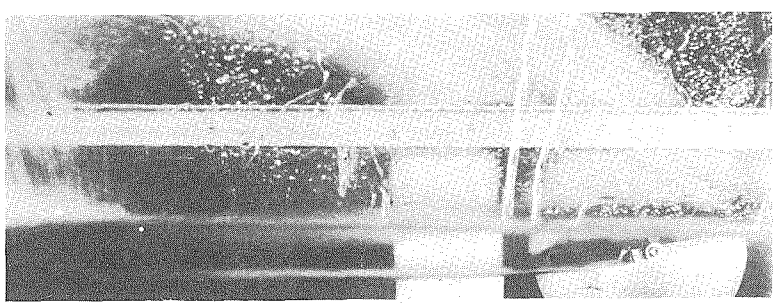

(f) s/c = 0.16, $\alpha = 16^{\circ}$, K = -0.003

Fig. 10 - Photos of Typical Cavities Under Varying Conditions which Show the Bowing of the Free Surface.

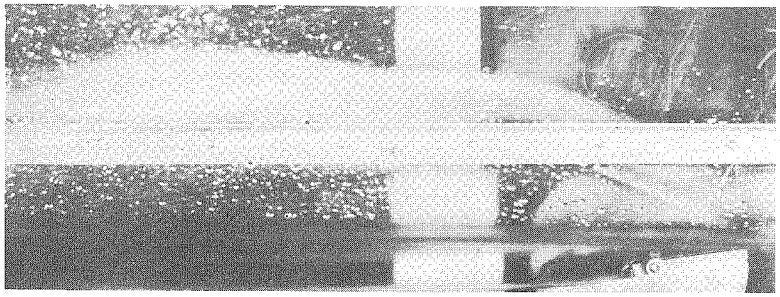

(a) s/c = 0.16, $\alpha = 14^{o}$, K = 0

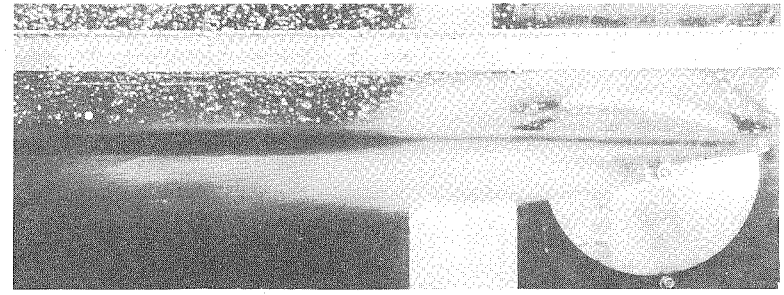

(b) s/c = 0.16, $\alpha = 14^{o}$, K = 0

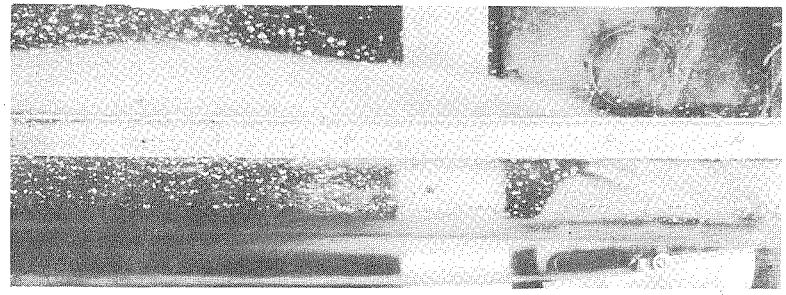

(c) s/c = 0.16, $\alpha = 12^{o}$, K = 0.005

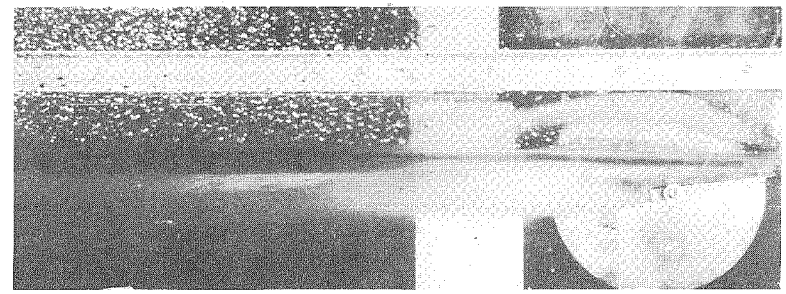

(d) s/c = 0.16, $\alpha = 12^{o}$, K = 0.055, $\ell/c = 2.26$

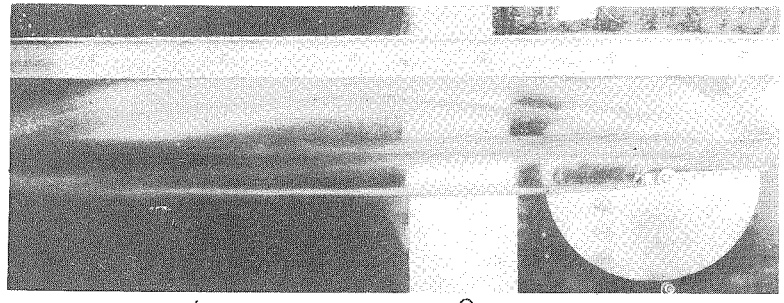

(e) s/c = 0.16, $\alpha = 8^{o}$, K = 0.016

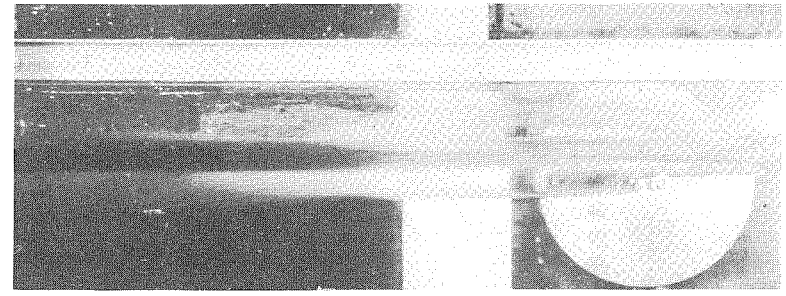

(f) s/c = 0.16, $\alpha = 8^{o}$, K = 0.039, $\ell/c = 2.80$

Fig. 11 - Photos of Typical Cavities Under Varying Conditions which Show the Bowing of the Free Surface.

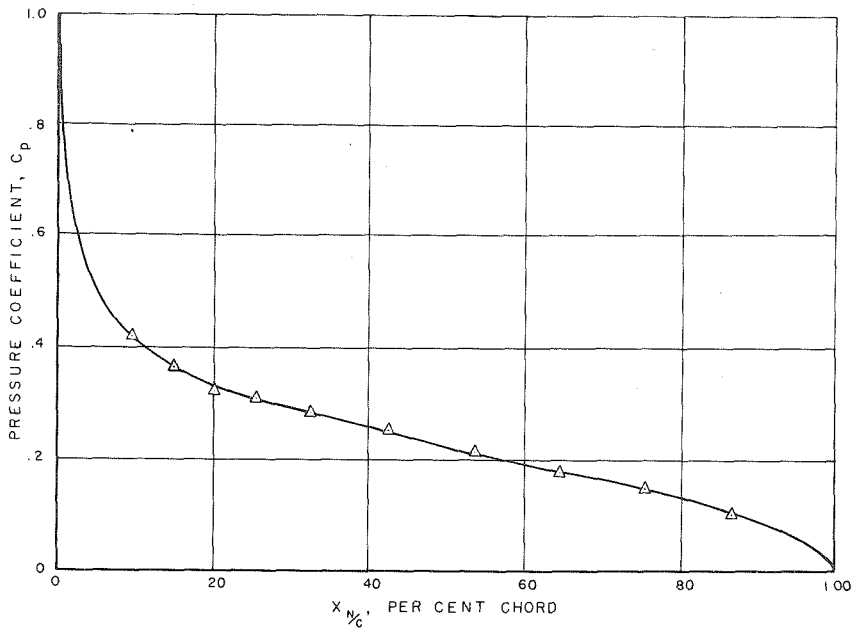

(a) s/c = 2.16, $\alpha = 8^{\circ}$, K = 0.115, $C_f = 0.252$

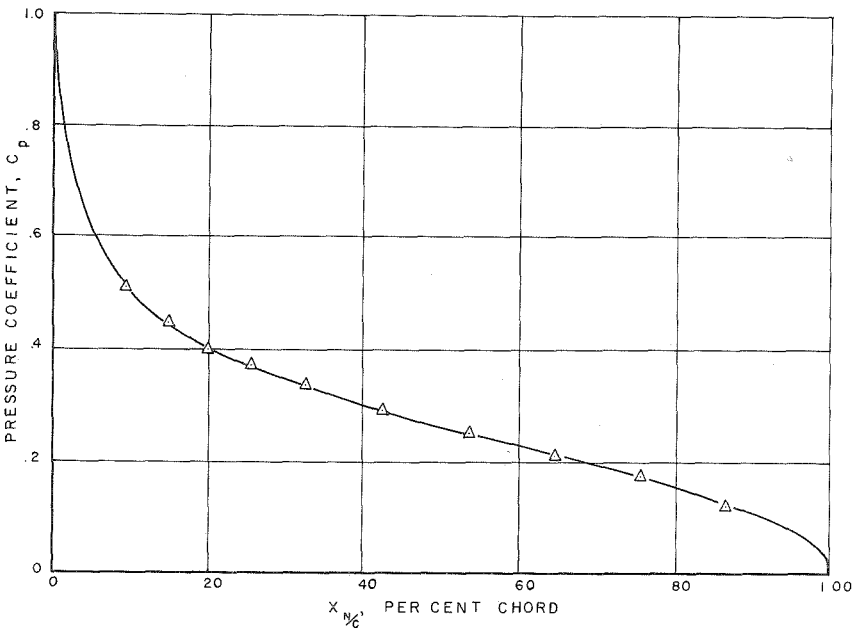

(b) s/c = 2.16, $\alpha = 10^{\circ}$, K = 0.111, $C_f = 0.294$

Fig. 12 - Plots of Pressure Distributions on a Fully Cavitating Flat Plate Hydrofoil at Various Submergences, Cavitation Numbers, and Angles of Attack.

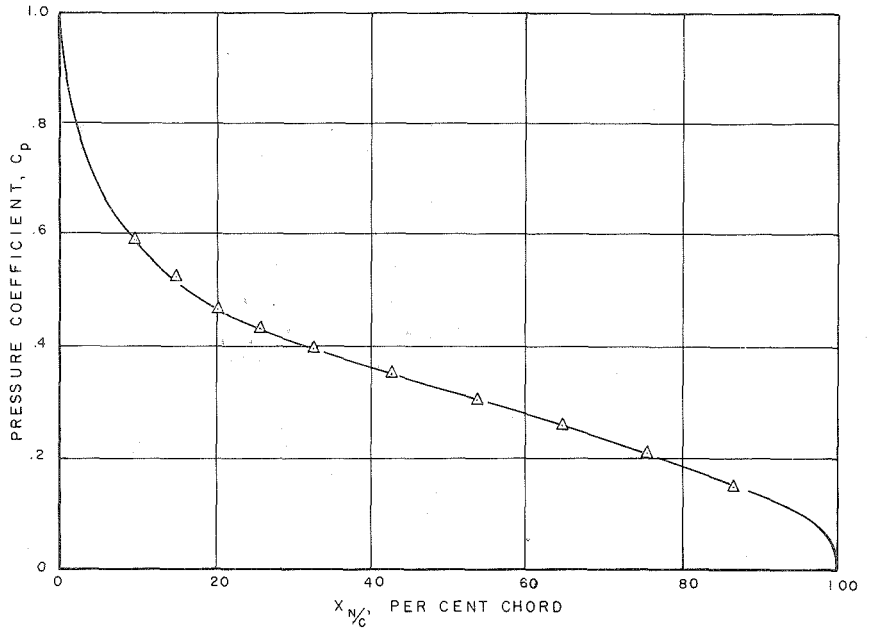

(a) s/c = 2.16, $\alpha = 12^{o}$, K = 0.127, $C_f = 0.343$

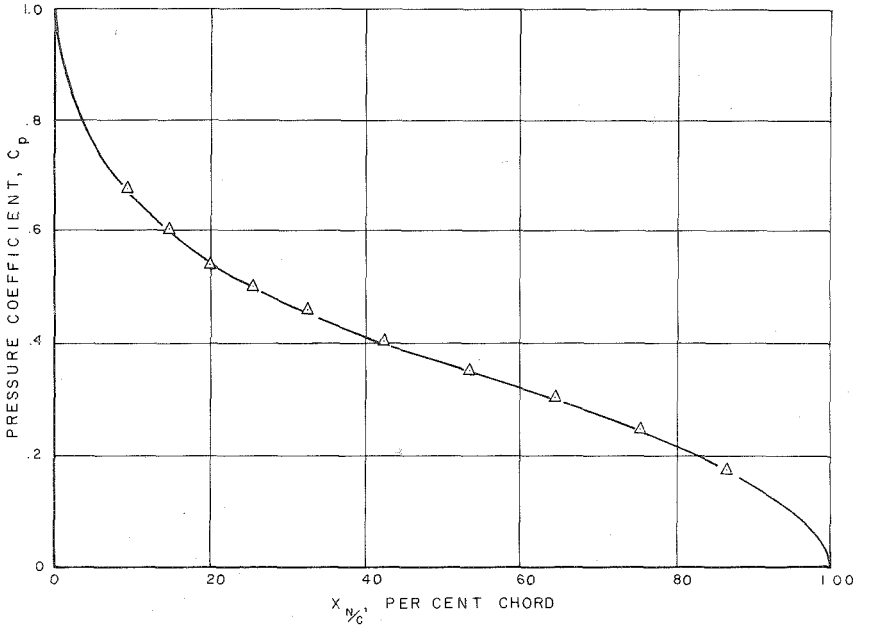

(b) s/c = 2.16, $\alpha = 14^{o}$, K = 0.120, $C_f = 0.391$

Fig. 13 - Plots of Pressure Distributions on a Fully Cavitating Flat Plate Hydrofoil at Various Submergences, Cavitation Numbers, and Angles of Attack.

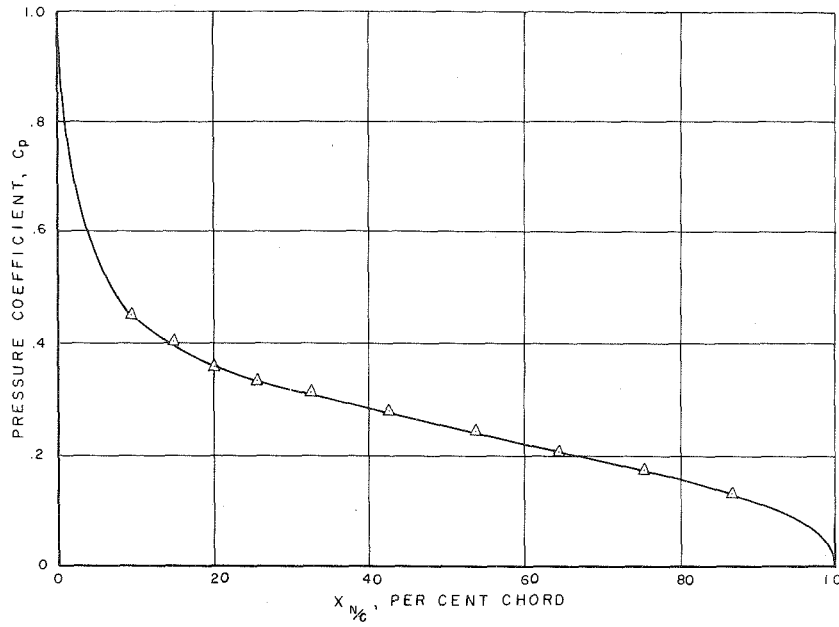

(a) s/c = 0.83, $\alpha = 8^{\circ}$, K = 0.128, $C_f = 0.278$

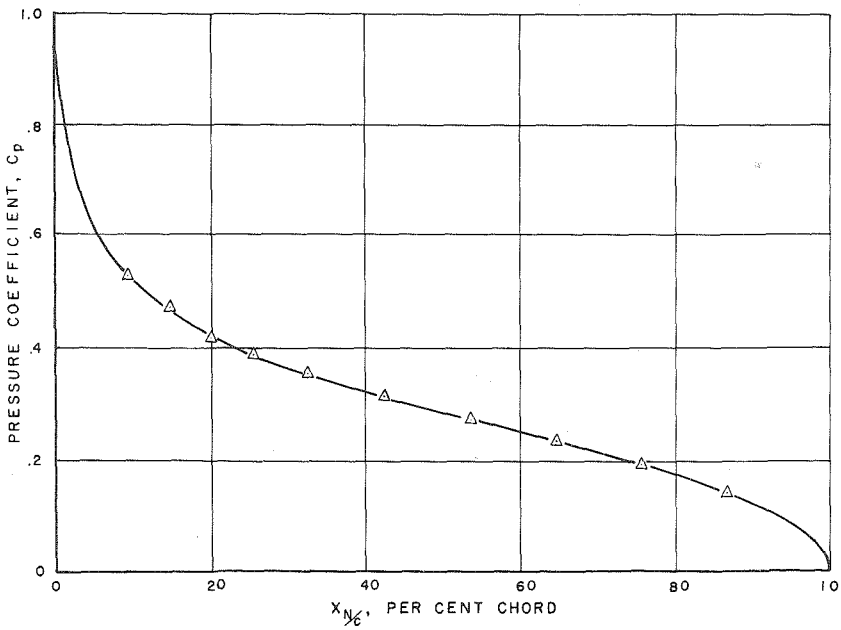

(b) s/c = 0.83, $\alpha = 10^{\circ}$, K = 0.123, $C_f = 0.313$

Fig. 14 - Plots of Pressure Distributions on a Fully Cavitating Flat Plate Hydrofoil at Various Submergences, Cavitation Numbers, and Angles of Attack.

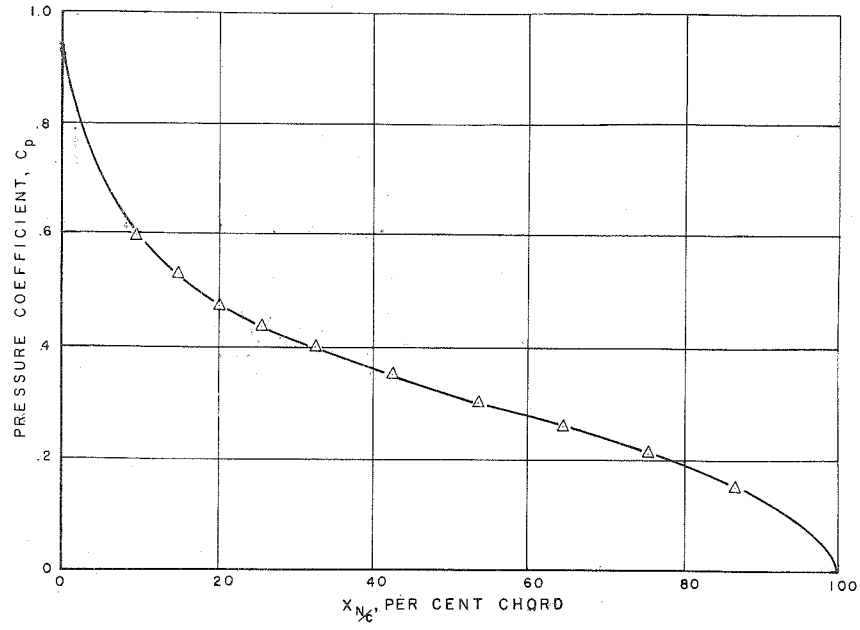

(a) s/c = 0.83, $\alpha = 12^{\circ}$, K = 0.118, $C_f = 0.346$

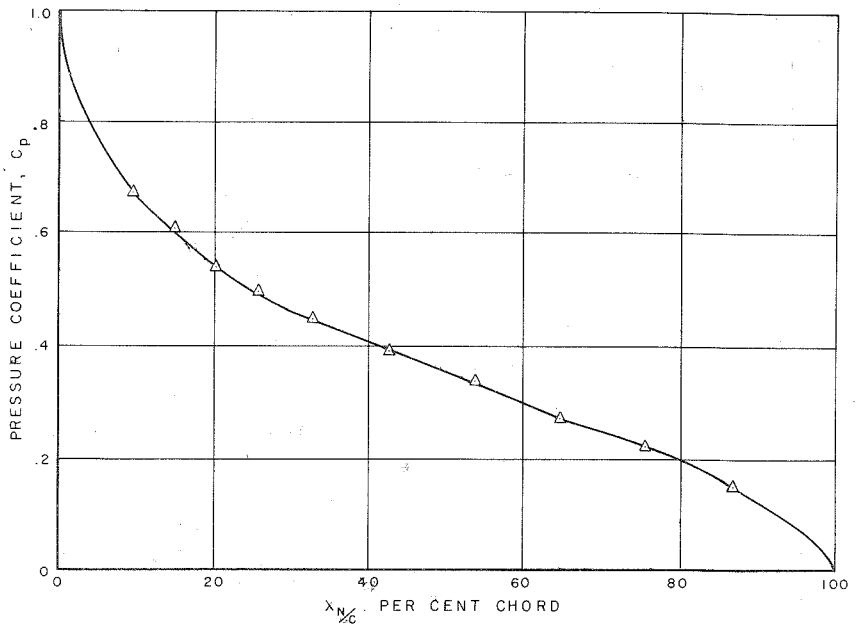

(b) s/c = 0.83, $\alpha = 16^{\circ}$, K = 0.079, $C_f = 0.380$

Fig. 15 - Plots of Pressure Distributions on a Fully Cavitating Flat Plate Hydrofoil at Various Submergences, Cavitation Numbers, and Angles of Attack.

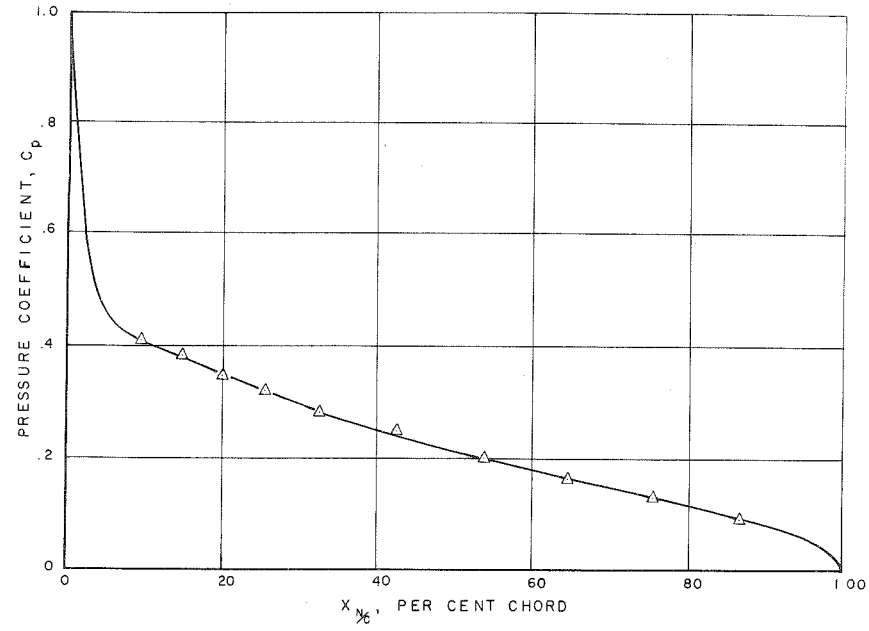

(a) $s/c = -0.06$, $\alpha = 8^{\circ}$, $K = -0.018$, $C_f = 0.217$

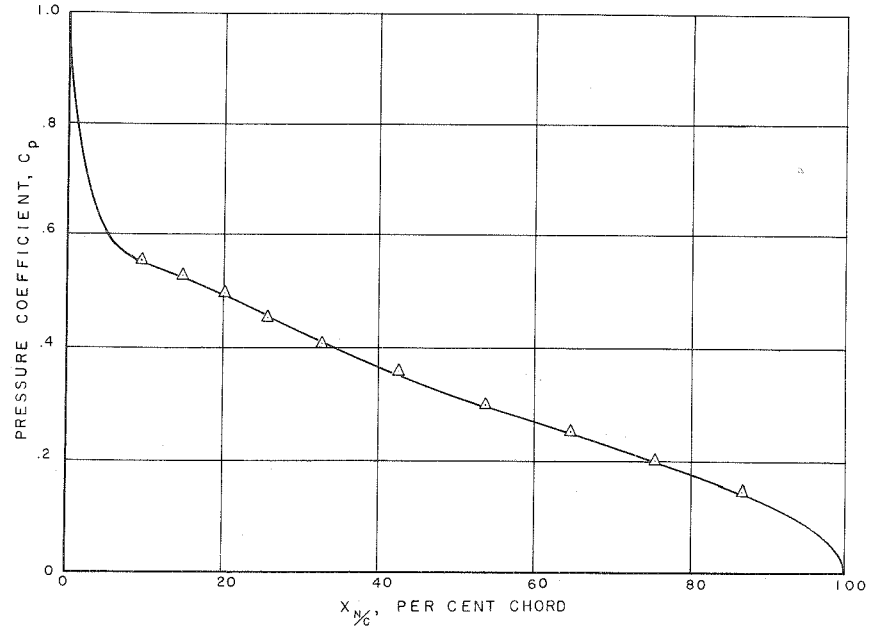

(b) $s/c = -0.06$, $\alpha = 12^{\circ}$, $K = -0.021$, $C_f = 0.339$

Fig. 16 - Plots of Pressure Distributions on a Fully Cavitating Flat Plate Hydrofoil at Various Submergences, Cavitation Numbers, and Angles of Attack.

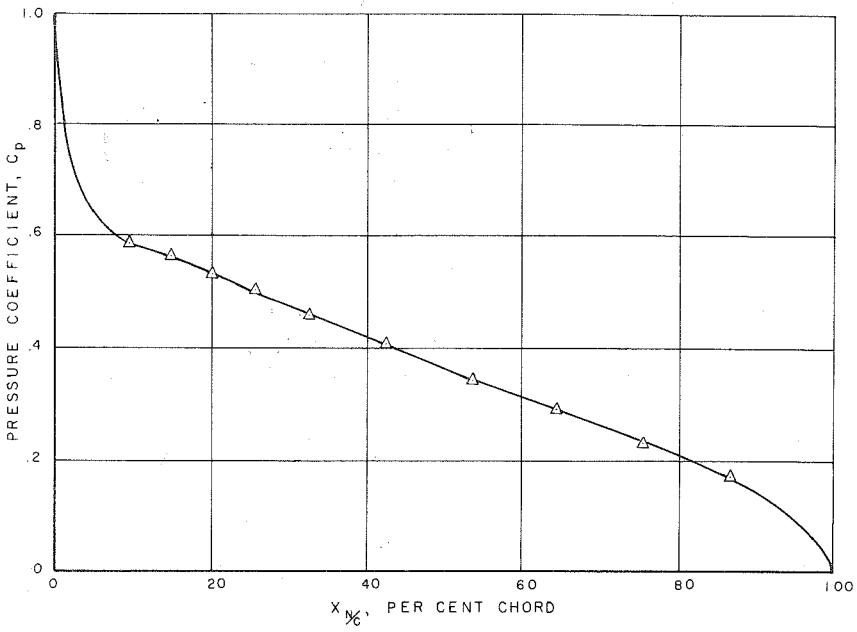

(a) $s/c = -0.06$, $\alpha = 14^{\circ}$, $K = -0.024$, $C_f = 0.377$

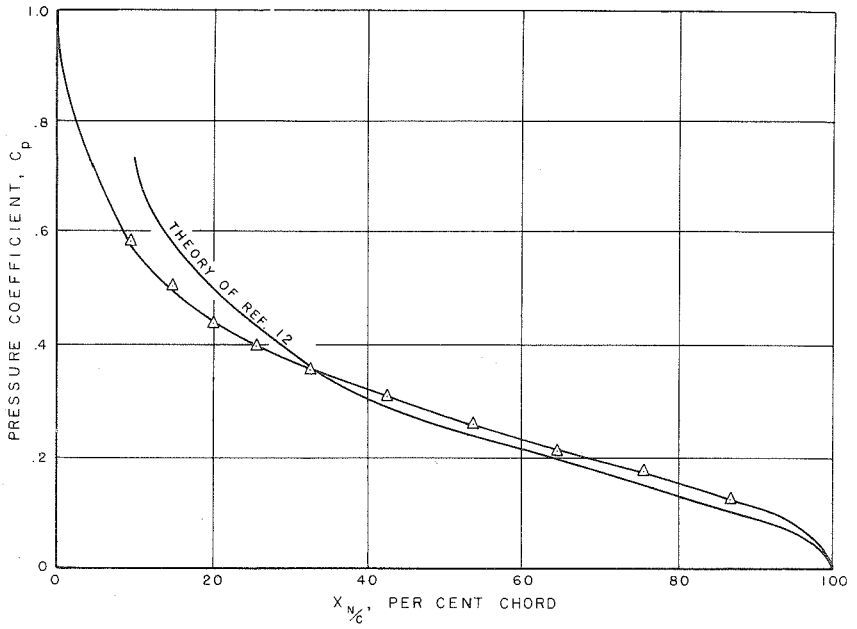

(b) $s/c = 0.09$, $\alpha = 10^{\circ}$, $K = -0.001$, $C_f = 0.312$

Fig. 17 - Plots of Pressure Distributions on a Fully Cavitating Flat Plate Hydrofoil at Various Submergences, Cavitation Numbers, and Angles of Attack.

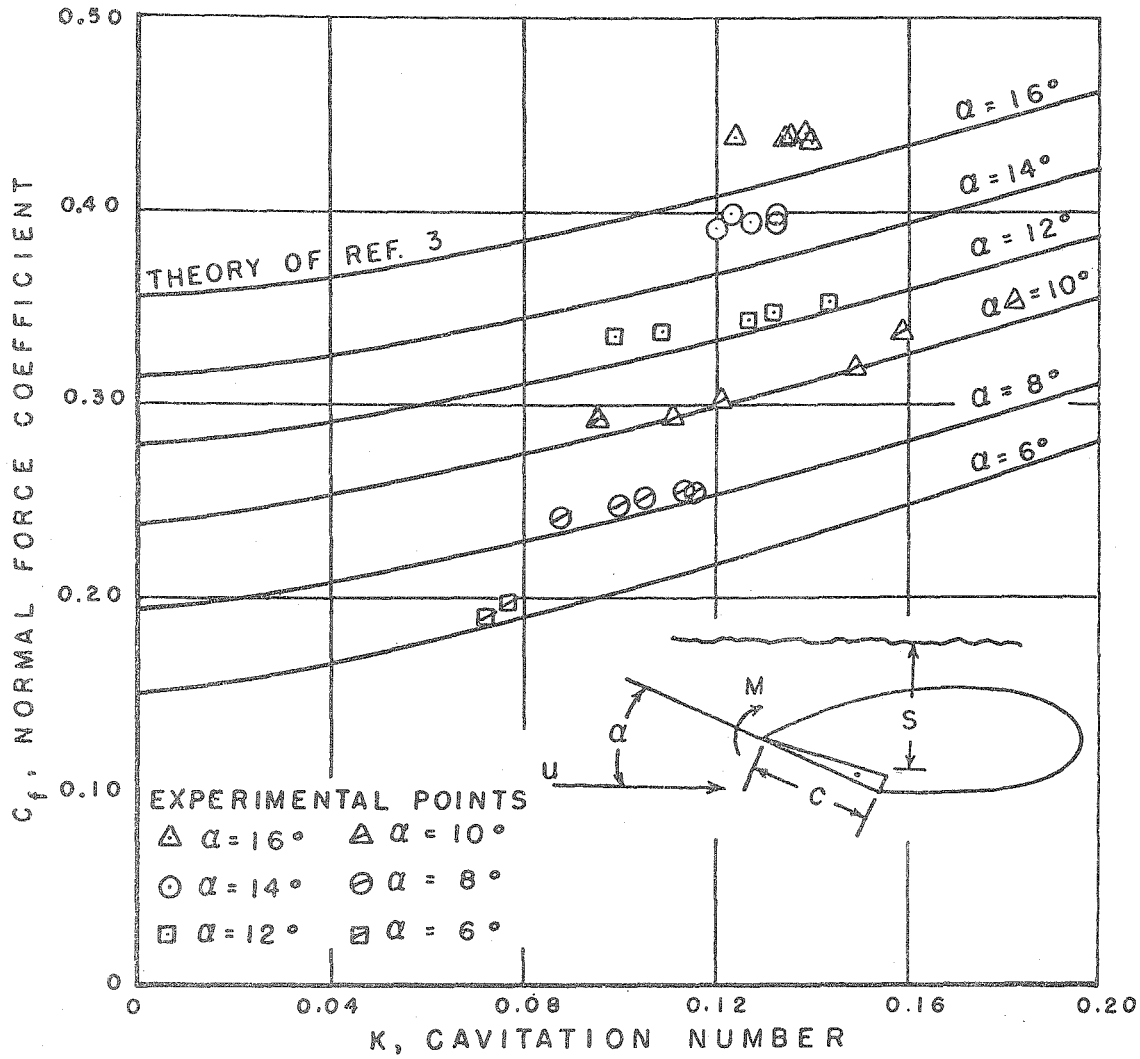

Fig. 18 - The Experimental Normal Force Coefficient versus Cavitation Number, at Six Angles of Attack and s/c = 2.16 as Compared to Wu's Exact Infinite Fluid Theory.

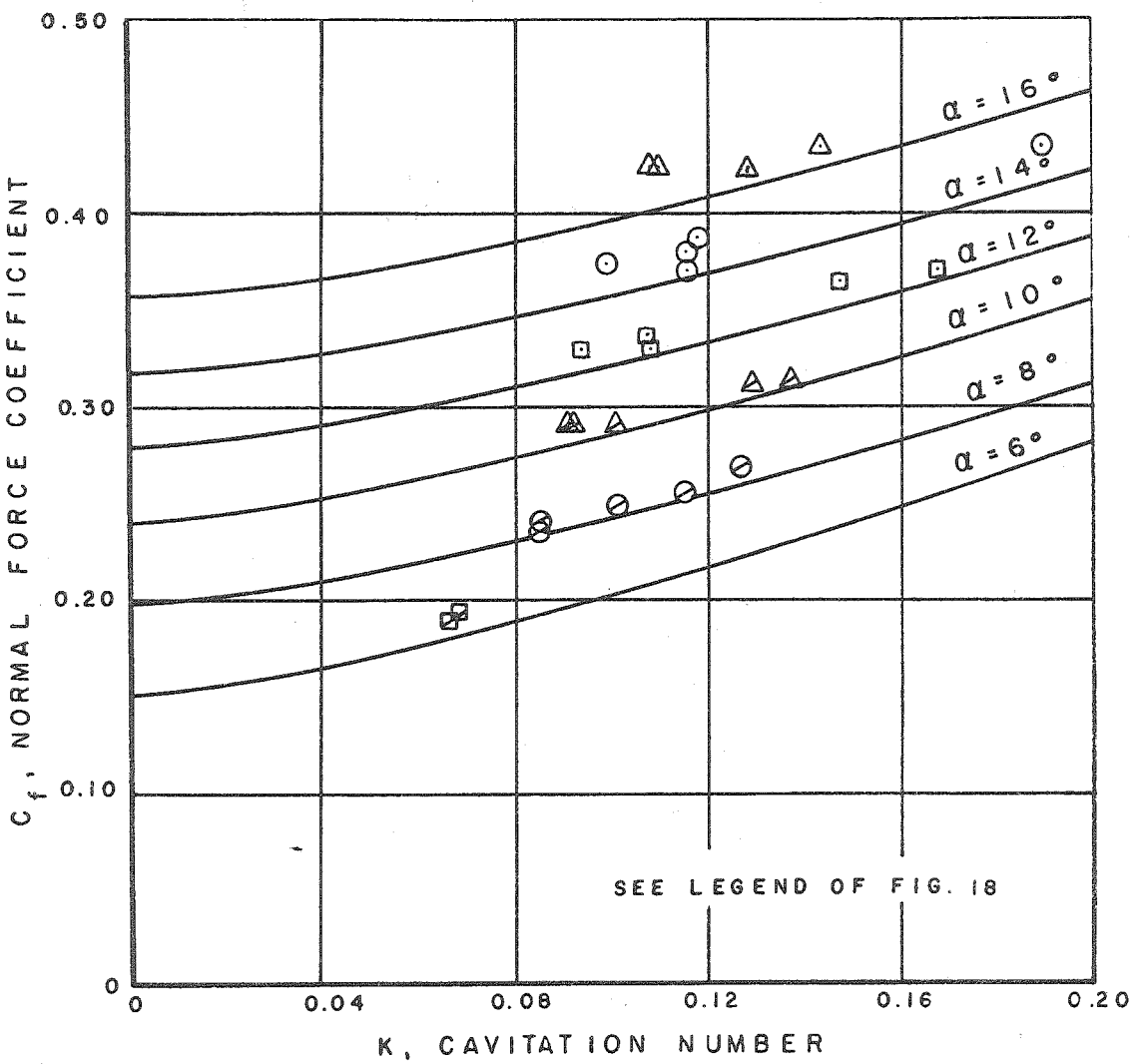

Fig. 19 - The Experimental Normal Force Coefficient versus Cavitation Number, at Six Angles of Attack and s/c = 1.50, as Compared to Wu's Exact Infinite Fluid Theory.

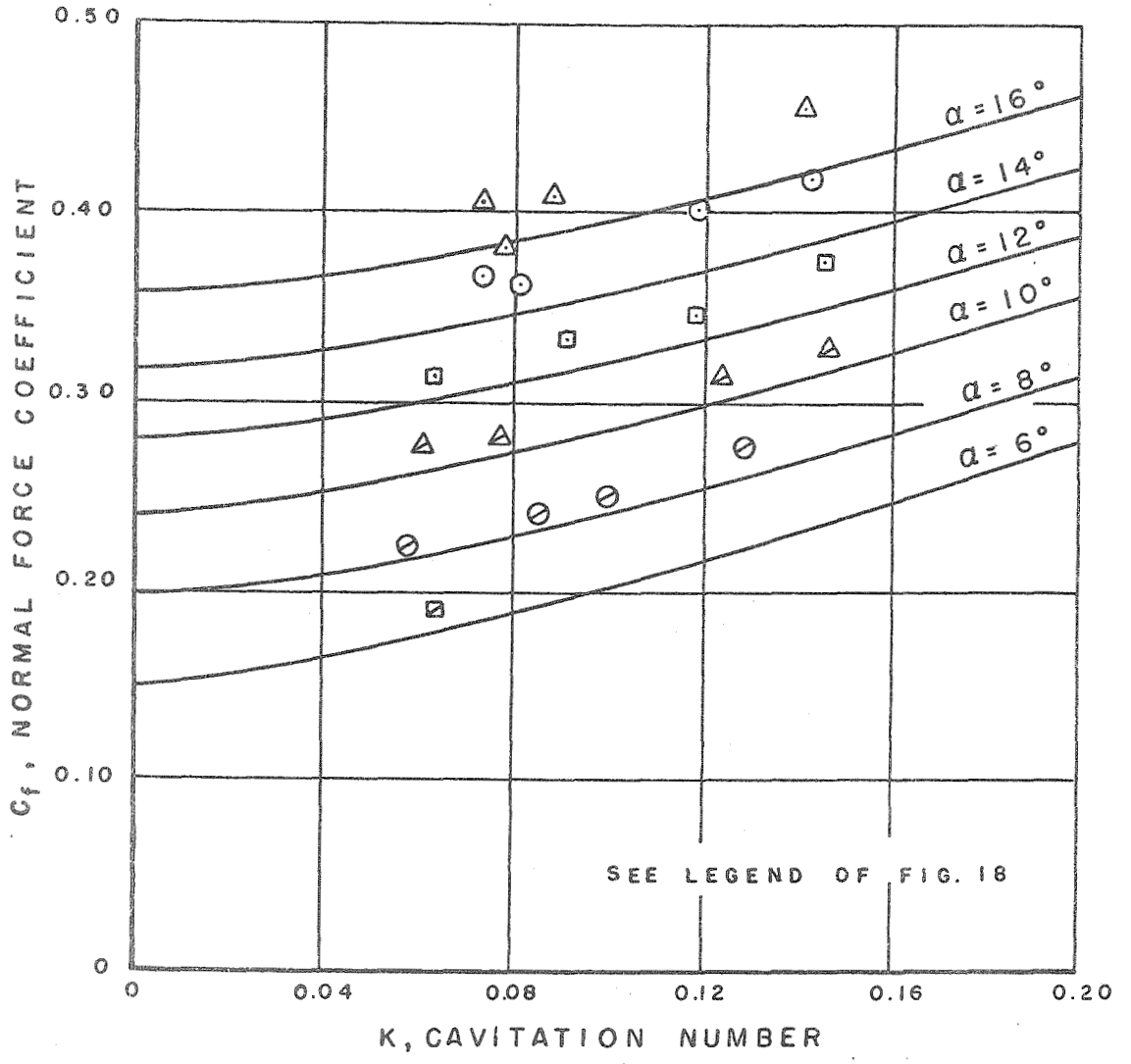

Fig. 20 - The Experimental Normal Force Coefficient versus Cavitation Number, at Six Angles of Attack and s/c = 0.83, as Compared to Wu's Exact Infinite Fluid Theory.

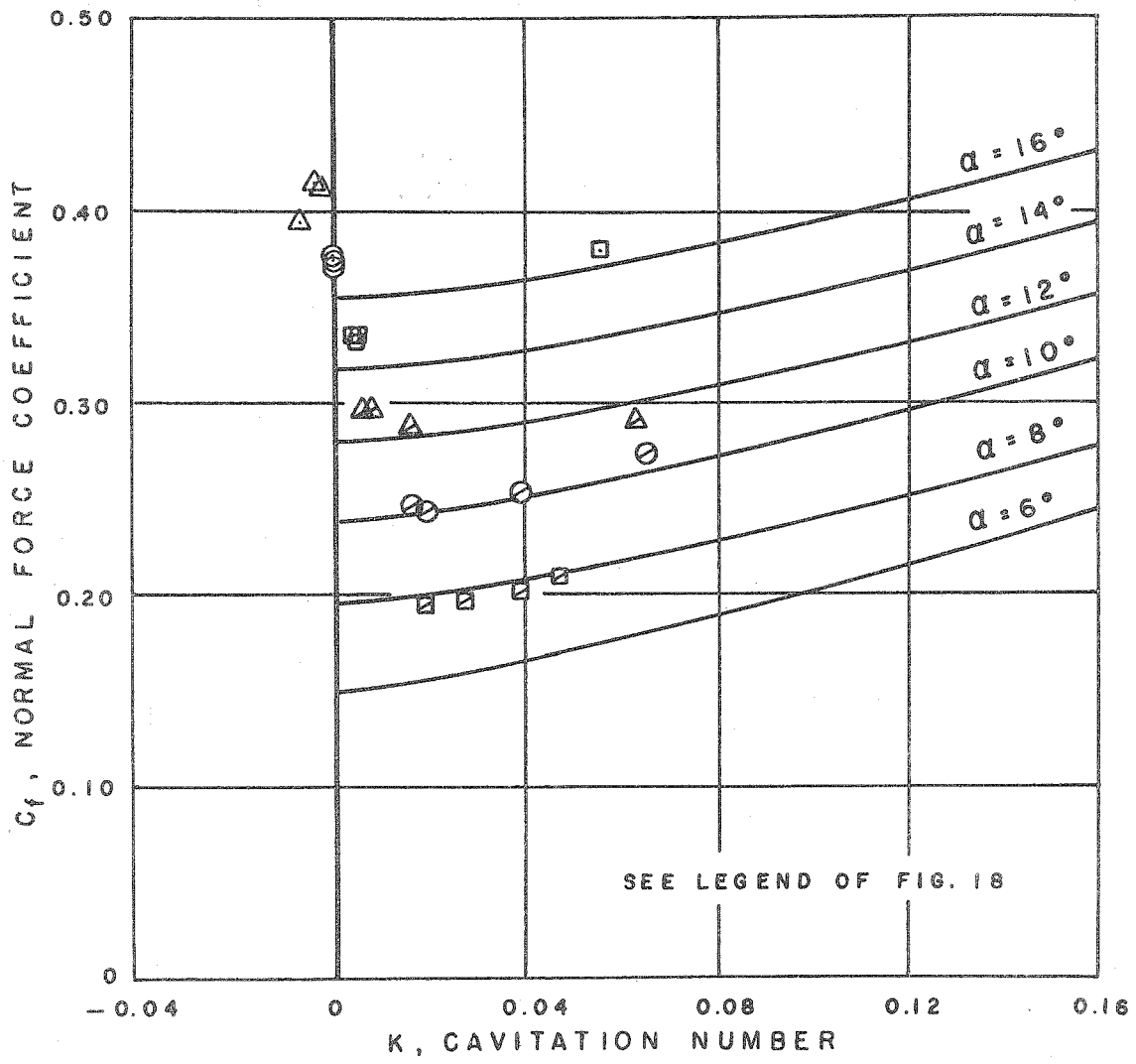

Fig. 21 - The Experimental Normal Force Coefficient versus Cavitation Number, at Six Angles of Attack and s/c = 0.16, as Compared to Wu's Exact Infinite Fluid Theory.

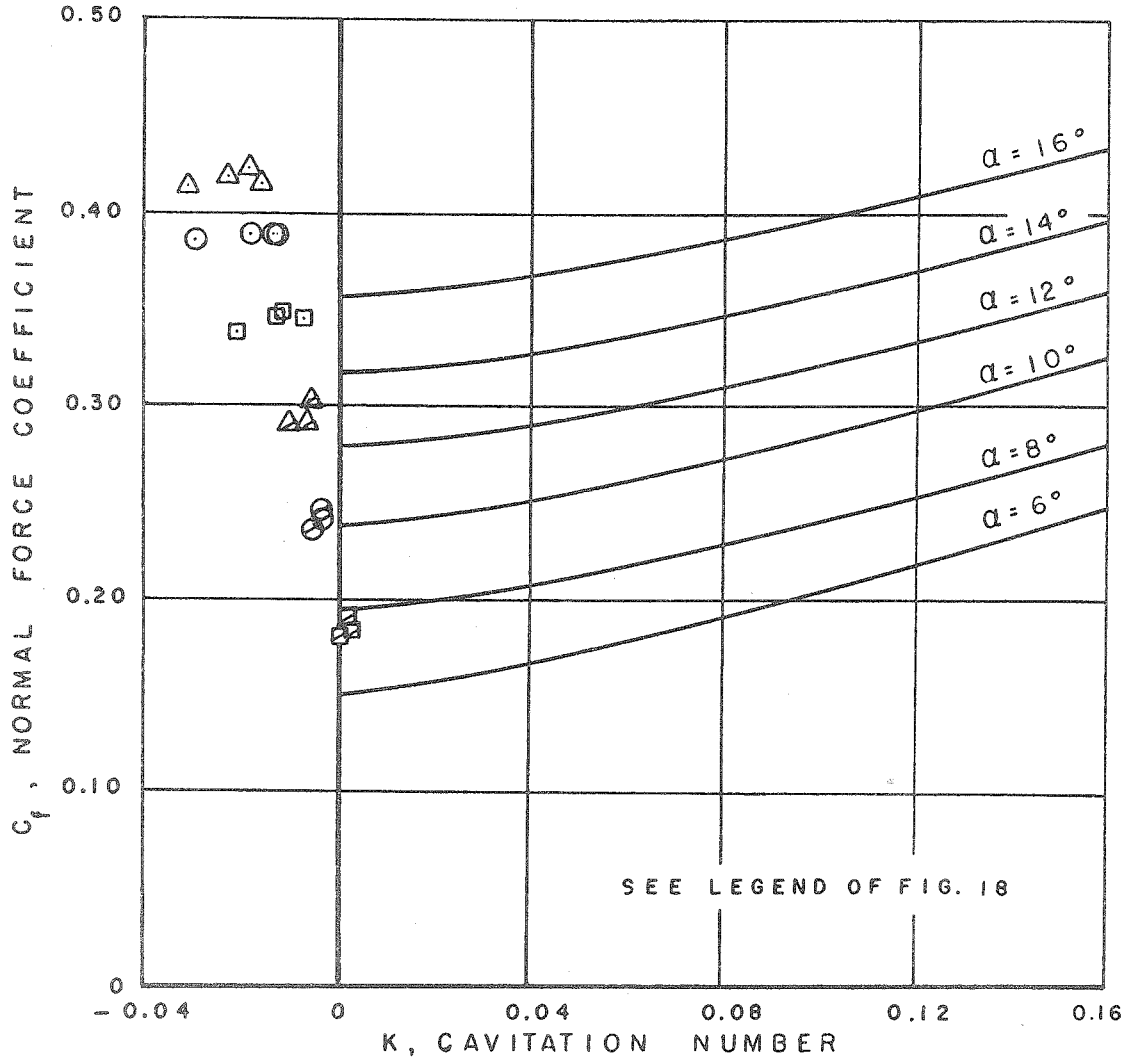

Fig. 22 - The Experimental Normal Force Coefficient versus Cavitation Number, at Six Angles of Attack and s/c = 0.05, as Compared to Wu's Exact Infinite Fluid Theory.

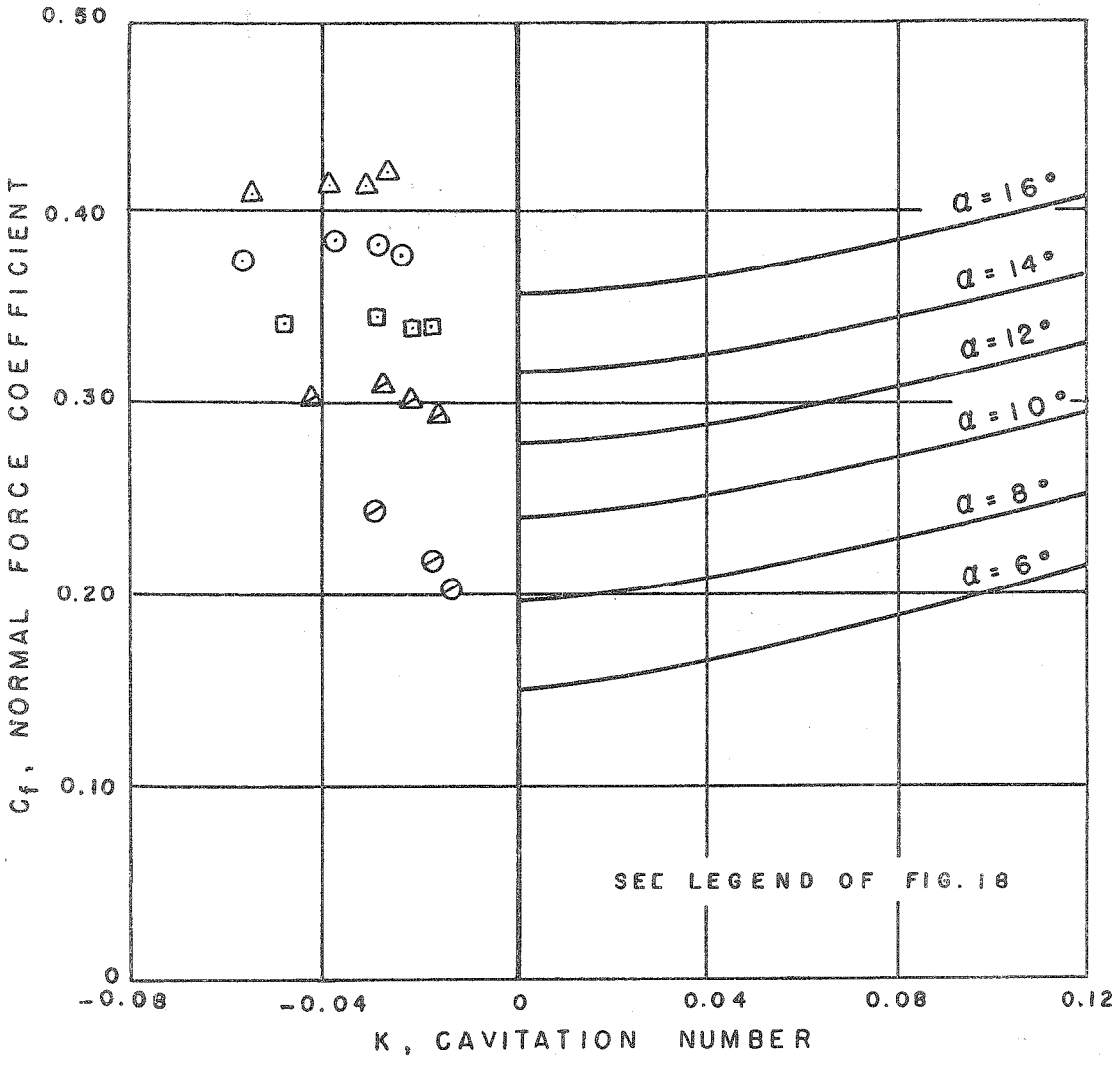

Fig. 23 - The Experimental Normal Force Coefficient versus Cavitation Number, at Six Angles of Attack and s/c = -0.06, as Compared to Wu's Exact Infinite Fluid Theory.

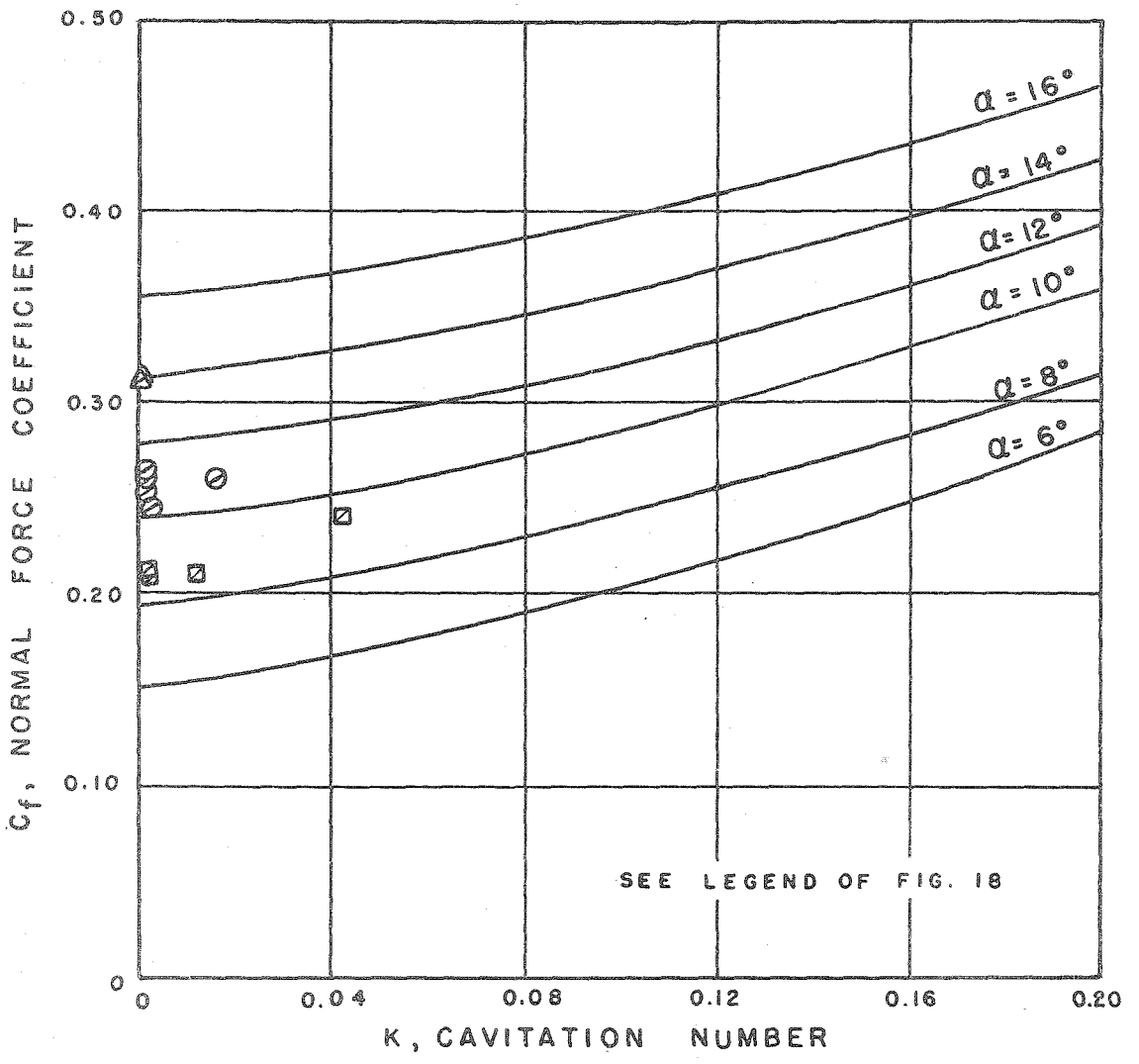

Fig. 24 - The Experimental Normal Force Coefficient versus Cavitation Number, at Three Angles of Attack and s/c = 0.09, as Compared to Wu's Exact Infinite Fluid Theory. Skimmer Unplugged.

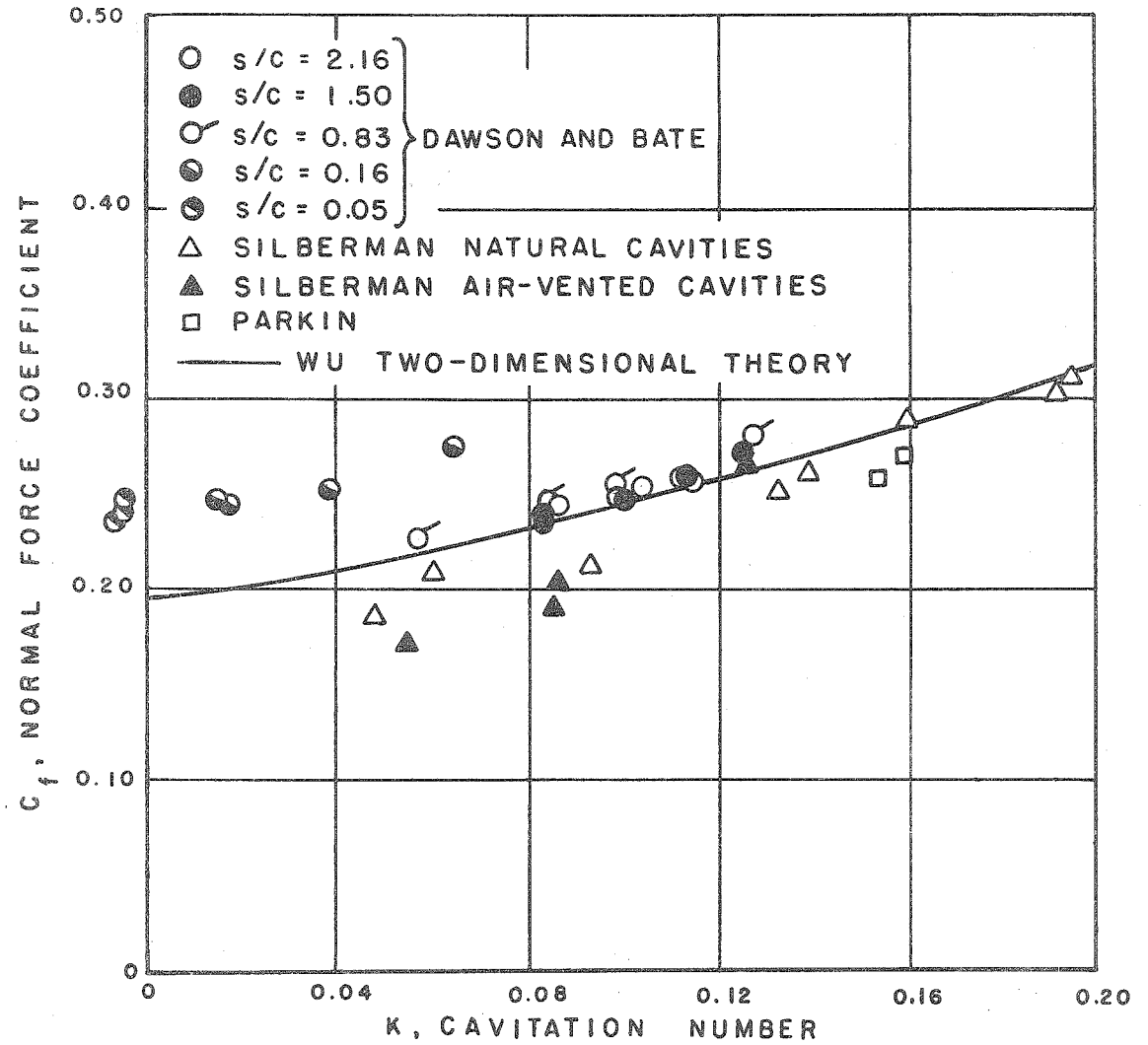

Fig. 25 - Comparison of Normal Force Coefficient with Silberman and Parkin for $\alpha = 8^{o}$.

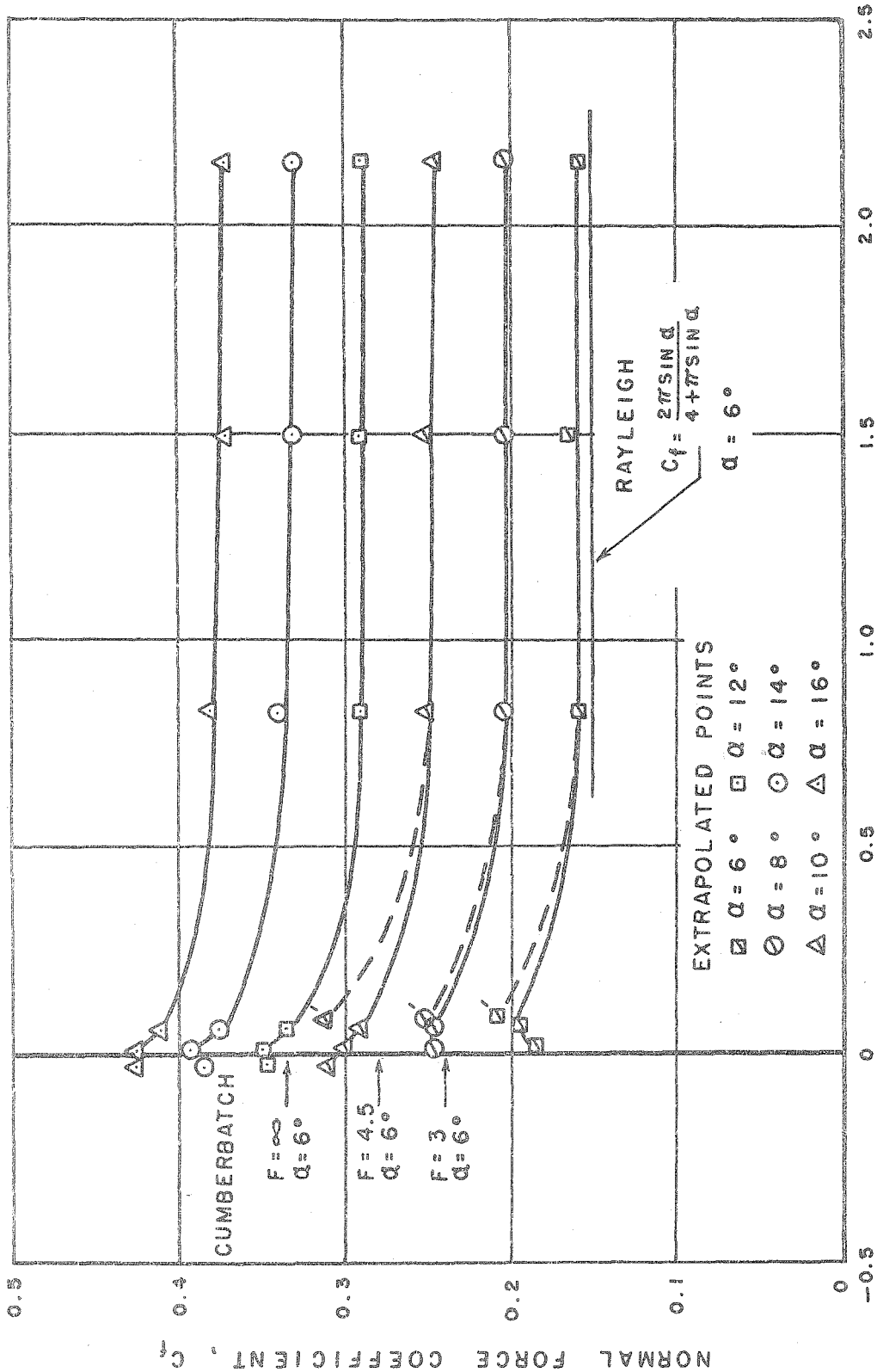

Fig. 26 - The Effect of Submergence on the Experimental Normal Force Coefficients at K = 0, Showing the Results Obtained by Rayleigh at Deep Submergences, and the Values at the Surface from the Theory of Cumberbatch for Three Froude Numbers. (The primed points are those obtained with the skimmer operating).

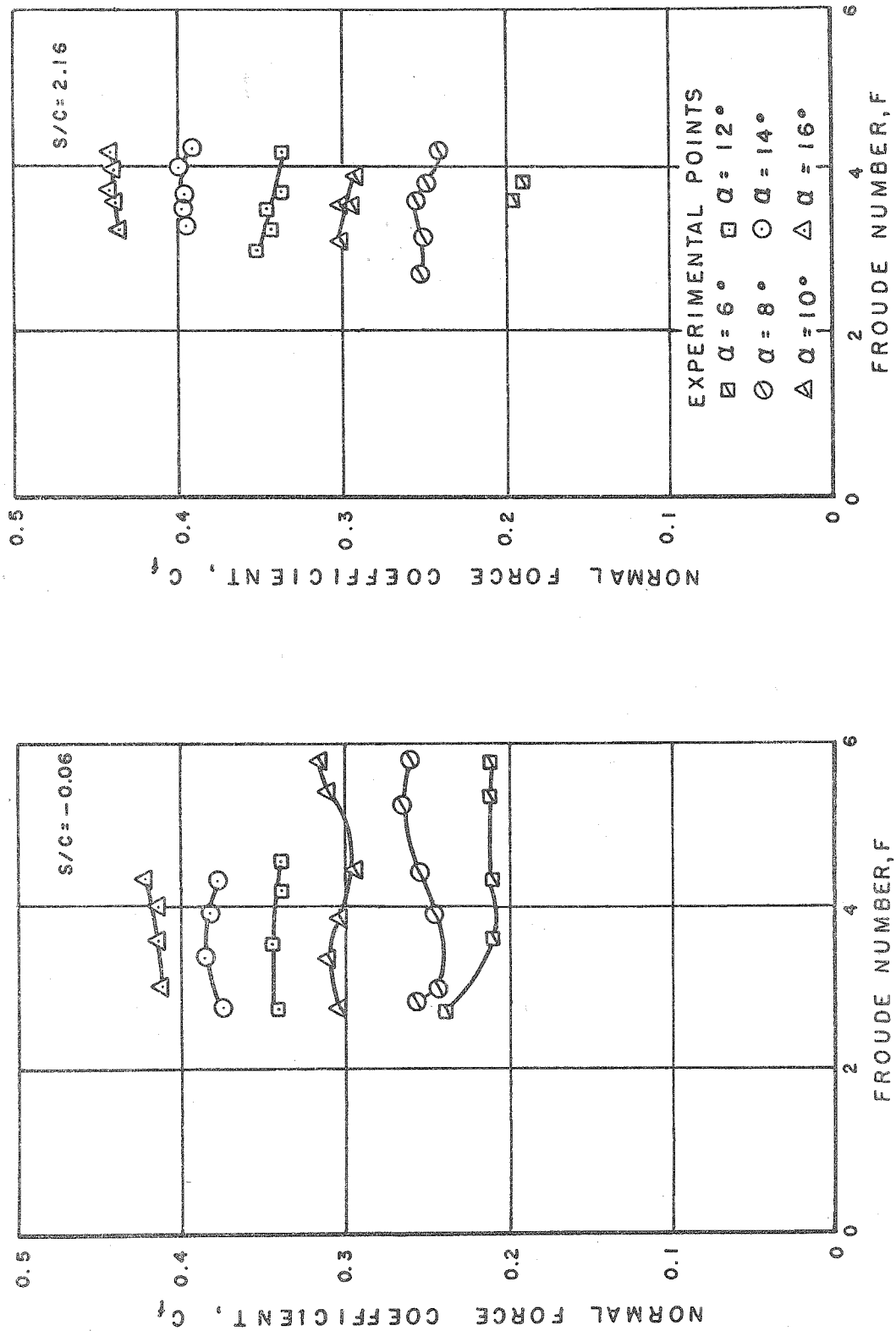

Fig. 27 - The Effect of Froude Number on the Normal Force Coefficient at Six Angles of Attack and Two Submergence Ratios.

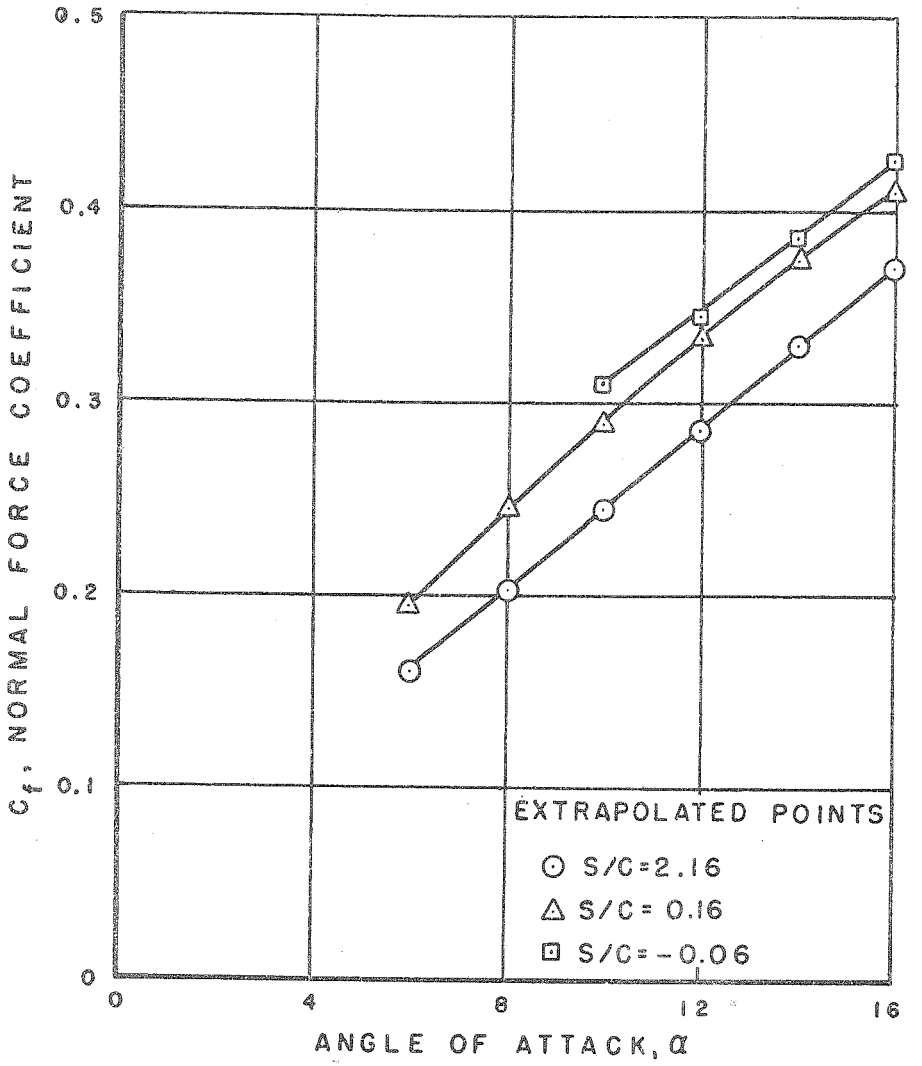

Fig. 28a - The Effect of Angle of Attack on the Normal Force Coefficient at K = 0 and Three Submergence Ratios.

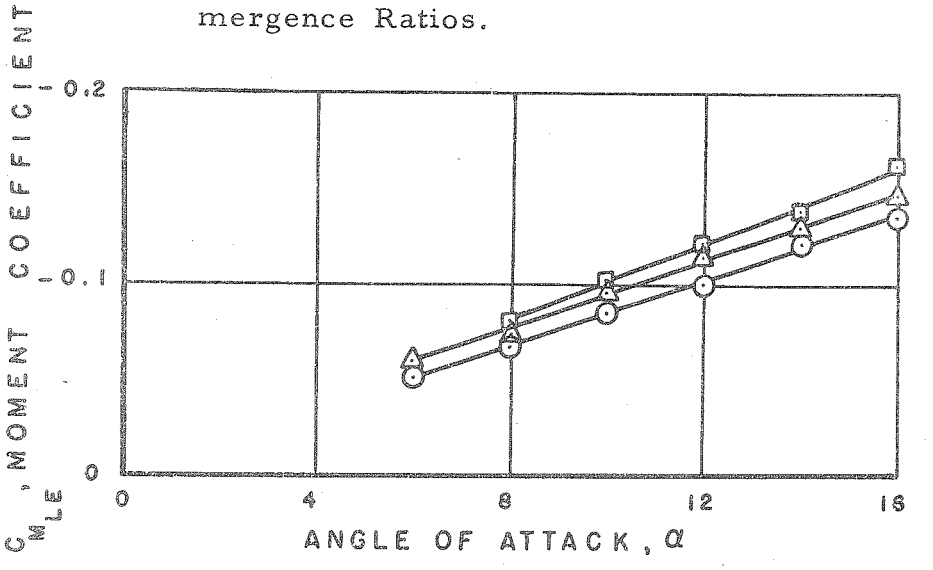

Fig. 28b - The Effect of Angle of Attack on the Moment Coefficient at K = 0 and Three Submergence Ratios.

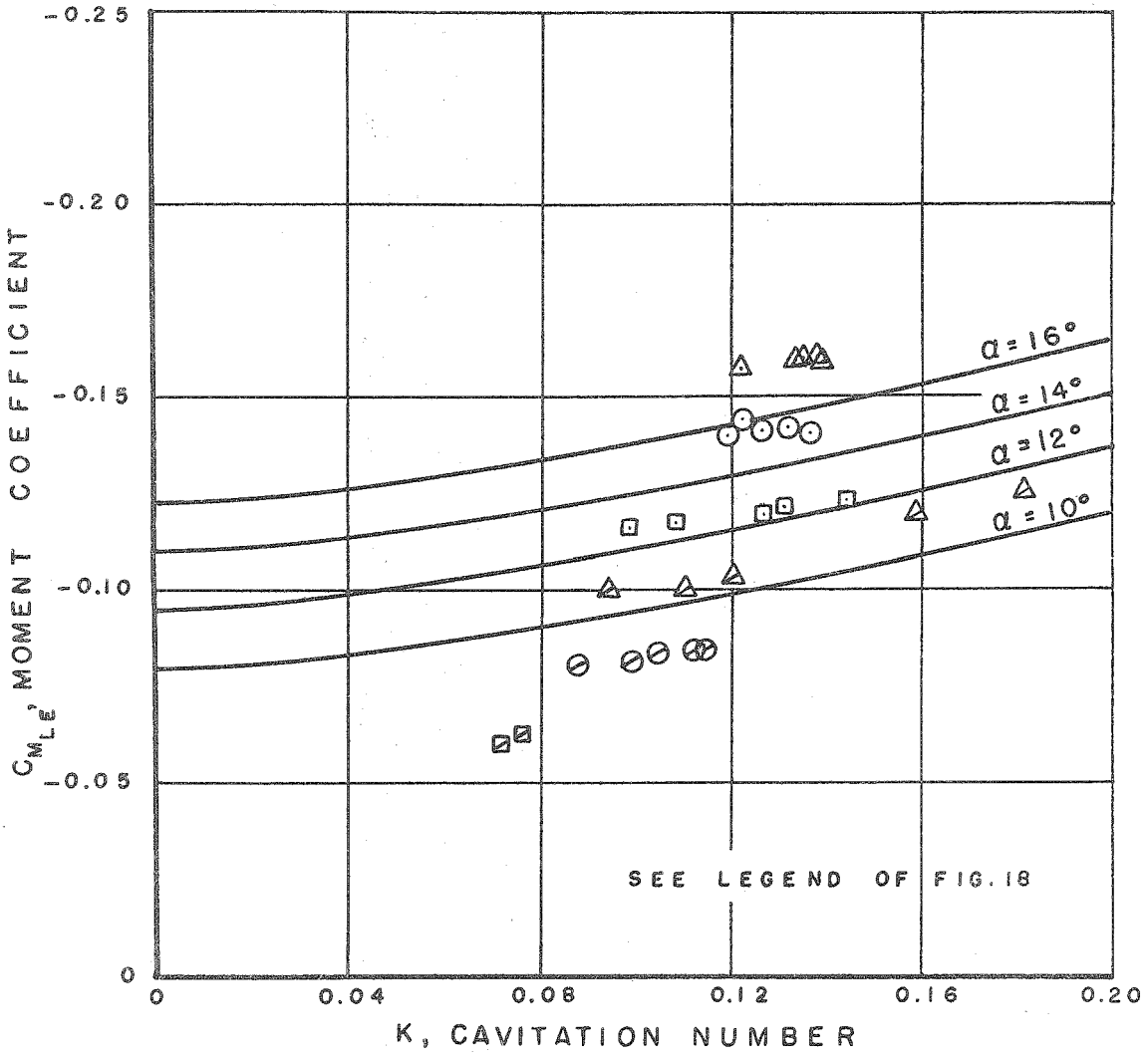

Fig. 29 - The Experimental Moment Coefficient about the Leading Edge versus Cavitation Number, at Six Angles of Attack and s/c = 2.16, as Compared to Wu's Exact Infinite Fluid Theory.

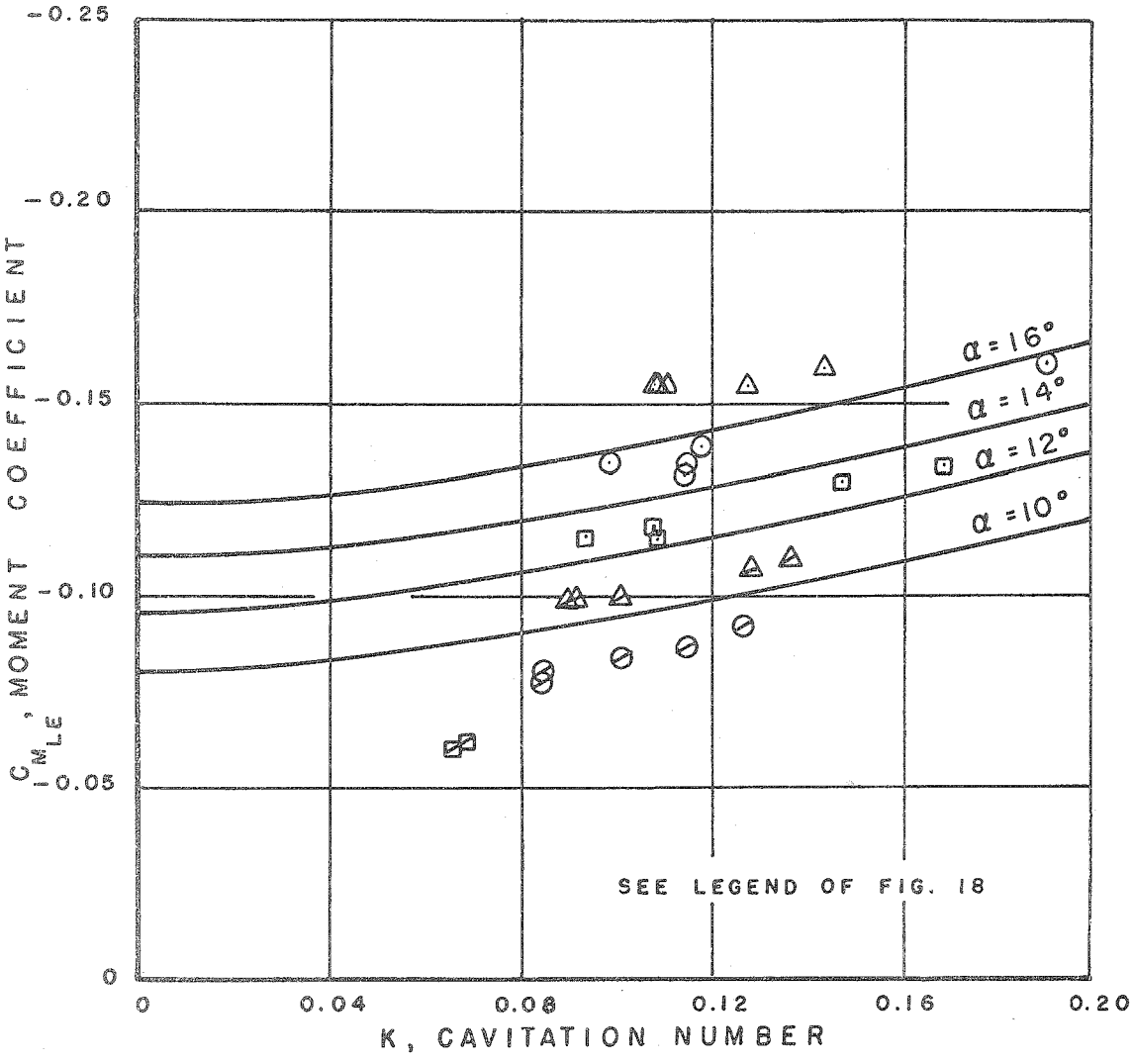

Fig. 30 - The Experimental Moment Coefficient about the Leading Edge versus Cavitation Number, at Six Angles of Attack and s/c = 1.50, as Compared to Wu's Exact Infinite Fluid Theory.

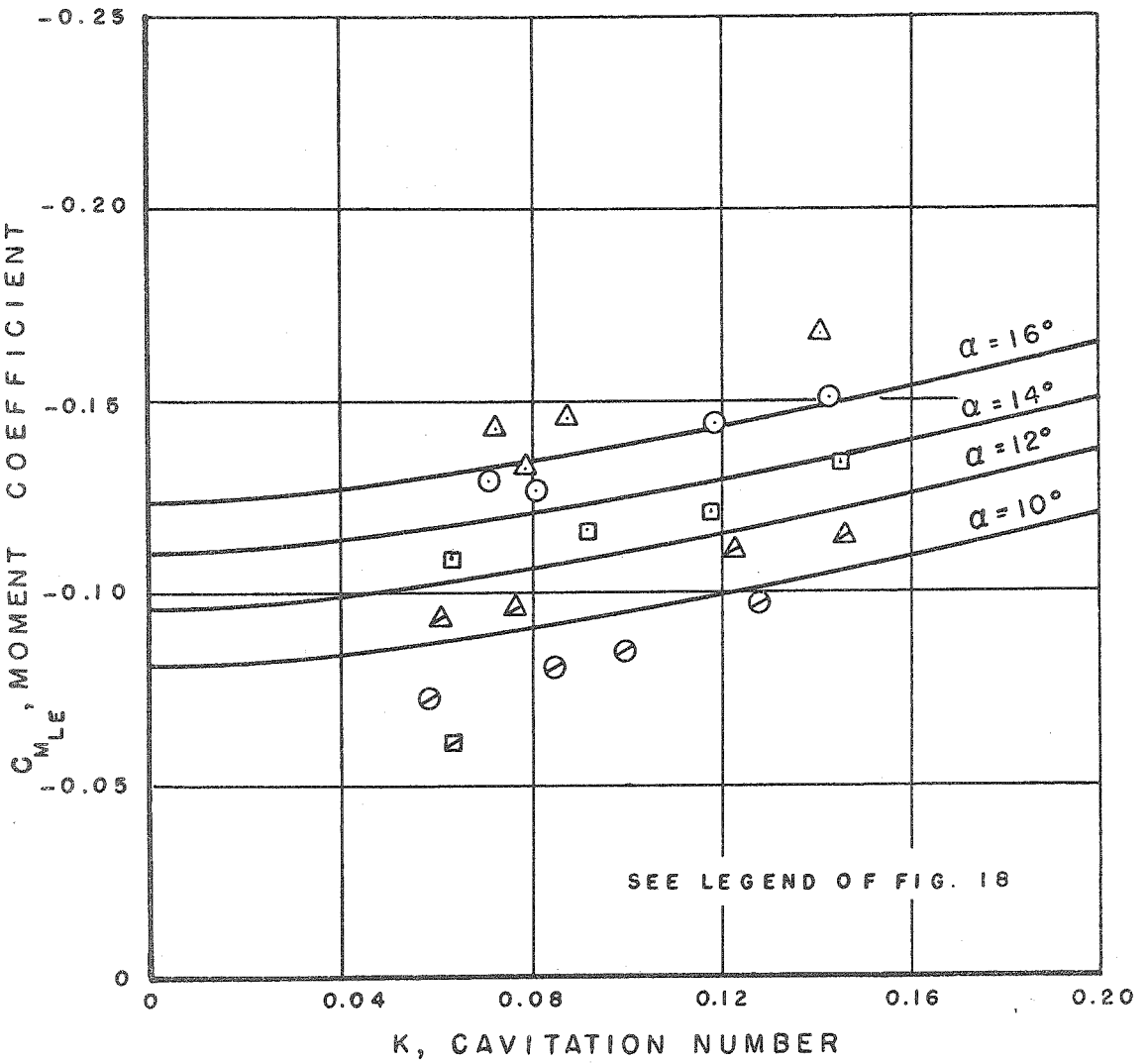

Fig. 31 - The Experimental Moment Coefficient about the Leading Edge versus Cavitation Number, at Six Angles of Attack and s/c = 0.83, as Compared to Wu's Exact Infinite Fluid Theory.

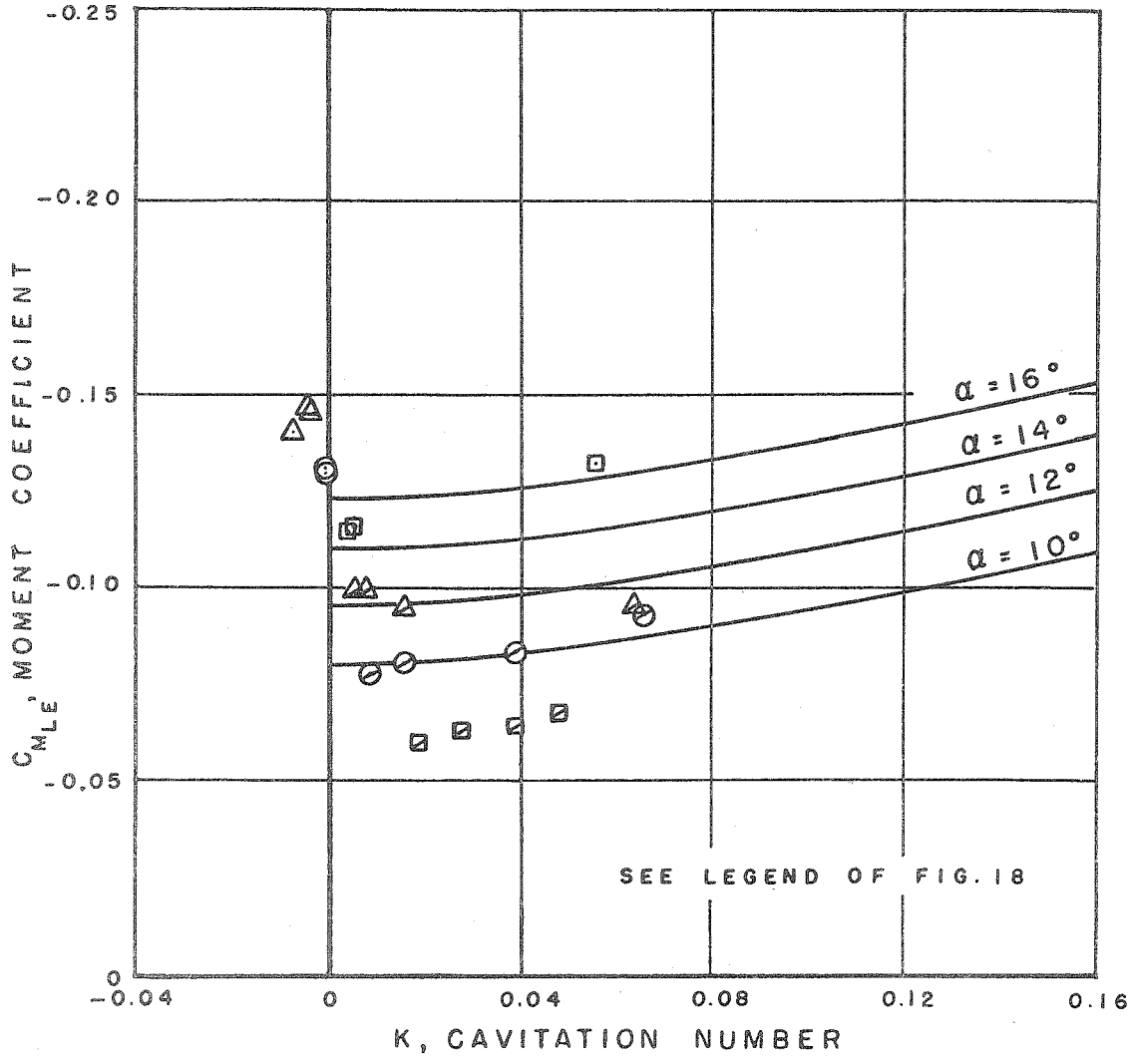

Fig. 32 - The Experimental Moment Coefficient about the Leading Edge versus Cavitation Number, at Six Angles of Attack and s/c = 0.16, as Compared to Wu's Exact Infinite Fluid Theory.

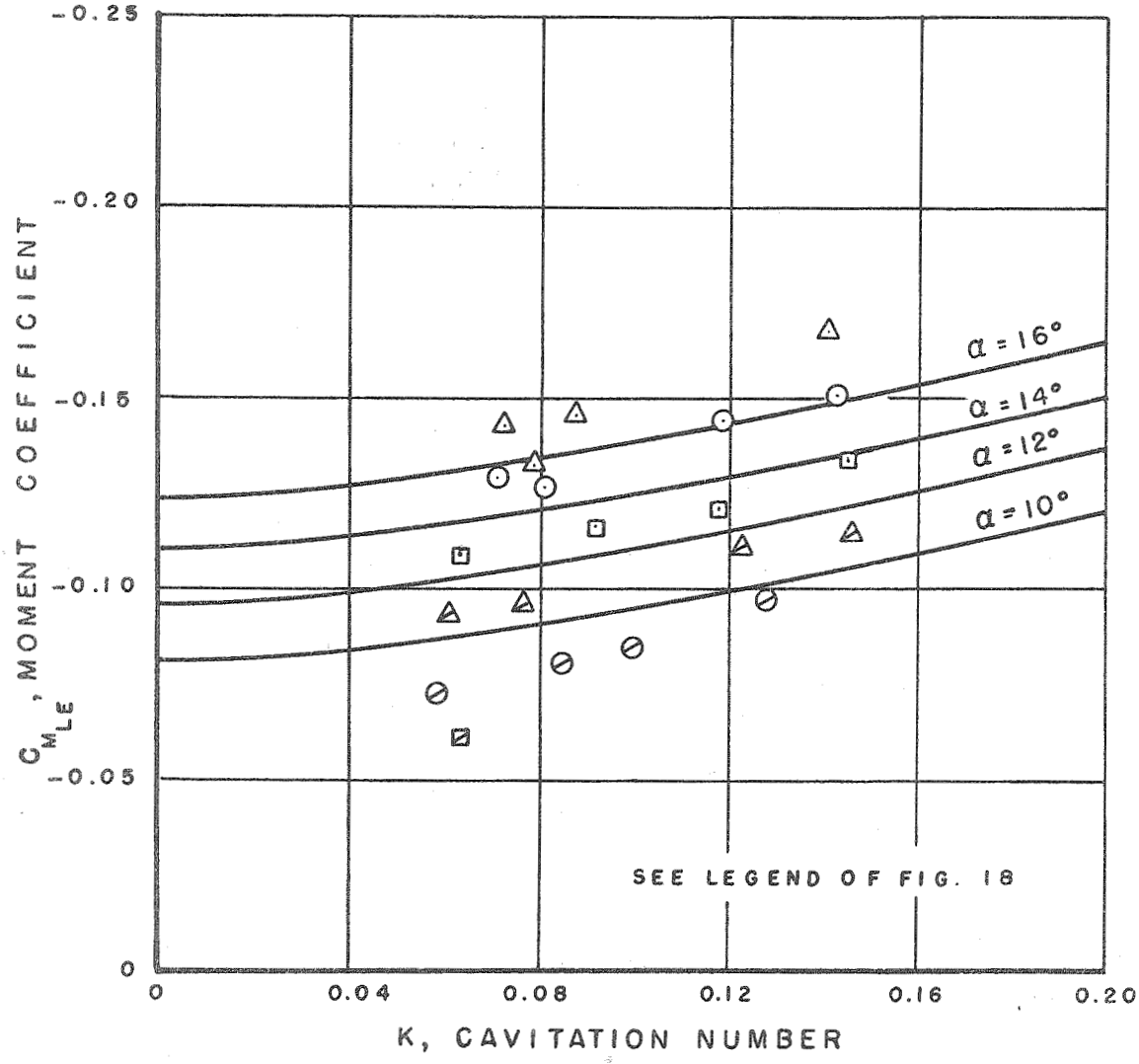

Fig. 31 - The Experimental Moment Coefficient about the Leading Edge versus Cavitation Number, at Six Angles of Attack and s/c = 0.83, as Compared to Wu's Exact Infinite Fluid Theory.

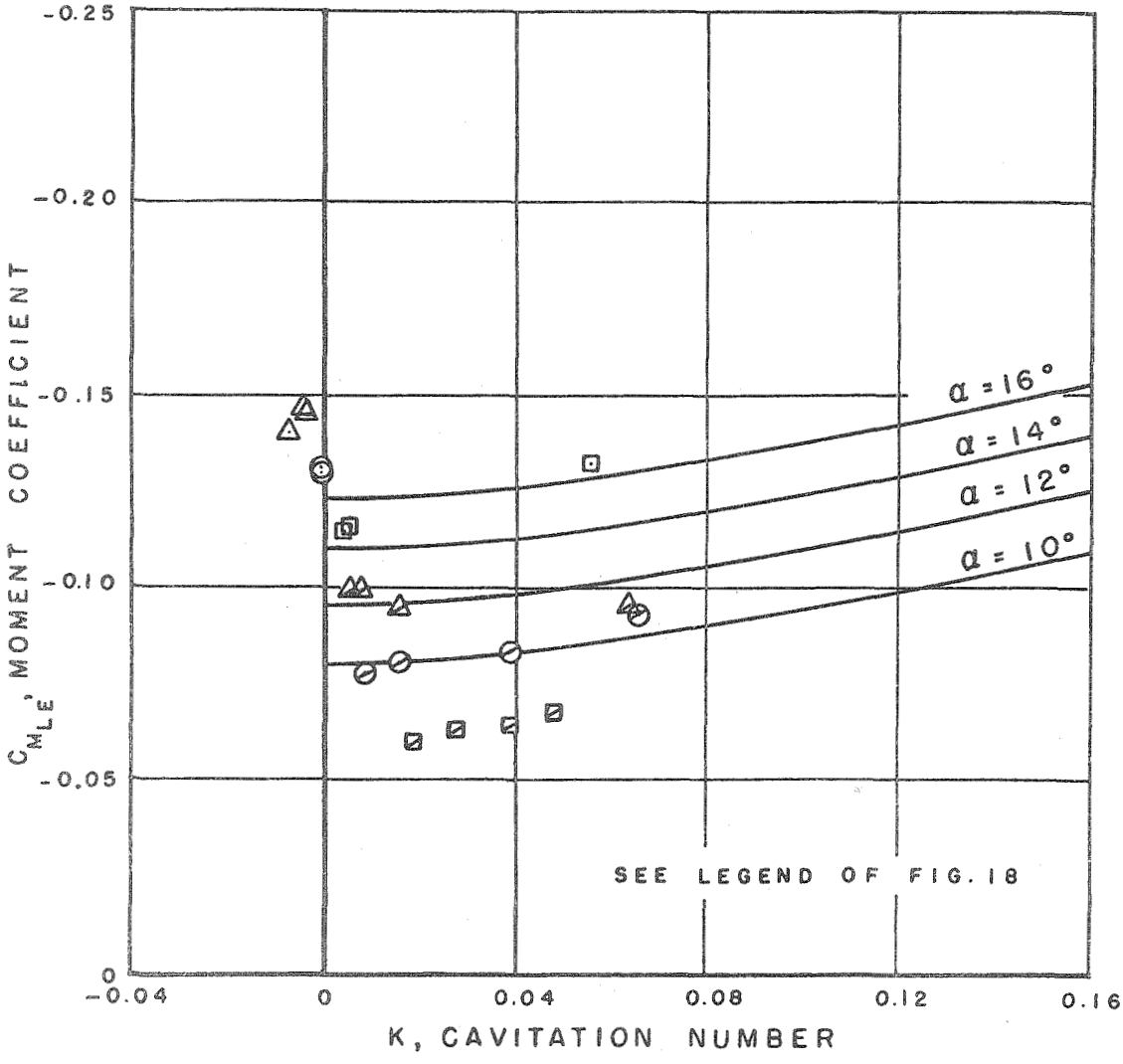

Fig. 32 - The Experimental Moment Coefficient about the Leading Edge versus Cavitation Number, at Six Angles of Attack and s/c = 0.16, as Compared to Wu's Exact Infinite Fluid Theory.

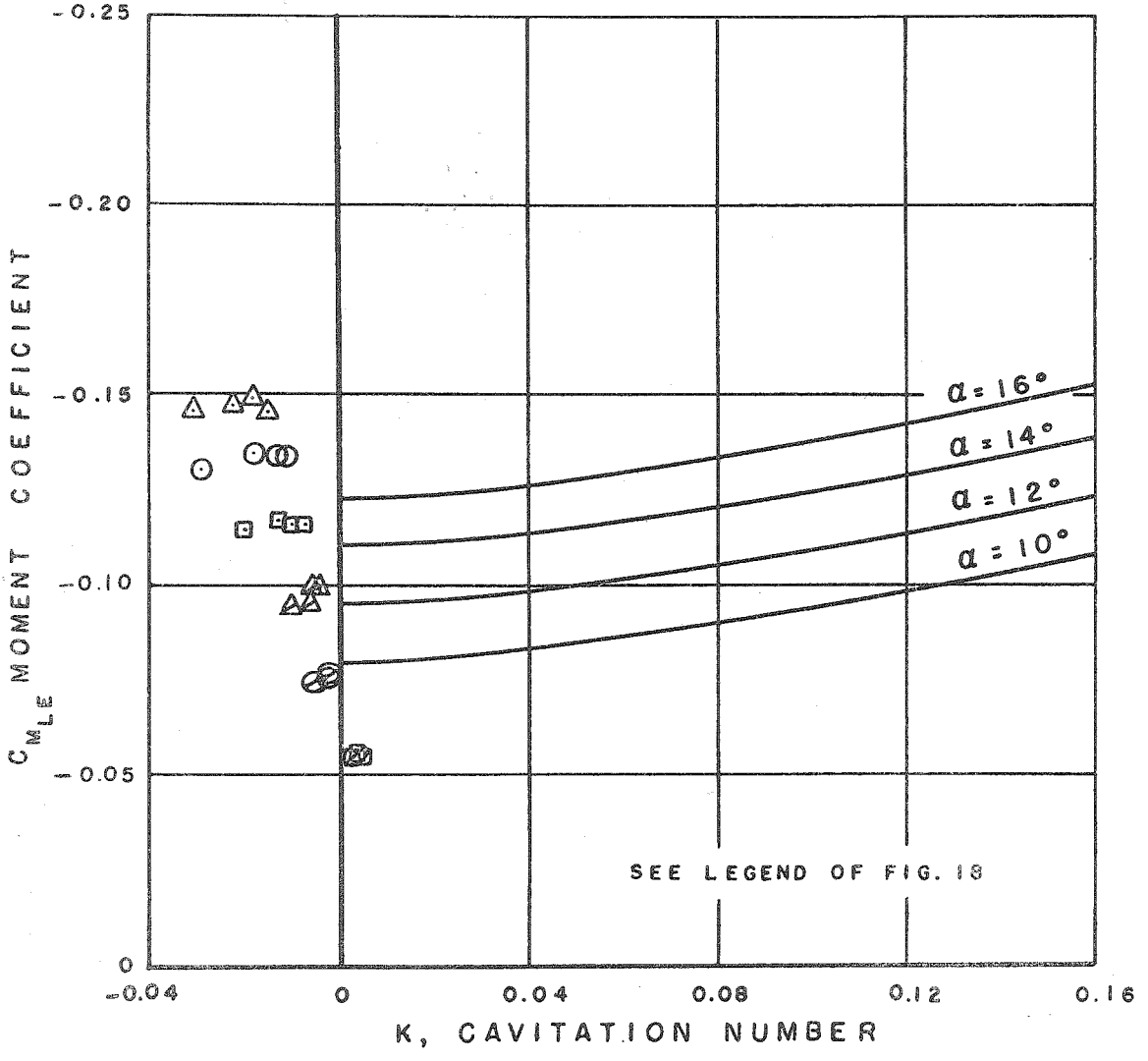

Fig. 33 - The Experimental Moment Coefficient about the Leading Edge versus Cavitation Number at Six Angles of Attack and s/c = 0.05, as Compared to Wu's Exact Infinite Fluid Theory.

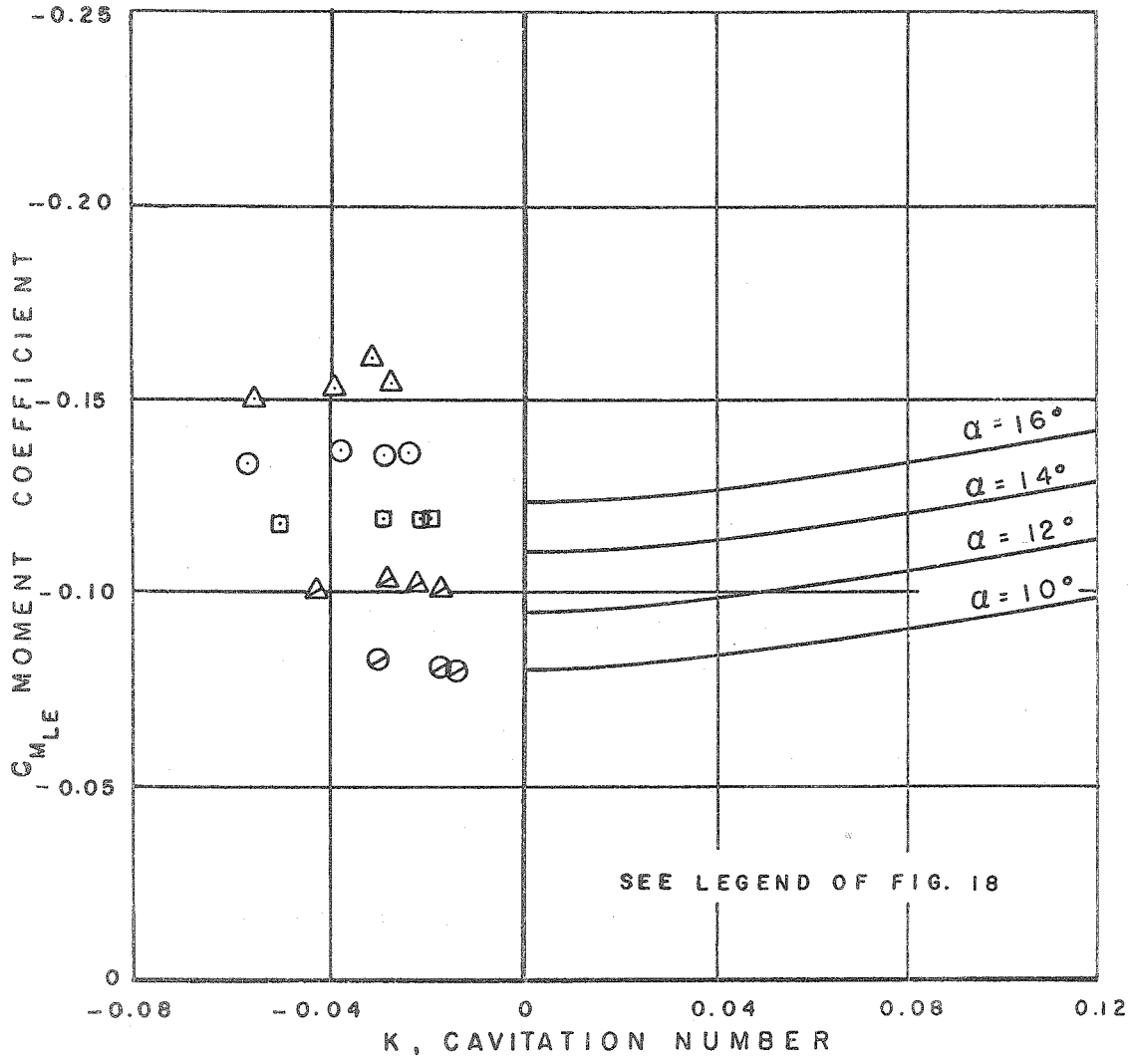

Fig. 34 - The Experimental Moment Coefficient about the Leading Edge versus Cavitation Number, at Six Angles of Attack and s/c = -0.06, as Compared to Wu's Exact Infinite Fluid Theory.

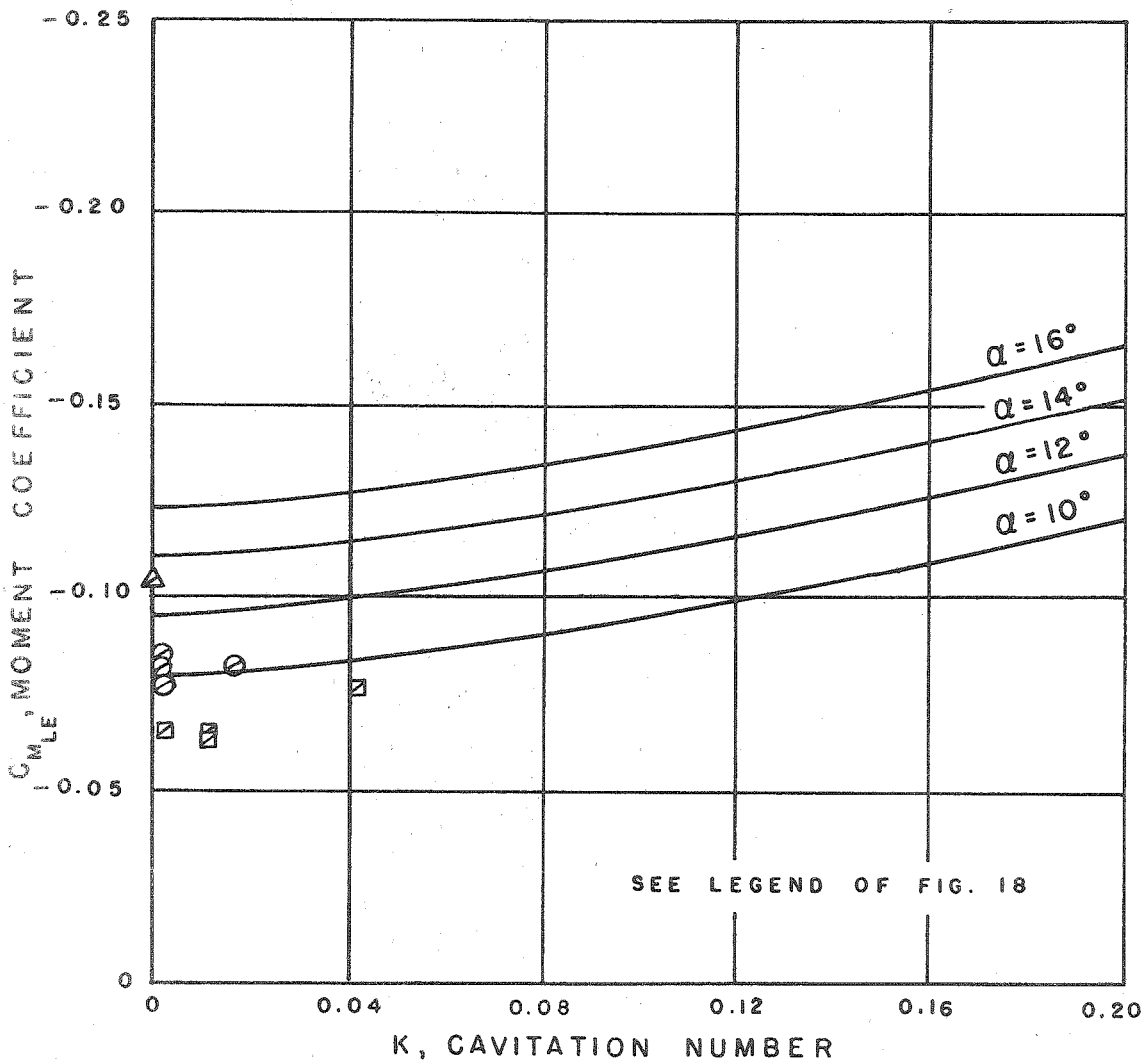

Fig. 35 - The Experimental Moment Coefficient about the Leading Edge at Three Angles of Attack and s/c = 0.09, as Compared to Wu's Exact Infinite Fluid Theory. Skimmer Unplugged.

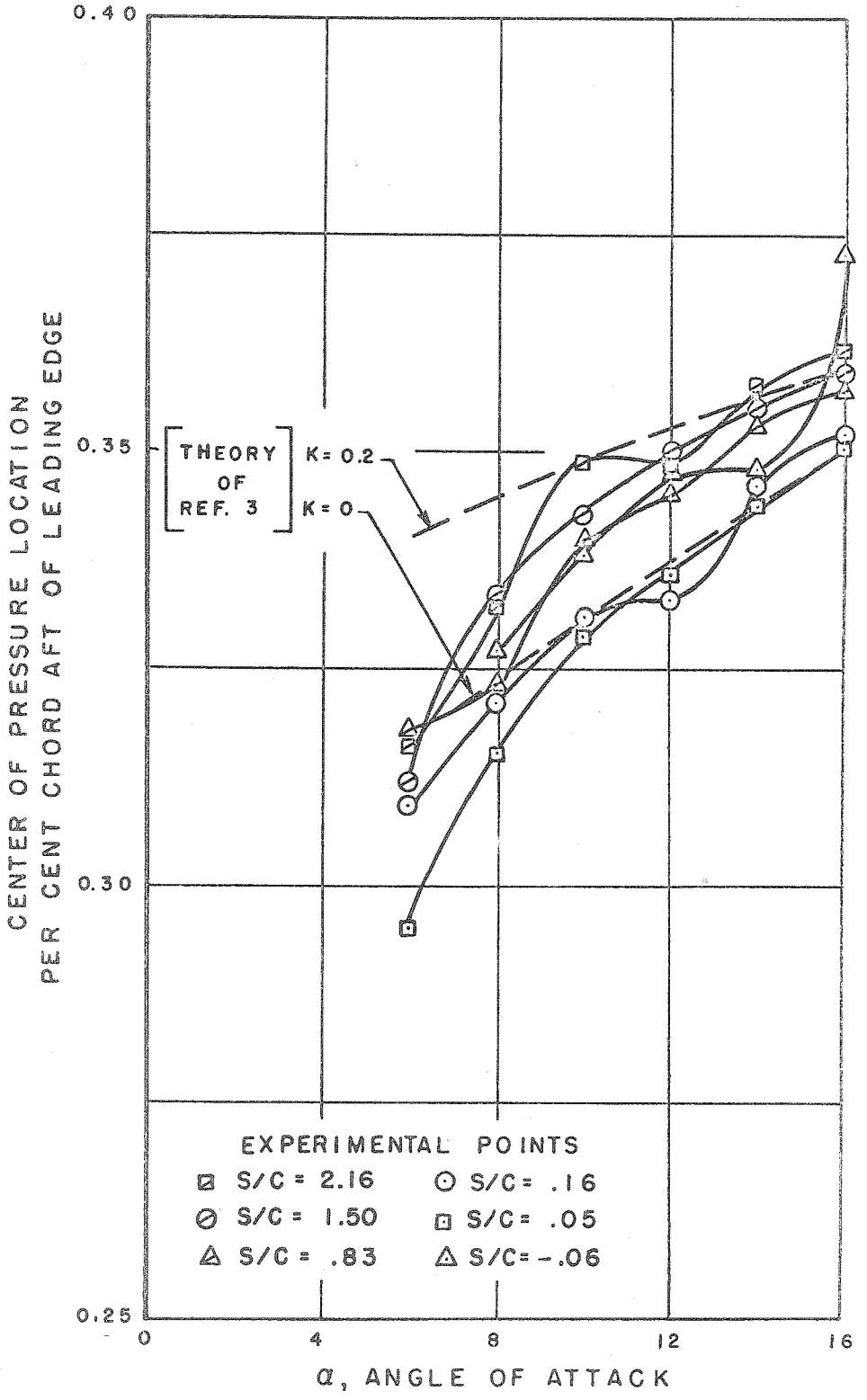

Fig. 36 - The Experimental Center of Pressure Location versus Angle of Attack at Six Submergence Ratios as Compared to Wu's Exact Infinite Fluid Theory.

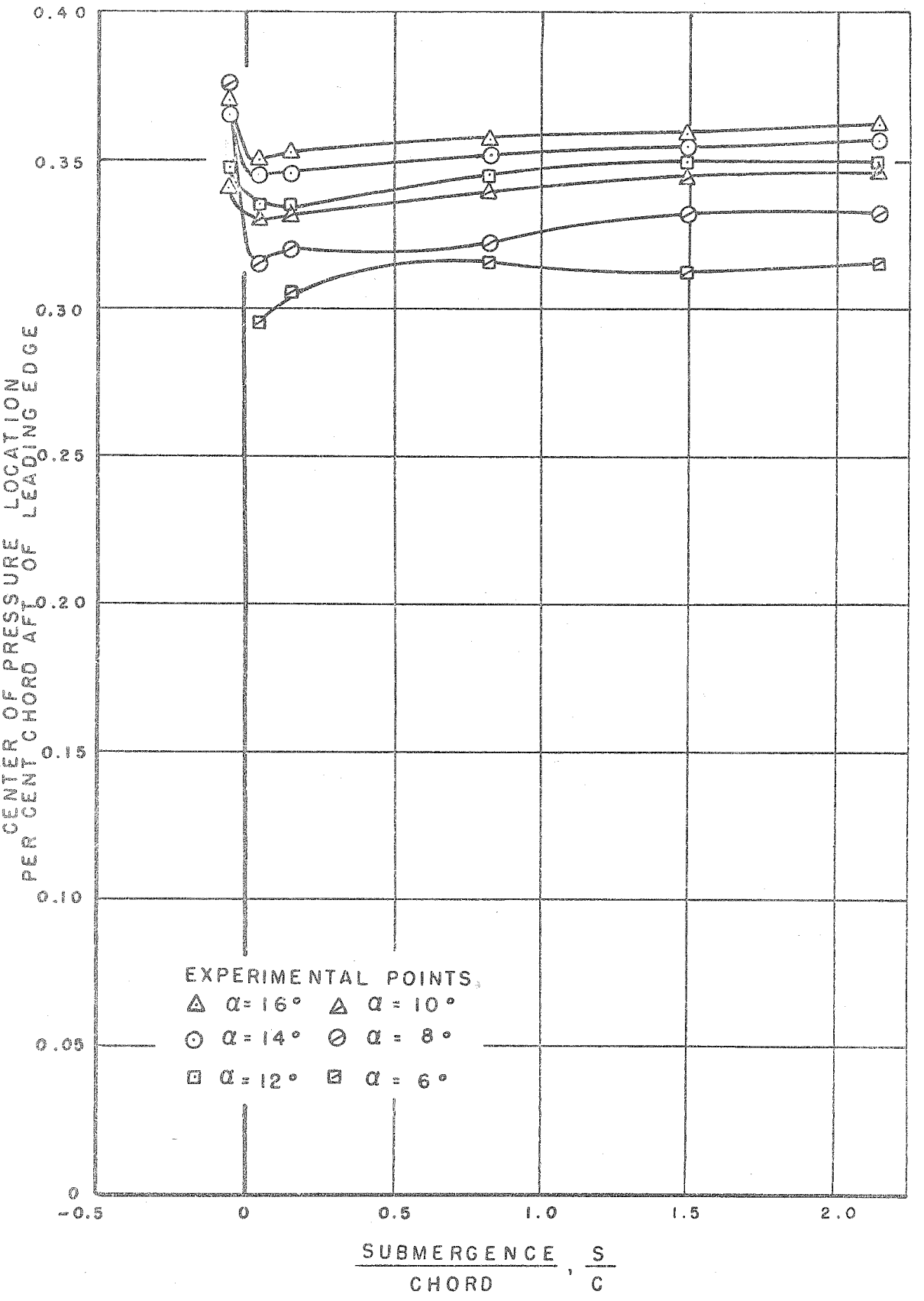

Fig. 37 - Center of Pressure Location versus Submergence at Six Angles of Attack.

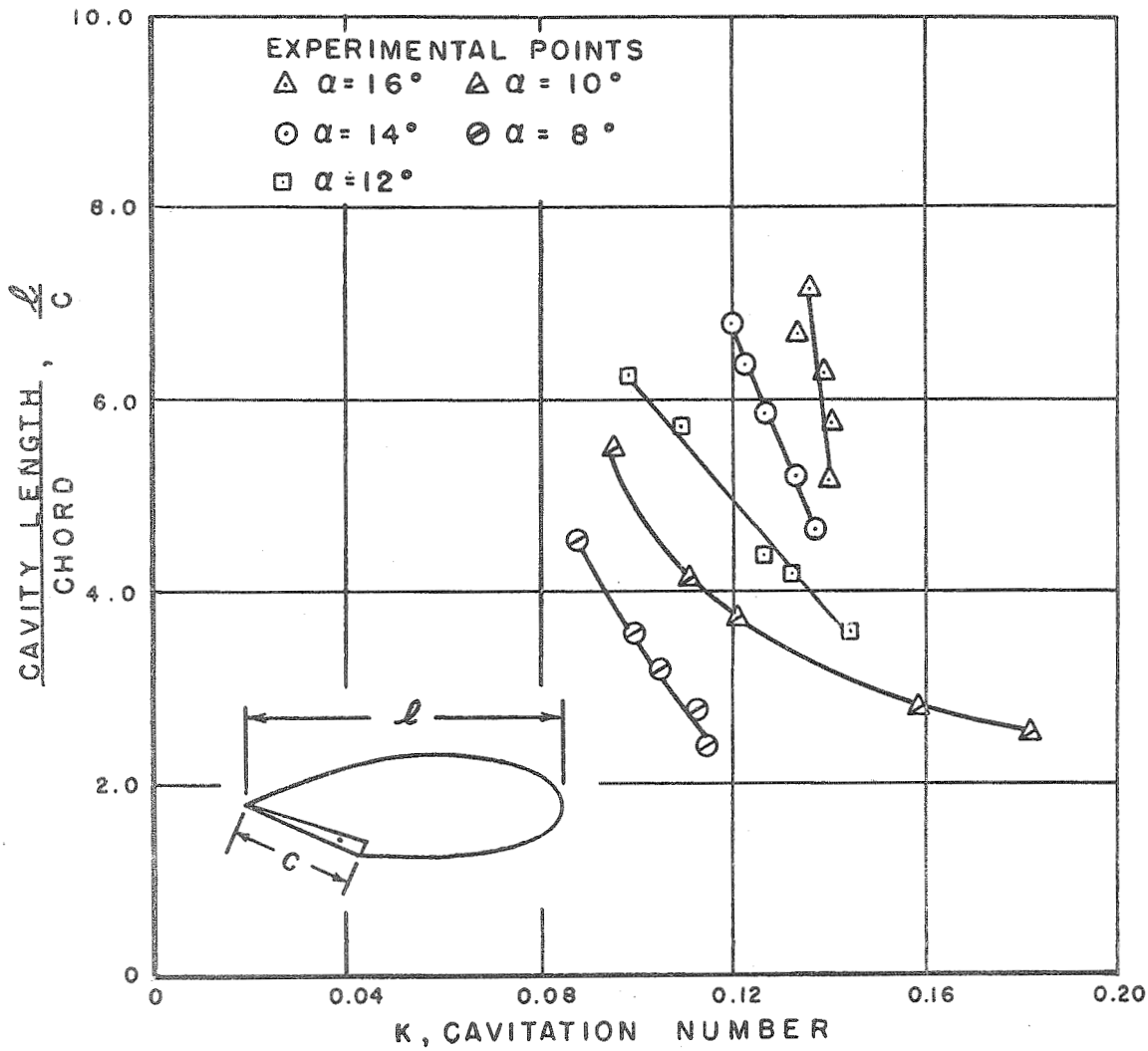

Fig. 38 - Cavity Length Ratios versus Cavitation Number at Five Angles of Attack and s/c = 2.16.

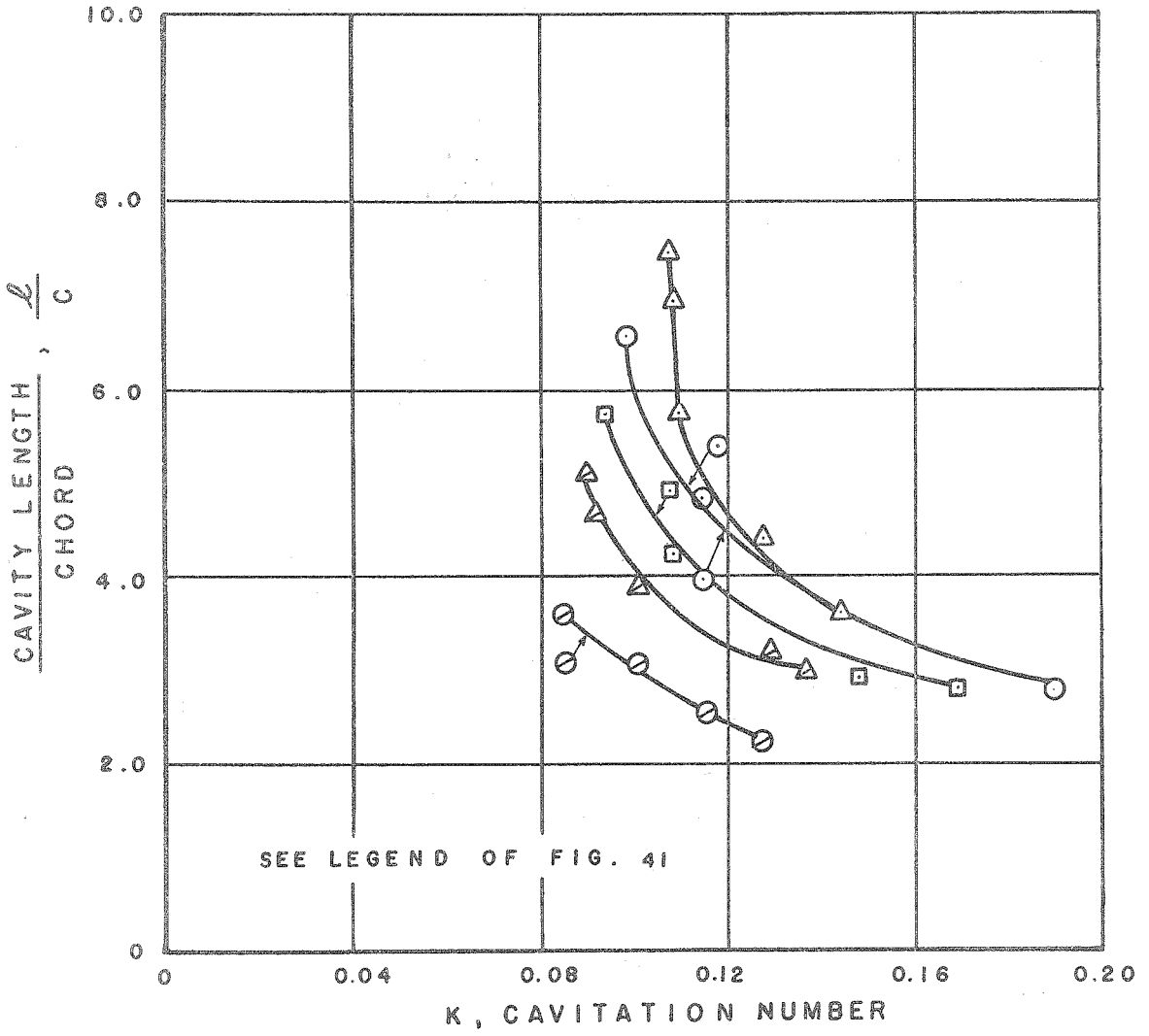

Fig. 39 - Cavity Length Ratios versus Cavitation Number at Five Angles of Attack and s/c = 1.50.

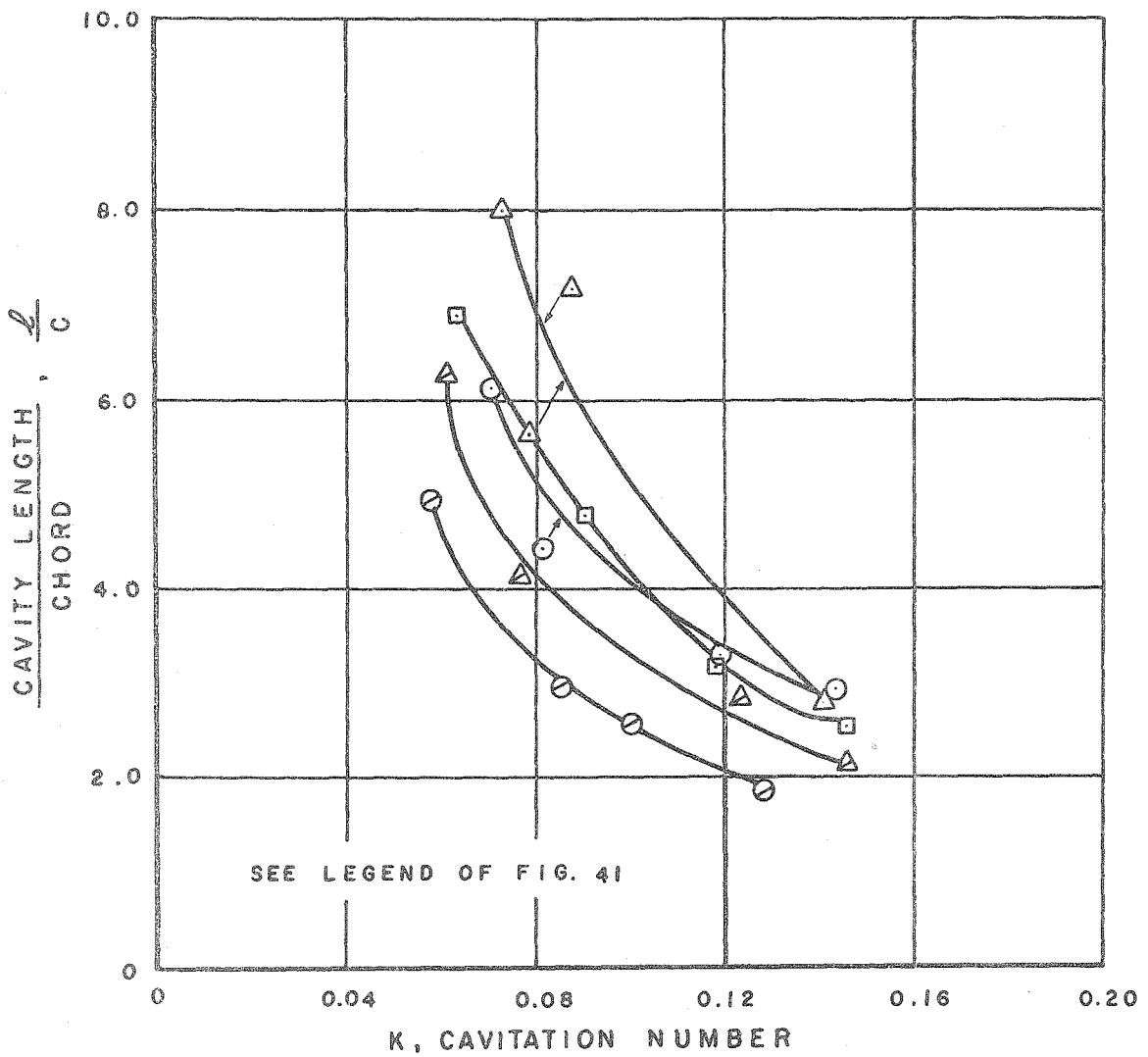

Fig. 40 - Cavity Length Ratios versus Cavitation Number at Five Angles of Attack and s/c = 0.83.

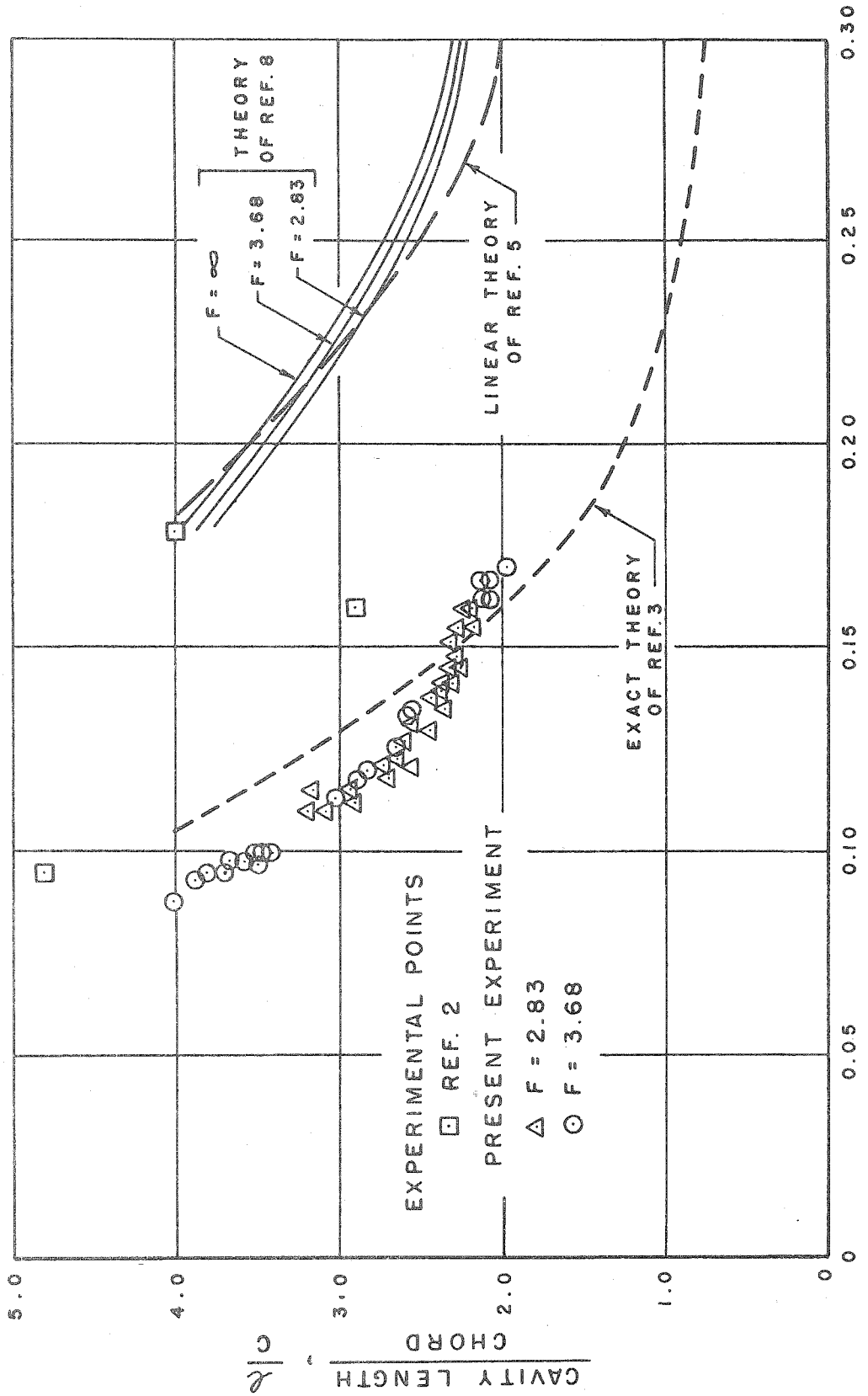

Fig. 41 - The Experimental Cavity Length Ratios at s/c = 1.60, α = 8°, F = 2.83 and F = 3.68, versus Cavitation Number as Compared to the Experiment of Silberman and the Theories of Wu and Parkin.

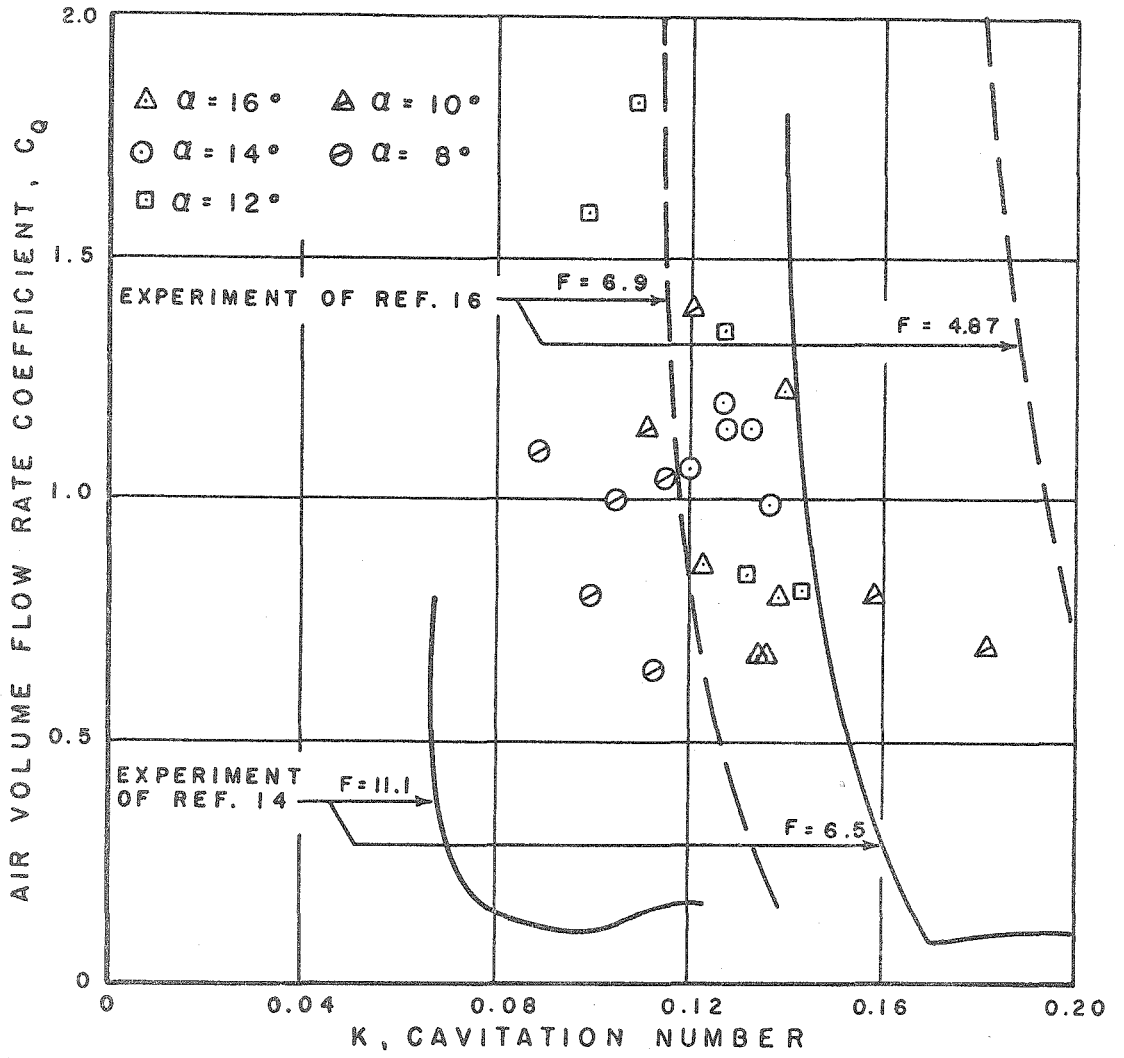

Fig. 42 - The Experimental Air Volume Flow Rate Coefficient versus Cavitation Number at Five Angles of Attack and s/c = 2.16 as Compared to the Experiments of Swanson and O'Neill and Cox and Clayden.

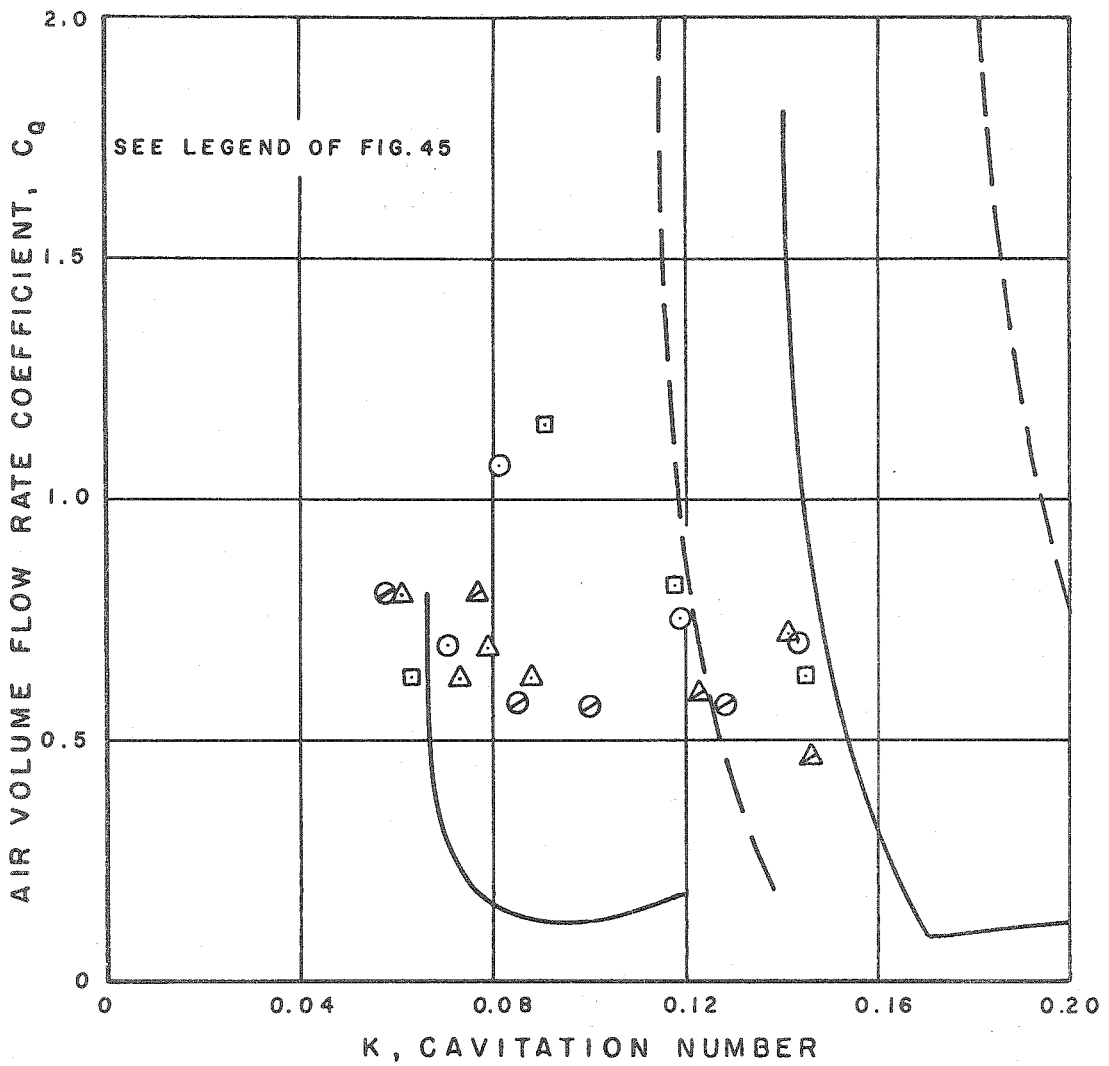

Fig. 43 - The Experimental Air Volume Flow Rate Coefficient versus Cavitation Number at Five Angles of Attack and s/c = 0.83 as Compared to the Experiments of Swanson and O'Neill and Cox and Clayden.

DISTRIBUTION LIST

Chief, Bureau of Naval Weapons
Department of the Navy
Washington 25, D.C.
Attn: Codes DL1-3 (1)
RAAD-3 (1)
RRRE (1)
RRRE-7 (1)
RUAW-4 (2)

Chief, Bureau of Ships
Department of the Navy
Washington 25, D.C.
Attn: Codes 335 (1)
421 (2)
442 (1)
644 (1)

Chief of Naval Research
Department of the Navy
Washington 25, D.C.
Attn: Codes 429 (1)
438 (1)
466 (1)

Commanding Officer and Director
David Taylor Model Basin
Washington 7, D.C.
Attn: Codes 142 (1)
500 (1)
526 (1)
591 (1)

Chief, Bureau of Yards and Docks
Department of the Navy
Washington 25, D.C.
Attn: Research Div. (1)

Commanding Officer and Director
U.S. Naval Eng. Experiment Sta.
Annapolis, Maryland
Attn: Librarian (1)

Superintendent
U.S. Naval Academy
Annapolis, Maryland
Attn: Librarian (1)

Superintendent
U.S. Naval Postgraduate School
Monterey, California
Attn: Librarian (1)

Commander
U.S. Naval Weapons Laboratory
Dahlgren, Virginia
Attn: Librarian (1)

Commanding Officer
U.S. Naval Underwater Ord. Sta.
Newport, Rhode Island
Attn: Librarian (1)

Commander
U.S. Naval Ordnance Laboratory
White Oak, Silver Spring, Md.
Attn: Desk DL (Library) (1)
XL (Aeroballistics)(1)

Commanding Officer and Director
U.S. Naval Civil Eng. Laboratory
Port Hueneme, California
Attn: Librarian (1)

Commander
U.S. Naval Ordnance Test Station
Pasadena Annex
3202 E. Foothill Blvd.
Pasadena, California
Attn: Codes P508 (2)
P804 (2)
P8074 (1)
P8076 (1)
P80962 (1)

Director
Naval Research Laboratory
Washington 25, D.C.
Attn: Librarian (1)

Commanding Officer and Director
U.S. Navy Underwater Sound Lab.
Fort Trumbull
New London, Connecticut
Attn: Librarian (1)

Commanding Officer and Director
U.S. Navy Electronics Laboratory
San Diego 52, California
Attn: Librarian (1)

Commanding Officer
U.S. Naval Air Developmt. Center
Johnsville, Pennsylvania
Attn: Librarian (1)

Commanding Officer
U.S. Navy Mine Defense Lab.
Panama City, Florida
Attn: Librarian (1)

Commander
U.S. Naval Ordnance Test Station
China Lake, California
Attn: Code 7533 (1)

British Joint Services Mission
(Navy Staff), via
Chief, Bureau of Naval Weapons
Department of the Navy
Washington 25, D.C.
Attn: Code DSC-3 (4)

Defense Research Member (W)
Canadian Joint Staff, via
Chief, Bureau of Naval Weapons
Department of the Navy
Washington 25, D.C.
Attn: Code DSC-3 (1)

ASTIA Reference Center
Technical Information Div.
Library of Congress
Washington 25, D.C. (1)

Document Service Center
Armed Services Tech. Inf. Agency
Arlington Hall Station
Arlington 12, Virginia (6)

Office of Technical Services
Department of Commerce
Washington, D.C. (1)

Director of Research
Nat. Aeronautics and Space Admin.
1512 H Street, N.W.
Washington 25, D.C. (6)

Director
National Bureau of Standards
Washington 25, D.C.
Attn: Fluid Mechanics Div. (1)

Coordinator for Research
Maritime Administration
441 G Street, N.W.
Washington, D.C. (1)

Director
Engineering Sciences Division
National Science Foundation
1520 H Street, N.W.
Washington, D.C. (1)

Commander
Air Research and Developmt. Command
Andrews Air Force Base
Washington 25, D.C. (1)

Air Force Office of Scient. Research
Mechanics Division
Washington 25, D.C. (1)

Commanding Officer
Office of Ordnance Research
Box CM, Duke Station
Durham, North Carolina (1)

Committee on Undersea Warfare
Nat. Academy of Sciences
National Research Council
2101 Constitution Avenue, N.W.
Washington 25, D.C. (1)

Director
U.S. Army Engineer Waterways
Experiment Station
Corps of Engineers
Vicksburg, Mississippi (1)

Superintendent
U.S. Merchant Marine Academy
Kings Point, Long Island, N.Y.
Attn: Librarian (1)

Massachusetts Institute of Tech.
Cambridge 39, Mass.
Attn: Dept. of Naval Architecture
and Marine Engineering,
Prof. L. Troost (1)
Hydrodynamics Lab.,
Prof. A. Ippen (1)

Applied Physics Laboratory
University of Washington
Seattle, Wash.
Attn: Librarian (1)

Director
St. Anthony Falls Hydraulic Lab.
University of Minnesota
Minneapolis 14, Minn. (1)

Stanford University
Stanford, California
Attn: Dept. of Mechanical Engrg.
Prof. B. Perry (1)
Head, Dept. of Math. (1)

Cornell University
Ithaca, New York
Attn: Director, Graduate School
of Aeronautical Engrg. (1)

Harvard University
Cambridge 38, Massachusetts
Attn: Dept. of Engineering Sciences
Prof. G.F. Carrier (1)
Dept. of Mathematics
Prof. G. Birkhoff (1)

Iowa Institute of Hydraulic Res.
State University of Iowa
Iowa City, Iowa
Attn: Prof. H. Rouse, Dir. (1)
Prof. L. Landweber (1)

Director
Alden Hydraulic Laboratory
Worcester Polytechnic Institute
Worcester, Massachusetts (1)

University of Wisconsin
Mathematical Research Center
1118 W. Johnson Center
Madison 6, Wisconsin
Attn: Prof. L.M. Milne-Thomson
(1)

Director
Garfield Thomas Water Tunnel
Ordnance Research Laboratory
Pennsylvania State University
P.O. Box 30
University Park, Pa. (1)

Davidson Laboratory
Stevens Institute of Technology
711 Hudson Street
Hoboken, New Jersey
Attn: Dr. J. Breslin (1)

Johns Hopkins University
Baltimore 18, Maryland
Attn: Prof. S. Corrsin, Head
Dept. of Mech. Engrg. (1)

Colorado State University
Fort Collins, Colorado
Attn: Prof. M. Albertson
Dept. of Civil Engrg. (1)

University of Michigan
Ann Arbor, Michigan
Attn: Prof. R.B. Couch
(Dept. NA and ME) (1)
Prof. V. Streeter
(Dept. Civ. Engrg.) (1)

Polytechnic Institute of Brooklyn
99 Livingston Street
Brooklyn 2, New York
Attn: Head, Dept. of Aero. Eng.
and Applied Mech. (1)

Brown University
Providence, Rhode Island
Attn: Div. of Appl. Math. (1)
Div. of Engineering (1)

University of California
Berkeley 4, California
Attn: College of Engineering
Prof. A. Schade (1)
Prof. I.V. Wehausen (1)

Webb Institute of Naval Architecture
Crescent Beach Road
Glen Cove, Long Island, N.Y.
Attn: Librarian (1)

New York State Maritime College
Fort Schuyler, New York
Attn: Librarian (1)

University of Kansas
Lawrence, Kansas
Attn: Dean J.S. McNown (1)

Lehigh University
Bethlehem, Pennsylvania
Attn: Prof. J.B. Herbich
Civil Engr. Dept. (1)

University of Notre Dame
Notre Dame, Indiana
Attn: Prof. A.G. Strandhagen
Dept. of Engineering Mech.
(1)

Rensselaer Polytechnic Institute
Troy, New York
Attn: Prof. H. Cohen
Dept. of Math. (1)

California Institute of Technology
Pasadena, California
Attn: Prof. F.C. Lindvall (1)
Prof. M.S. Plesset (1)

University of Illinois
Urbana, Illinois
Attn: College of Engineering
Prof. J. Robertson (1)

Scripps Institution of Oceanography
University of California
La Jolla, California
Attn: Librarian (1)

Woods Hole Oceanographic Institution
Woods Hole, Massachusetts
Attn: Librarian (1)

Case Institute of Technology
Cleveland, Ohio
Attn: Librarian (1)

Institute of Fluid Mechanics
and Applied Mechanics
University of Maryland
College Park, Md.
Attn: Librarian (1)

Yale University
Mason Laboratory
400 Temple Street
New Haven 10, Connecticut
Attn: Librarian (1)

Philco Corporation
4700 Wissahickon Avenue
Philadelphia, Pennsylvania
Attn: Eng. Librarian (1)

Vitro Corporation of America
962 Wayne Avenue
Silver Springs, Maryland
Attn: Eng. Librarian (1)

Gibbs and Cox
21 West Street
New York 6, New York
Attn: Dr. S. Hoerner (1)

Hydronautics, Inc.
Pindell School Road
Laurel, Md.
Attn: Mr. P. Eisenberg (1)

Technical Research Group
2, Aerial Way
Syosset, New York
Attn: Library (1)

Aerojet General Corporation
6352 North Irwindale Avenue
Azusa, California
Attn: Mr. J. Levy (1)

The Martin Company
Baltimore 3, Maryland
Attn: Science Tech. Librarian
Mail No. J398 (1)

North American Aviation, Inc.
International Airport
Los Angeles 45, California
Attn: Engineering Librarian
Dept. 56 (1)

Lockheed Aircraft Corporation
2555 N. Hollywood Way
Burbank, California
Attn: Engineering Librarian
Bldg. 63, Factory A1 (1)

Douglas Aircraft Company, Inc.
El Segundo, California
Attn: Mr. A.M.O. Smith (1)

Bell Aerosystem Company
P.O. Box 1
Buffalo 5, New York
Attn: Engineering Librarian (1)

McDonnell Aircraft Corp.
P.O. Box 516
St. Louis 3, Missouri
Attn: Engineering Librarian (1)

Chance Vought Aircraft, Inc.
P.O. Box 5907
Dallas 22, Texas
Attn: Engineering Library (1)

Republic Aviation Corporation
Farmingdale, Long Island, N.Y.
Attn: Engineering Librarian (1)

EDO Corporation
College Point, New York
Attn: Engineering Librarian (1)

The RAND Corporation
1700 Main Street
Santa Monica, California
Attn: Librarian (1)

Electric Boat Division
General Dynamics Corp.
Groton, Connecticut
Attn: Engineering Librarian (1)

Hydrodynamics Laboratory
Convair Division
General Dynamics Corp.
P.O. Box 1950
San Diego 12, California
Attn: Mr. H.E. Brooke (1)

Goodyear Aircraft Company
Akron 15, Ohio
Attn: Engineering Librarian (1)

Grumman Aircraft Eng. Corp.
Bethpage, Long Island, N.Y.
Attn: Engineering Librarian (1)
Plant 5

Aeronutronic Division
Ford Motor Company
Ford Road
Newport Beach, California
Attn: Engineering Librarian (1)

Director
Department of Applied Mechanics
Southwest Research Institute
8500 Culebra Road
San Antonio 6, Texas (1)

Boeing Airplane Company
P.O. Box 3707
Seattle, Washington
Attn: Aero-Space Div. Librarian
Org.No. 2-5190, Mail Stop
1384 (1)

Hughes Tool Company
Florence and Trole
Culver City, California
Attn: Librarian Bldg. 2,
Mail Station 5 (1)

United Technology Corporation
P.O. Box 358
Sunnyvale, California
Attn: Dr. D.A. Rains (1)

Cleveland Pneumatic Ind., Inc.
Adv. Systems Development Div.
1301 El Segundo Blvd.
El Segundo, California
Attn: Mr. S. Thurston (1)
Mr. W. Ellsworth (1)

Westinghouse Electric Corp.
Baltimore Division
P.O. Box 1897
Friendship Int'l Airport, Md.
Attn: Engineering Librarian (1)

General Electric Corp.
Ordnance Dept.
100 Plastics Ave.
Pittsfield, Mass.
Attn: Engineering Librarian (1)

Society of Naval Architects and
Marine Engineers
74 Trinity Place
New York 6, N.Y. (1)

Applied Mechanics Reviews
American Soc. Mech. Eng.
29 West 39th Street
New York, N.Y. (1)

Engineering Societies Library
29 West 39th Street
New York 18, N.Y. (1)

OCEANICS, Inc.
Technical Industrial Park
Plainview, L.I., New York
Attn: Dr. P. Kaplan (1)

General Electric Corporation
LME Dept., Bldg. 28
No. 1 River Road
Schenectady 5, New York
Attn: Engineering Librarian (1)

Clevite Brush Development
Clevite Research Center
540 E. 105th Street
Cleveland, Ohio
Attn: Engineering Librarian (1)

AVCO Manufacturing Company
2385 Revere Beach Parkway
Everett 49, Mass.
Attn: Engineering Librarian (1)

Inst. of the Aerospace Sciences Library
2 East 64th Street
New York 21, N.Y. (1)

New York Naval Shipyard
Material Laboratory
Brooklyn, N.Y.
Attn: Mr. D. Kallas (2)

Laboratorio Hidrotecnico Salturnino
de Brito
Rua Ferreira Pontes 637
Rio de Janeiro, Brazil
Attn: Mr. V.F. Motta (1)

Commander
Office of Naval Research
USN, Fluid Dynamics Branch,
Washington 25, D.C.
Attn: Mr. A.J. Coyle (6)